Summer 6-28-2023

Gold Thin Film Electrodes for High Sensitivity & Selectivity Electrochemical Detection of Arsenite in Water

Tybur Q. Casuse Driovínto
University of New Mexico

Tybur Q. Casuse-Driovínto

Candidate

Civil, Construction, & Environmental Engineering

Department

Approval signatures from committee for acceptable publication:

Dr. Jose M. Cerrato, Co-Advisor

Dr. Fernando H. Garzon, Co-Advisor

Dr. Kerry Howe

Dr. Abdulmehdi Ali

Dr. Juan M. Feliu

Gold Thin Film Electrodes for High Sensitivity & Selectivity Electrochemical Detection of Arsenite in Water

By

Tybur Q. Casuse-Driovínto

Bachelor of Science, Chemical Engineering, University of New Mexico, 2017

Master of Science, Civil Engineering, University of New Mexico, 2019

DISSERTATION

Submitted in Partial Fulfillment of the

Requirements for the Degree of

Doctor of Philosophy

Engineering

The University of New Mexico

Albuquerque, New Mexico

August 2023

Dedication

This dissertation is dedicated to my ancestors and future generations.

Ahéhee', Thank you, Danke, y Gracias!

Hozho Nahasdlii'

All is Beautiful Again

Alles ist wieder schön

Todo es hermoso de nuevo

Acknowledgments

Aqua es vida, Tó éí iiná, Water is Life.

The PhD journey was made possible, and profoundly enlightening, thanks to the loving support of my mom, Nyra, my dad, Richard, and my wife, Marisol. The sagacious guidance and friendship of my advisors Jose M. Cerrato and Fernando H. Garzon helped me to build my own way of generating knowledge and curiosity. The land of New Mexico created me, and I thank all human and non-human relatives that help to create the beauty of the world surrounding.

Gold Thin Film Electrodes for High Sensitivity & Selectivity in Electrochemical Detection of Heavy Metals in Water

By

Tybur Q. Casuse-Driovínto

B.S.CHE in Chemical Engineering, University of New Mexico, 2017

M.S. in Civil Engineering, University of New Mexico, 2019

Ph.D. in Engineering, University of New Mexico, 2023

Dissertation Abstract

This is partial fulfillment of a dissertation defense on electrochemical detection of Arsenic (As) in water using gold (Au) nanofilms as sensing electrodes. The maximum contaminant level of Arsenic in drinking water is set at 10 μg L^{-1} by the WHO and USEPA. Electrochemical detection by linear stripping voltammetry has comparable detection limits to more expensive laboratory-based methods but with added benefits of being portable and manufacturable. The work has developed sputtered and crystallographically oriented nanofilms for detection of trace As (III). Ultraflat Au(111) oriented thin films, Au(UTF), were compared to single crystal model electrodes to identify the impacts of controlled surface atom geometry during fundamental electrochemistry studies. We found that the Au(111) surface structure had the highest sensitivity and selectivity for As (III) detection and the Au(UTF) performed very similar to the Au(111) single crystal model electrode for

detection of As (III). The Au(UTF)s were then tested to determine the ability to detect trace As when its primary competing contaminant, Cu (II), was also present. Experiments with As & Cu mixtures provided evidence of an intermetallic alloy which had a large impact on the ability to detect trace As at the Au(UTF) surface. This study has implications for manufacturable and low Au loading sensing electrodes. The work is intended to increase availability of high sensitivity detection of As in drinking water for rural areas where mining legacies and groundwater usage have resulted in increased exposure to As (III).

Table of Contents

List of Figures

List of Tables

Chapter 1. Introduction

Arsenic, As, is a carcinogen and toxin commonly found in drinking water sources around the world. [1, 2] It can be mobilized into a soluble form from anthropogenic sources, such as use of arsenical pesticides, [3] or natural geological processes in groundwater systems. [4, 5] The world health organization (WHO) and United States Environmental Protection Agency (USEPA) have both determined 10 $\mu g\ L^{-1}$ to be the maximum contaminant level (MCL) of As in drinking water. [6-8] If daily drinking water contains a high concentration of As the person which relies on that water may begin to experience chronic arsenic poisoning which can result in a myriad of health concerns ranging from skin rashes and digestive issues to skeletal disorders and various forms of cancer. [9] Increased use of ground water and mining legacies have contributed to increased exposure of rural communities to unsafe concentrations of water. [10-12] The ability to identify and assess As contamination is essential to promoting both public and environmental health.

The goal of this dissertation is to identify a material which provides increased accessibility, sensitivity, and selectivity for electrochemical detection of arsenite, As (III), in water. This dissertation is divided into five chapters and three appendix sections. Chapter two provides a brief background to the presence of Arsenic, aqueous chemistry, electrochemical reactions, electrochemical analysis methods, and knowledge gaps in the form of a literature review. Chapters three, four, and five make up much of the dissertation and are formatted for submission to scientific journals. Chapters three and four have been published in Sensors Plus and Journal of Physical Chemistry C, respectively. The fifth chapter has been formatted

for submission to Physical Chemistry Chemical Physics and will be submitted shortly after the submission of this dissertation to the University of New Mexico repository.

Chapter 3 has been published in the Electrochemical Society *Sensors Plus* journal (https://doi.org/10.1149/2754-2726/ac6d67) and develops the use of a Au nanofilm direct current (DC) sputtered onto carbon paper as an ultralow Au loading (~13 μg) and manufacturable method to generate low-cost As sensing electrodes. The DC sputtered Au electrodes were evaluated by x-ray fluorescence, scanning electron microscopy, and electrochemical analysis. This chapter focuses on the accessibility of electrochemical As sensing electrodes and demonstrates that sputtering of Au electrodes are a facile and rapid electrode generation method capable of detecting As in both laboratory and natural waters below the 10 μg L^{-1} MCL.

Chapter 4 of this study is published in the *Journal of Physical Chemistry C* (https://doi.org/10.1021/acs.jpcc.2c05541) and develops the surface structure-activity-detection relationship for Au electrodes by use of single crystal model electrodes and commercially available well oriented Au(111) thin films, Au(UTF). The work was done at the Universidad de Alicante with the mentorship and guidance of Dr. Juan M. Feliu and other excellent collaborators in the Instituto de Electroquimica in Alicante, Spain. The basal plane Au(111), Au(110), and Au(100) single crystal model surface electrodes and an electrochemical quartz microbalance were used to identify the impact of surface orientation on As redox. The Au(111) surface showed the highest sensitivity and selectivity for As detection and the Au(UTF) performed very similar to the Au(111) electrode. In addition to electrochemical characterization, the Au(UTF) electrodes were characterized for surface

structure and morphology using scanning electron microscopy, transmission electron microscopy and electron backscatter diffraction.

Chapter 5 is formatted for submission to *Physical Chemistry Chemical Physics* and investigates the ability to utilize the Au(UTF) for As (III) detection with co-occurring Cu (II) in solution. Electrochemical cyclic voltammetry and linear stripping voltammetry analysis was performed in mixtures with high and trace concentrations of As and Cu with the Au(UTF) electrodes. The study shows that a Cu_3As alloy is formed during LSV detection at the highly oriented Au(111) surface of the Au(UTF) electrode. The Cu-As intermetallic formed during the deposition step of LSV analysis was characterized with angle resolved x-ray photoelectron spectroscopy and aqueous chemistry modelling. During experiments with mixtures of As and Cu the formation of the intermetallic caused significant shifts in peak shape and position during detection even when only 25 $\mu g\ L^{-1}$ Cu (II) was present. The limit of detection for As (III) was increased from 0.6 to 43 $\mu g\ L^{-1}$ As (III) when 1500 $\mu g\ L^{-1}$ Cu (II) was present in solution. This study provides new insights into alloy formation as a significant mechanism of As detection interference from Cu (II) and has important implications for the development of well oriented sensing electrodes.

Chapter 2. Literature Review

2.1 Arsenic Chemistry

Arsenic (As) can be dissolved and mobilized into potential drinking water sources through natural or anthropogenic causes. [2, 4, 13-16] Groundwater in arid regions is likely to have high concentrations of As due to the reducing potential and contact with Arsenic containing compounds. [17] Humans have contributed to an increase in As concentrations in

surface waters due to mining operations, pesticides and effluents from various manufacturing industries. [3, 11] The health impacts of As in drinking water sources are widespread and severe. [10] Some of the myriad risks of chronic exposure to high concentrations of As include increased child morbidity, skin lesions, diabetes, and renal cancers. [9, 18] Development of accurate methods for on-site determination of drinking water sources is an invaluable tool for aiding public and environmental health.

The chemical speciation and complexation of As controls the toxicity and ability to detect it using electrochemistry. [17] Organic and inorganic species of As have four possible valences of As including As^{-3}, As^{0}, As^{+3} and As^{+5}. [19] Arsenite, As (III), in its inorganic form is the most toxic with the pentavalent species being the second most concerning followed by some organic species. Arsenite is the most readily detectable using electrochemical methods due to the non-reversible redox between As (III) and As (V). Chemical reduction methods using reducing agents have been developed to determine As (V) by using a subtractive method where the As (III) is analyzed before and after chemical reduction of As (V) to As (III). [20-23]

2.2 Electrochemical Detection of As (III)

Electrochemical detection of As can be portable, low cost, and accurate at part per billion ($\mu g\ L^{-1}$) concentrations. These factors make the technology ideal for on-site sensors and was established as a USEPA standard method in 1996. [24] Detection of As (III) can be performed using linear, square wave or differential pulse stripping voltammetry techniques. [22, 25-30] Before describing the process of As detection, an understanding of the components of the electrochemical cell will be helpful for readers unfamiliar with voltammograms. Stripping analysis is typically performed in a three electrode cell configuration consisting of

a working electrode (WE), counter electrode (CE), and reference electrode (RE) and is controlled by a specialized instrument called a potentiostat. [31] The focus of the electrochemical study is on the processes occurring on the working electrode. The potential on the working electrode is controlled in comparison to a reaction with a fast and known potential occurring at the reference electrode. The electric current which is passed during the reaction is passed between the WE, electrolyte solution, and CE. As the potential is swept positively or negatively at a constant rate over time (usually measured in mV s^{-1}) if an electrochemical reaction occurs at the surface of the WE the current will increase or decrease depending on if it is an oxidation or reduction reaction, respectively. A voltammogram is generated by plotting the potential on the x axis, and the current on the y axis. Chemical reactions are then observed by analyzing any peaks, waves, or plateaus in the voltammogram. The redox potential of a reaction is the potential where a reaction will begin to occur and the standard state thermodynamic potential is the potential where the reaction will occur if the concentration of oxidized and reduced species are equal, 1 atm of pressure, and 298 K. If the reaction is diffusion limited the current vs. potential plot will result in a current peak beginning near the reaction potential and ending once the reaction has finished or reached a stead state. The shape, height, and width of a peak related to an electrochemical reaction contains many valuable insights into the reaction mechanisms occurring. Table 1 presents the electrochemical reactions and their standard state thermodynamic potentials for As (III), Cu (II) and Cu_3As, which are the subject of this work. [32, 33]

Table 2-1 Chemical reactions and thermodynamic potential

Reactions of Interest

Reduction process	Chemical Reaction	Thermodynamic Potential V vs. SHE
As(III)/As(0)	$3\ H^+ + \ H_3AsO_3 + 3\ e^- \leftrightarrow As + 3\ H_2O$	0.248
Cu(II)/Cu(0)	$Cu^{2+} + 2\ e^- \leftrightarrow Cu$	0.342
Cu(II) + As(III)/Cu-As	$H_3AsO_3 + 3\ Cu^{2+} + 3\ e^- \leftrightarrow Cu_3As + \ 1.5\ O_2 + 3\ H^+$	-

Now that the foundation of the electrochemical experiment has been described the process of stripping voltammetry can be more easily communicated. The general procedure of each of stripping voltammetry techniques is a three step procedure beginning with equilibration, followed by deposition, and finally stripping. [34] For anodic stripping voltammetry detection of As (III) the equilibration step is a period of time where the potential of the WE is held at a potential which is positive compared to the thermodynamic potential of As (III) reduction to As (0). This step ensures that the electrode does not have any of the reduced species pre-adsorbed and increases the consistency of results. After equilibration, the potential is quickly stepped to a potential below the thermodynamic potential and the reduction of As (III) to As (0) begins to occur. The deposition step is held at the reducing potential for a period of time and as time increases the amount of As adsorbed also increases. Finally, the stripping step is a sweep from the deposition potential back to the equilibrium potential and a plot of the current vs. potential during the stripping step shows an oxidation peak related to the dissolution of As(III) back into solution.

Dr. Compton and his group have provided seminal work on the detection of As at gold electrodes in the early 2000s and continue to do so today. [35-38] A wide variety of alternative structures and materials such as mercury, silver, platinum and carbon electrodes

have been investigated. [39, 40] However, Au is advantageous because of its nobility, reversible As (III) redox reaction, and relatively low hydrogen evolution overpotential. [41] Recent advances in detection have found that shape-controlled nanoparticles with preferred surface orientation present increased selectivity and sensitivity for As (III) detection. [25, 42, 43] Selective detection is essential for accurate results when performing analysis in complex aqueous systems such as natural waters and wine which contain additional cations and anions which may impact the faradaic and capacitive currents observed during analysis. [20, 44, 45]

Copper is commonly cited as the most concerning interfering ion for electrochemical detection and is used as an indicator for selectivity for As. The close thermodynamic redox potential proximity between As (III)/As (0), 0.248 V vs. standard hydrogen electrode (SHE), and Cu (II)/Cu (0), 0.34 V vs. SHE, is cited as the reasoning for interference.[32, 33] An intermetallic alloy of As and Cu is expected to contain Cu_3As and can be formed electrochemically. [20, 46, 47] Figure 2.1 is a phase diagram for the Cu-As system produced by Shishin et al in which they compare their thermodynamic modelling to that of others from past studies. [47] The phase diagram shows that at ratios between 0.05 and 0.11 As/(As+Cu) a stable intermetallic Cu_3As is favorable at room temperature. However, the phase diagram is a metallurgical study and shows a solid-state stability, so it is necessary to also consider if it is likely to form in an aqueous system as well. Figure 2.2 presents a thermodynamic model using geochemists work bench for a solution containing 1 mg L^{-1} Cu (II) and 750 μg L^{-1}. This figure shows that it is also thermodynamically favorable to form a Cu-As intermetallic in an aqueous solution and will be further analyzed in chapter 5.

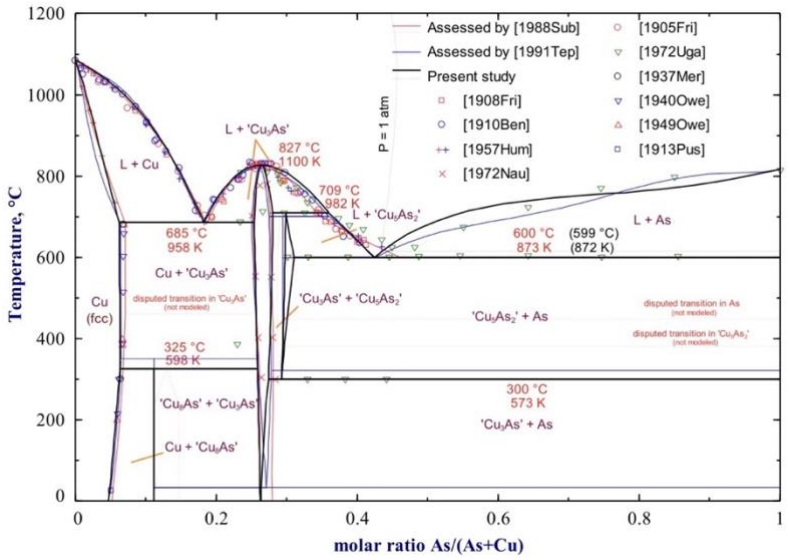

Figure 2.1 Phase diagram of the Cu-As system From Shishin et al. [47] Thin red lines are adapted from the assessment of Subramanian and Laughlin (1988). Thin blue lines are calculated using model parameters of Teppo and Taskinen (1991). Thick black lines are calculated using model parameters of the present study. Symbols are experimental data. (For interpretation of the references to color in this figure legend, the reader is referred to the web version of this article.)

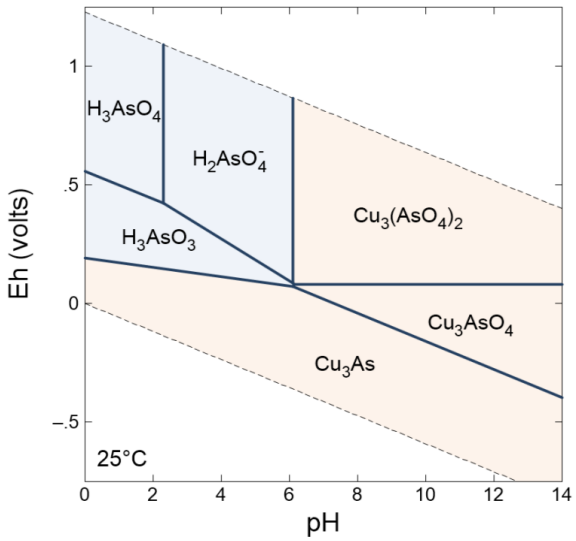

Figure 2.2 Eh vs. pH diagram for 750 μg L^{-1} As (III), 1 mg L^{-1} Cu (II) at 25 ° C and 1.013 bars, generated using geochemist's workbench.

2.3 Gaps and Limitations in Existing literature

This dissertation addresses gaps in existing literature related to accessibility, controlled surface morphology, and interference from Cu-As intermetallic formation for As (III) detection. The overall goal of this work is to identify a highly effective system which may be developed into a

Chapter 3 seeks to address a gap in accessibility to electrochemical As analysis in drinking water for household use. Arsenic levels in drinking water sources can vary between safe and dangerous levels throughout the year due to environmental changes. [48] Therefor if a house relies on a groundwater source at risk of toxic As concentrations the water may be safe to drink at certain times of the year and unsafe at other times. In this case the snapshot in time analysis provides by laboratory techniques such as inductively coupled plasma mass spectrometry (ICP-MS), or atomic absorption spectrometry (AAS) may not have the

temporal resolution to determine the safety of the water. An additional barrier to household use is the cost of publicly oriented electrochemical As detection systems. Systems which have been geared toward the public specifically for As are often expensive, with portable potentiostats costing over $1,000 and compatible electrodes costing hundreds of dollars each. [49] Although electrochemical cleaning of the electrode can allow for repeatable use of the electrodes, fouling of the electrode will occur and accuracy will decline with each additional use, leading to single use electrodes being the most practical for a household. [50] This cost is significantly less than the cost of ICP-MS or AAS equipment and may be a great alternative for a business or governmental organizations. However, for the average household hundreds of dollars per month for As sensing is not accessible. In chapter 3 we introduce a DC sputtered Au nanofilm sputtered on carbon paper as an ultralow Au loading electrode capable of detecting As (III) in laboratory and natural waters below the MCL of As in drinking water. This chapter seeks to increase accessibility of As detection to households by using low-cost and non-precious metal substrates with less than 10 μg of Au to allow for cost effective replacement of sensing electrodes.

Recent studies have investigated the use of shaped Au nanoparticles on carbon substrates to observe how surface geometry impacts selectivity for As detection. [25, 42, 43, 51] It has been found that the Au(111) surface shows higher sensitivity and selectivity compared to the other surface geometries. However, the use of nanoparticles inherently causes imperfections in surface geometry due to edges caused by the 3-dimensional structure and variable quality of result in shape control during synthesis. To fully understand the impacts of surface geometry of Au electrodes on As detection a more ideal surface is necessary. Single crystal model electrodes are commonly used to provide fundamental insights into

electrochemical reactions due to surface geometry and provide an ideal surface which can provide more systematic data relating the structure and electrochemical activity. [52-61] Chapter 4 utilizes single crystals to elucidate the structure-activity-selectivity relationship between the Au basal plane surfaces and As detection. This study was performed in collaboration with the Instituto de Electroquimica at the Universidad de Alicante and shows that the Au(111) surface had the highest sensitivity and selectivity for As detection of the model electrodes.

Chapter 5 combines the benefits of low Au loading from chapter 3 and findings of controlled surface morphology from chapter 4 by investigating a commercially available ultraflat Au(111) thin films, Au(UTF), for As (III)detection with co-occurring Cu (II). The use of thin films on the order of 10 – 100 nm thickness allows for increased surface area to Au consumption. [62, 63] It was expected that the increased selectivity and sensitivity of the Au(111) surface would allow for separation of As (III) and Cu (II) oxidation peaks. However, the use of the Au(UTF) showed that the formation of a Cu-As intermetallic during the LSV deposition step severely impacted the capability to detect trace As (III) even when only 25 μg L^{-1} Cu (II) was in solution. The formation of Cu-As intermetallic have been studied for metallurgical purposes but have not been thoroughly investigated in relation to detection of As at electrodes with controlled surface morphologies. Chapter 5 provides a systematic study showing the impacts of co-occurring Cu (II) on trace As (III) detection at an Au(111) surface. This study identified alloy formation as the primary cause of interference at Au(111) electrodes and provides new electrochemical and physical insights into the formation of Cu_3As.

2.4 Research Objectives

The aim of this dissertation was to investigate and develop sensitive and selective gold (Au) nanofilm sensing electrodes for electrochemical detection of arsenite, As (III), in water. The work develops two nanofilm Au electrodes, a facile and rapid fabrication method and a commercially available ultraflat well oriented Au(111) for trace As detection. The relationship of surface structure and detection sensitivity and selectivity were assessed by use of specialized fundamental electrochemistry techniques and compared to the thin film electrodes.

The overall goal of the research is to increase accessibility to effective and manufacturable electrochemical sensors for As detection in water and assess the benefits and challenges of using controlled surface morphology. Figure 2.3 presents a schematic of the research considerations overarching our goal of developing an accessible electrode which is effective at detecting As (III) at in conditions relevant to unsafe human exposure. The specific objectives and hypothesis of the following three chapters are:

Objective 1: Determine the sensitivity of a DC sputtered ultralow loading Au nanofilm for As (III) detection in laboratory and natural waters below the 10 μg L^{-1} maximum contaminant level set by the USEPA and WHO.

Hypothesis 1: The DC sputtered Au nanofilm will allow for detection below the 10 μg L^{-1} maximum contaminant level.

Objective 2) Develop understanding of surface structure dependence for As redox using single crystals and ultraflat Au(111) thin films.

Hypothesis 2: The Au(111) surface will show the highest sensitivity and selectivity for electrochemical As (III) deposition and stripping.

Objective 3) Assess selectivity for As (III) detection in water containing Cu (II) when using ultraflat Au(111) thin film electrodes.

Hypothesis 3: Isolation of As (III) and Cu (II) during LSV cannot be resolved using ultraflat Au(111) thin films at trace concentrations, due to electrochemical formation of a new phase during the deposition step of LSV.

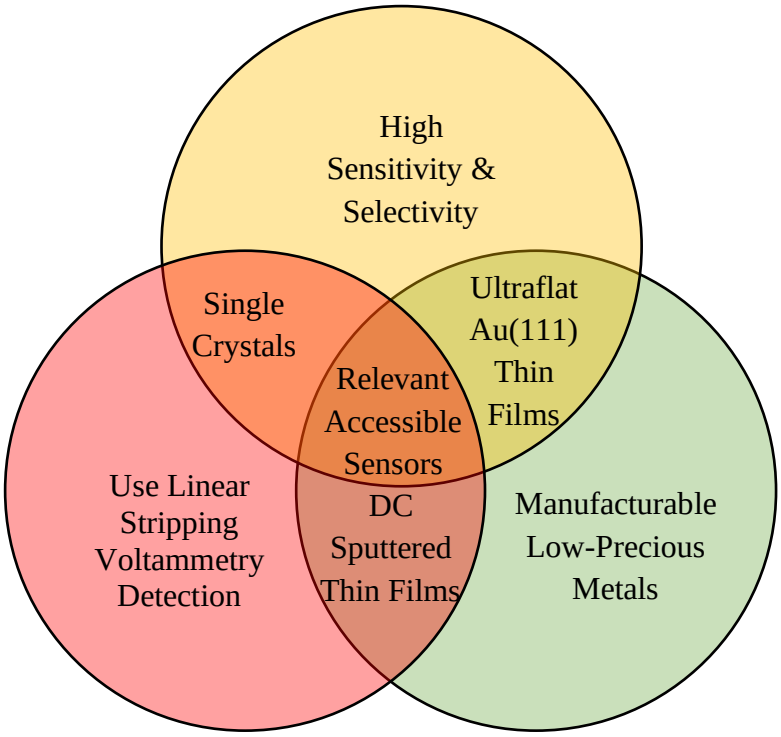

Figure 2.3 Schematic of the intersections of this PhD work with the goal being toxicologically and environmentally relevant sensors which are accessible by researchers and the public.

Chapter 3. DC Sputtered Ultralow Loading Gold Nanofilm Electrodes for Detection of As (III) in Water

Authors names: Tybur Q. Casuse [1], Angelica Benavidez [2], John B. Plumley [2], Lok-kun Tsui [2], Abdul-Mehdi Ali [3], José M. Cerrato [1], and Fernando H. Garzon [2z]

z Corresponding authors' email address: garzon@unm.edu

[1] Department of Civil, Construction & Environmental Engineering, MSC01 1070, 1 University of New Mexico, Albuquerque, New Mexico 87131, USA

[2] Center for Micro Engineered Materials, 1001 University Dr., Albuquerque, New Mexico 87106, USA

[3] Department of Earth & Planetary Sciences, MSC03 2040, 1 University of New Mexico, Albuquerque, New Mexico 87131, USA

Submitted to *Electrochemical Society Sensors Plus* and published May 2023

Keywords: Arsenic, Aqueous Electrochemical Detection, Gold Electrode, Thin Films, Accessible Electrochemistry

3.1 Abstract

This study investigates the use of DC sputtering, physical vapor deposition as a facile method for creating ultralow loading, Au/C electrodes for use in the detection of As (III) in water. The sputtered nanofilm electrodes on carbon papers, substantially reduces the amount of Au consumed per electrode, <10 μg cm^{-2}, compared to use of wire, foil, or screen-printed electrodes. Linear stripping voltammetry (LSV) was chosen for analytical simplicity and ease of automation. Electrodes using Au nanoparticles supported on Vulcan XC 72R carbon were also investigated but were not viable for LSV analysis due to capacitive current charging of the high surface area carbon. The DC sputtered, Au nanofilm electrodes were used to create calibration curves for concentrations of As (III) between 5 and 50 μg L^{-1} and the standard addition method was used in a surface water sample with 5.5 μg L^{-1} total As. Peak areas plotted against concentration displayed strong linear correlation with meaningful detection below the USEPA maximum contaminant level (MCL) of 10 μg L^{-1}. To our knowledge, this is the first study which utilizes DC sputtering to produce ultralow Au loading and low cost As (III) sensing electrodes. The results of this study have implications for the development of single use, low-cost nanofilm electrodes for field As (III) electroanalysis.

3.2 Introduction

Unsafe concentrations of arsenic (As) in drinking water are a global health hazard afflicting many areas of the world such as Argentina, United States, Bangladesh and Vietnam [4, 17]. Concentrations as low as 10 μg L^{-1} in daily drinking water have been identified to cause chronic detrimental health effects according to The United States Environmental Protection Agency (USEPA) and World Health Organization (WHO) [6, 64]. The solubilization of As (III) is commonly performed through microbial respiration in anoxic soils and is dependent on a multitude of variables including temperature and presence of elements such as iron, sulfide, manganese and carbon [11, 14, 65-68]. Many naturally occurring minerals contain As which can be mobilized into ground or surface waters by either reducing or oxidizing conditions to form oxyanions primarily containing arsenite, As (III), and arsenate, As (V), respectively [13]. Arsenic can be found in valence states of -3, -1, 0, +3 and +5, however +3 and +5 are the most common forms in natural waters and present the most concern for toxicity from ingestion. The mobilization of As (III) in anoxic soils can lead to unsafe concentrations in aquifers which may unknowingly be used as a potable water source.

Several methods for quantitative analysis of μg L^{-1} As concentrations are available both in the laboratory and in the field [48, 69]. Laboratory methods include atomic absorption spectroscopy, inductively coupled plasma mass spectrometry and atomic fluorescence spectroscopy. High cost per sample and transport to a capable facility are limitations when conducting studies that require many sample sites, remote locations, or time dependence. Currently, in field measurements can be done by colorimetric techniques and electrochemical sensors [49, 70]. For example, Metrohm produces a three-electrode sensor which uses a Au wire working electrode (WE) with a 0.3 μg L^{-1} limit of detection (LOD) and results are obtained in

around 2 minutes [71]. Creating electroanalysis calibration curves in field samples helps to investigate novel electrodes for their in-situ capabilities and identify competing ion effects [35, 72]. Electroanalysis has many advantages for in situ applications including lightweight materials, low detection limits, and rapid on-site results, which is especially valuable in well bore installation applications or testing in remote locations.

Nano-structured electrodes offer increased surface area to volume ratio compared to macroelectrodes, such as wires. Gold (Au), platinum (Pt) and silver (Ag) are the most commonly studied electrode materials due to their catalytic activity, stability and wide potential range for analysis [73, 74]. Gold is the most ideal of these options due to its high overpotential for hydrogen evolution and stability within the potentials at which As (III) is reduced and oxidized between the zero and trivalent state [75]. Gold nanoparticles and films have been synthesized in a variety of methods using chemical deposition or electrodeposition onto conductive substrates, typically electrically conductive carbons [35, 44, 76-84]. The use of nanostructures such as nanoparticles and nanofilms increases the useable surface area per mass of Au for the electrode, leading to a decrease in precious metal consumption.

Thin films of Au with nanoscale thicknesses generated with physical vapor deposition (PVD) techniques can be used for fabricating ultralow loading electrodes. Direct current (DC) or Radio Frequency (RF) sputter deposition is a particularly common manufacturing method for coatings of thin films in large production operations such as the automotive and textile industries [85, 86]. Physical vapor deposition of Au thin films has also been used with various substrates such as TiO_2, quartz glass, and poly(methyl methacrylate) (PMMA) substrates and used for other electrochemical applications [63, 87-89]. Due to a global need for detection of As (III) in remote and developing world locations, low-cost and high-volume

manufacturing of these electrodes would help to increase the availability of potentially lifesaving knowledge to vulnerable communities. Our study is aligned with recent efforts to develop facile and low-cost electrode fabrication methods beyond screen printing and Au wire electrodes, which could increase access to electrochemical detection [90-94]. Therefore, this study seeks to investigate the suitability of electrodes prepared by DC sputtered to be used as an alternative to nanoparticle, screen printing, and wire electrodes.

This is the first investigation presenting the use of ultralow (<10 μg cm^{-2}) gold loading on carbon, formed using sputter deposition, to detect As (III) in water. This method may significantly impact the development of low-cost systems that use linear stripping voltammetry for As (III) detection and could be economically accessible to under-served communities. Regional As prevalence investigations may require the analysis of hundreds to thousands of water samples. Near real-time measurements of water samples during well drilling operations are particularly valuable in selecting appropriate aquifers with low As concentrations. While in some cases, bulk Au electrodes may be cleaned and reused, practical field cleaning is problematic and time consuming. The replacement cost of single use, stripping electrodes may limit the scope of timely field investigations. Implementation of this electrode fabrication method contributes to in situ trace As detection by generating consumable electrodes that are analytically effective, ultralow Au loading, and scalable by using existing manufacturing techniques. Herein, we investigate the use of DC sputter deposition, Au nanofilms on carbon paper supports to detect below the MCL of As (III) in ultrapure water as well as a complex surface water sample which was comprehensively analyzed for species present using spectroscopic and chromatography laboratory techniques.

3.3 Experimental

3.3.1 Generation of Au Nanofilm and Nanoparticle Electrodes

We fabricated two types of Au nanostructured electrodes, one with DC sputter deposition of Au nanofilm s and another with chemical deposition of Au nanoparticles onto carbon nanoparticles then bonded onto carbon support. Both methods provide means for very low - cost synthesis of consumable electrodes for field investigations. Electrodeposition of Au nanoparticles onto conductive supports, although viable, was not explored due to the increased cost and complexity of deposition for large numbers of electrodes. For the DC sputtered electrodes, Au was deposited directly onto both sides of a 1 cm wide by 5 cm long Sigracet 29AA carbon paper. Sputter coaters manufactured by Polaron or SPI DC were used for Au deposition, voltage 1.7 kV, current 18 mA, and deposition times from 60 to 120 seconds. An Au lead wire was woven into the dry portion of the carbon paper, providing a robust method of electrode current collection.

The nanoparticles were synthesized using Vulcan XC 72R (~250m^2 /g surface area, 50nm particle size) carbon supports. The XC 72R was functionalized in a 24-hour reflux of 2.5% nitric acid at 93° C. [95] A ratio of 0.62 wt/wt% polyvinyl alcohol (PVA) to Au was used to create a colloidal solution. [96] Sodium borohydride ($NaBH_4$) was added in four times the molar concentration of Au to reduce the Au solution. The solution color changed from a transparent yellow to a deep violet color upon addition of the $NaBH_4$. The Au solution was then slowly dripped into a sonicating bath of the functionalized XC 72R in deionized (DI) water over approximately 15 minutes. The solution was sonicated in the bath for an additional hour and left to settle overnight. The solution was then centrifuged, and the supernatant was replaced with fresh DI water. The carbon with Au was mixed into the new

DI water and centrifuged again. The rinsing process was repeated until the pH of the supernatant was the same as the DI water, typically four rinses. The Au on carbon was then allowed to dry at 60° C in air and scraped into a crucible for a reduction process. The reduction was conducted in 3% H_2 balance N_2 at 320° C for five hours with a ramp rate of 5° per minute from room temperature to 320° and allowed to cool to room temperature under the 3% H_2 flow. The powder was then made into an ink using 15 wt/wt% Nafion to Au/XC 72R and ethanol. The entirety of the ink was evenly painted onto both sides of a 1 x 1 cm square at the end of a 1 cm wide by 5 cm long strip of Sigracet 29 AA using a small paintbrush. Creative Materials GPC 251 electrically conductive adhesive was used to attach the carbon strip to a 1 cm wide strip of copper foil or nickel wire, which were used as a lead material. Crystal Bond 509 was used to mask the areas of the electrodes besides the Au electrode area.

An Au wire electrode was created for a comparison to a macroelectrode. Alfa Aesar 0.1 mm diameter Au wire (99.95%) was polished using an alumina slurry and wrapped around a polished nickel wire which acted as the lead and structural support of the electrode. Crystal Bond 509 was used to isolate a 3.3 cm length of the Au wire and keep the nickel wire from interacting with the electrolyte solution. A voltmeter was used to confirm conductivity between the Au and Nickle wire after Crystal bond was applied.

3.3.2 Solutions

Calibration curves were created in 18 MΩ deionized (DI) water and a river water sample collected directly from the Rio Paguate River, which is downstream of the Jackpile mine in Laguna, New Mexico. A previous study from our group has provided a detailed characterization of the water quality and environmental conditions of this site [97]. For As (III)

detection the solutions were acidified to 0.5 M H_2SO_4. The solution was bubbled with nitrogen and stirred using a stir bar on a moderate setting which was consistent during the deposition processes. Stirring was stopped during the stripping process. Sigma Aldrich sodium (meta)arsenite salt, $NaAsO_2$, was used to create a stock solution of 10^{-3} M As (III) in ultrapure water. This concentration was used to determine the amount of stock solution to add to the electrolyte to create additions of 5, 10, 25, 50 and 75 μg L^{-1} As (III) for LSV analysis.

3.3.3 Linear Stripping Voltammetry

In-field electrochemical sensing typically utilizes the linear stripping voltammetry method, which is comprised of a pre-conditioning, pre-concentration and stripping periods. In the case of anodic stripping voltammetry, the preconditioning period is when the electrode surface is held at a potential positive to that of the analytes oxidation to strip any remaining analyte from the surface before analysis. During the preconcentration period the electrode potential is stepped to a potential which negative to the reduction of the analyte and held for a consistent amount of time for all analysis. Finally, in the stripping step the potential is gradually swept positively until it is well beyond the peak caused by oxidation of the analyte. The potential on the Au electrodes was held at -0.1 V for 60 seconds to concentrate As (III) onto the electrode, a Pine Research, single junction, saturated silver chloride (Ag/AgCl) reference electrode was used as the reference electrode for all electrochemical experiments. Subsequently, the voltage was swept to 0.5 V at a rate of 10 mV s^{-1}. The standard potential for As (III) redox is expected to be near 0.051 V vs Ag/AgCl so this potential region is sufficient to observe the stripping reaction. Peak area was calculated by using the difference between the known standard addition curve and the baseline curve by aligning the two curves

at the beginning and end of the oxidation peak.

3.3.4 Material Characterization

X-ray diffraction (XRD) analyses were conducted in a PANalytical Xpert pro instrument using Cu Kα radiation operated at 40 kV and 40 mA. The data were analyzed by the MDI Jade (version 9) software package using the Whole Profile Fitting (WPF) feature. The data was taken from 2θ = 10 ° to 100 ° with a scan rate of 3 ° per minute. Scanning electron microscopy (SEM) analyses were conducted using a Hitachi S5200 nano SEM instrument with 10 kV and 8 mA. Transmission electron microscopy (TEM) analyses were performed with a Joel 2010F field emission gun operated at 200 kV and the images were recorded and analyzed using digital micrograph software. X-ray fluorescence (XRF) measurements were performed under vacuum with an EDAX Orbis Micro-XRF at 20 kV and 400 mA and a spot size of 1 mm in diameter. The Orbis Film builder application was utilized to compare intensity of the film to the intensity of a thick standard piece of Au to estimate mass loading of the Au film. Thermogravimetric analyses were performed using a TA instruments SDT-Q600 in air from room temperature to 800 ° C at a scan rate of 5 ° per minute.

3.3.5 Statistical Analysis

Anova single factor tests ($\propto = 0.05$) were used in excel software to determine statistically significant differences of Au reduction max peak current potential (V) between the three Au electrodes. Plots representing three of each electrode were created and the minimum current for Au reduction at a scan rate of 50 mV s^{-1} was used to analyze significant variation of reduction peak potentials. Anova analysis was also performed on the area (µA V) between 5, 10 and 15 µg L^{-1} standard additions curves and the baseline curve of the As (III) in acidified

ultrapure and river water. The anova tests were used to determine statistically significant differences between the three lowest concentrations and verify the ability to detect below 10 µg L^{-1}. Plots were generated using OriginPro software and the LSV data was smoothed using 5 points of window with adjacent averaging as well as vertically translated to represent the data analysis process and make the curve easier to interpret visually. Limits of detection were determined using the equation LOD = (k * Sb)/ m, where k was equal to 3 for a 98.3 % confidence level, Sb is the standard deviation for analysis of three blank curves, and m is the slope of the calibration curve.

3.3.6 River Water Sample Analysis

The river water sample was collected directly from the Rio Paguate Moquino River on September 21st, 2020, on Laguna reservation in New Mexico, USA. The sample was not filtered or acidified at collection but was acidified to 0.5 M H_2SO_4 before LSV analysis. For Inductively Coupled Plasma (ICP) analysis the sample was filtered through a 0.45 µm membrane and acidified below pH 2 (by adding 2% HNO_3). The original pH at collection was measured to be 8.36. A PerkinElmer Optima 5300DV ICP Optical Emission Spectrometer (ICP-OES) was used to identify the major contributions of metal ions to the water matrix and analyzed Al, As, Ca, Cr, K, Mg, Na, Pb, and U. A PerkinElmer NexION 300D (Dynamic Reaction Cell) ICP Mass Spectrometer (ICP-MS) was used for trace element (As, Pb, U and Cr) analysis. Chloride, nitrate, and sulfate were measured using ion chromatography. Alkalinity was measured via acidimetric titration. The results presented in Table 1 of this manuscript reports only the elements which had concentrations above the limit of detection for the ICP and IC analysis.

3.4 Results and Discussion

3.4.1 Physical Characterization of Au Nanofilm and Au Nanoparticles

A nanofilm of Au was sputtered over the top of a conductive carbon paper to create the Au nanofilm electrode. The Au on carbon was analyzed by XRF and SEM. For a 60 second deposition, X-ray fluorescence analysis reported a thickness of 6.82 ± 0.42 nm with an assumption of a continuous nanofilm (Table S1). The nanofilm is dispersed over the top layer of the carbon and is not continuous, because the DC sputtering process coats the fibrous carbon with a porous film nonuniformly (Figures 1.1A and 1.1B). Decreased Au consumption per electrode has important implications for in-situ implementation in an As sensor with consumable electrodes. Over the lifetime of the electrodes many determinations of As will eventually lead to fouling of the Au surface. Electrochemical cleaning of the Au nanofilms can extend the life of the electrode, [50] but eventually replacement will be necessary. The facile DC sputtering method can make electrode replacement less supply prohibitive and consumptive by producing large batches of low Au loading electrodes. The conditions of DC sputtering in this study did not result in a strong preferred orientation. However, by implementing annealing processes, and/or potential cycling, preferred orientation may be developed while still utilizing a low loading of Au [63, 88, 98-100].

The synthesis of the chemically deposited nanoparticles on XC72R carbon produced a powder that was analyzed with XRD and TEM. X-ray diffraction peaks showed that the Au nanoparticles deposited onto Vulcan XC 72R presented peaks that aligned well with International Centre for Diffraction Data (ICDD) card (PDF# 00-066-0091) peak positions

for Au and gave an average crystallite size of 8 nm (Fig. S1A). The synthesis was done five separate times and resulted in average particle sizes ranging from 3 to 8 nm in size (Table S2). The crystallite size was determined using the full width and half max of the XRD peaks in the MDI Jade (version 9) software, and the Scherrer equation. Figure S1B presents a high-resolution TEM image representative of the sample and corroborates the nanoparticle size determined by XRD. The image also shows that the Au particles are embedded into the carbon substrate, which will provide a physical path for electrical conductivity from the particle to the substrate. However, a portion of the surface of the particle is still exposed to the electrolyte solution, which allows the Au to interact with the ions in solution. Dark field TEM imaging showed that the Au nanoparticles were well-dispersed on the carbon support (Fig. S1C). Active sites for electrochemical reactions with redox active ions in the solution are increased by the presence of many small particles dispersed across the surface of the carbon. Using thermogravimetric analysis, the Au/C ratio was found to be 17.8 wt/wt% (Fig. S2). The geometric surface areas of Au nanoparticles and XC 72R were estimated to be near 460 cm^2 and 13,700 cm^2, respectively, by using the diameters of the particles. This Au nanoparticle electrode generation process was not as scalable as the vapor phase Au nanofilm generation process. The Au to carbon surface area ratio was much lower for the nanoparticles than the nanofilm electrode. Additional cyclic voltammetry analysis was conducted with the Au nanofilm and Au nanoparticles to evaluate their electrochemical response.

3.4.2 Cyclic Voltammetry of Au Nanofilm and Au Nanoparticle Electrodes

The Au nanofilm and Au nanoparticle electrodes were compared to Au wire electrodes using cyclic voltammetry (CV) and evaluated for their ability to perform LSV. The nanofilm

electrode resulted in a CV shape similar to the Au wire with an increased background current at 50 and 100 mV s^{-1}. The nanoparticle electrode presented capacitive masking of faradaic peaks at typical scan rates for LSV and showed a similar CV shape to the Au wire only at very low scan rates (Fig. 3.2).

The Au nanofilm was determined to be viable for LSV, because the capacitance and therefore the background current was low and allowed for consistent analysis in a large range of scan rates. Scan rates of 50 mV s^{-1} and 100 mV s^{-1} with the Au nanofilm produced peaks to background ratios similar to the Au wire with a manageable amount of capacitive current in the response (Fig. 3.2A, B). The reduction peak potential for the Au nanofilm was not significantly different ($p = 0.25$) from the Au wire (Fig. S3). Electrochemical surface area (ECSA) of the Au nanofilm was estimated to be 22.0 cm^2 by calculating the Au reduction peak as compared to an Au wire swept to 1.4 V at a scan rate of 10 mV s^{-1} and a specific capacitance of 400 µC cm^{-2}. When performing the standard addition method in the river water sample the Au reduction peak was compared to that of the ultrapure solution to estimate electrochemical surface area due to an interfering peak at high potentials. When using the Au nanofilm electrode the capacitive current increased but did not obscure the peak due to reduction of the Au surface (Fig. 3.2B, Peak 2). The capacitance due to the carbon paper is represented by the widening with increasing scan rate observed in the region between 0.45 and 0.8 V.

The Au reduction peak with the Au nanofilm was not statistically different from the Au reduction peak on the Au wire. This could be indicative that the nanofilm is not presenting increased catalytic activity or peak shifting due to nanostructure strain. [101] However, a shift in reduction peak maximum potential for the Au nanoparticles could also be caused by

resistance due to the high surface area of the XC-72 carbon support.

The Au nanoparticle electrode presented a high capacitive current from XC 72R, which masked faradaic current peaks for Au reduction. Cyclic voltammetry between 0.45 and 1.3 V was performed at 1, 50 and 100 mV s^{-1}. The difference in reduction peak minimum for the Au nanoparticles was statistically significant ($p = 0.0002$). The nanoparticle electrodes Au reduction potentials were lower than that for the Au wire. This is likely due to the high surface area and surface strain of the Au nanoparticles. Gold nanoparticle electrodes prepared on low surface area carbon supports do not necessarily result in masking of the Au reduction peak from capacitive current [35, 42, 76, 77, 83]. In our study, the use of Au nanoparticles supported on high surface area carbons, and use of LSV instead of pulse stripping voltammetry, resulted in a large amount of capacitive current and masking of faradaic currents and peaks. Linear stripping voltammetry relies on a high peak to background area for detection of trace As (III), thus the use of XC 72R to create an Au nanoparticle electrode was determined to be unsuitable for As (III) detection. Differential pulse voltammetric methods are capable of greatly decreasing the capacitive background. However, a goal of this study is to minimize the time and complexity of the test procedure and data analysis so that non electrochemist professionals would be capable of performing the analysis without assistance.

The DC sputtering method for generating Au nanofilm electrodes results in a comparatively reduced background, is facile, and is potentially scalable by using already existing large scale manufacturing technologies. In our study DC sputtering benefited from coating a larger amount of carbon support surface area than the chemically deposited nanoparticles, which mitigated masking of faradaic peaks which were observed in the Au nanoparticle cyclic voltammetry. The stability of the DC Sputtered thin films was found to be

better than that of the Au nanoparticles because when gas evolution would occur on the electrodes the Au nanoparticles would show a decrease in Au peaks to the point of completely absent. The DC sputtered Au nanofilms could withstand gas evolution without the electrochemical activity of the Au being completely lost. Further study of detection of trace As (III) was conducted only with the Au DC sputtered nanofilm electrodes.

3.4.3 Detection of Arsenite in Ultrapure conditions with Au Nanofilm

The Au nanofilm showed a statistically significant difference in peak area for oxidation of As (0) to As (III) between standard additions of 5, 10 and 15 μg L^{-1} As (III) (Anova p = 1.67E-05, Table S3) in 18 MΩ DI water acidified with 0.5 M H_2SO_4. Figure 3.3A shows the linear sweep data for standard additions of 5, 10, 15, 25, and 50 μg L^{-1} As (III). The limit of detection was determined to be 0.15 μg L^{-1} for the ultrapure calibration curve. The peak area correlated to As oxidation was analyzed by determining the difference between curves and the blank between the beginning and end of the peak. The stripping peak has a shoulder at a slightly more positive potential which can be attributed to a polycrystalline surface with multiple surface energies resulting in multiple peak potentials of stripping [51, 53]. The peak was originally thought to be potentially caused by Cu (II) contamination because of the well-known interference of Cu with the As (III) oxidation during stripping analysis. Careful preparation measures and thorough cleaning procedures were performed to ensure that this was not the case. Figure 3.3B shows the area under the As (III) peak versus the concentration with error bars representing the standard deviation from analysis of four LSV determinations conducted successively in each concentration during a single standard additions experiment. The plot has an R^2 value of 0.996 showing a good linear trend between 5, 10, 15, 25, and 50

$\mu g \cdot L^{-1}$, and that the DC sputtered electrode was able to detect As (III) at environmentally and toxicologically important values by creating a calibration curve while using a low loading nanofilm of Au per electrode.

Again, linear stripping was chosen instead of pulse stripping techniques because it does not require individual electrode evaluation. Pulse stripping is effective in reducing background due to capacitive current, but it also requires defining additional parameters such as pulse height, frequency, and pulse width. [30, 102] In the effort to generate electrodes which can be used for in-field measurements, a reproducible and simple technique for workers which outlines the need for acidification, how to perform standard additions with stock solutions, deposition potentials and time as well as scan rate could make performing electrochemical detection accessible to workers unfamiliar with electrochemistry. [103]

3.4.4 Detection of Arsenite in River Water Sample with Au Nanofilm

The DC sputtered Au nanofilm electrode was used to detect standard additions of 5, 10, 15, 20, 25, 50, 75, 100, 125 and 175 $\mu g\ L^{-1}$ As (III) to a river water sample (Fig. 3.4A). There was not an observed peak from As (III) in the river water sample initially, but there was statistically significant difference in standard additions of 5, 10 and 15 $\mu g\ L^{-1}$ curve area above the baseline (Anova $p = 0.00021$, Table S4). The limit of detection was determined to be 4.7 $\mu g\ L^{-1}$ for the river water sample calibration curve. Metal ion analysis with ICP-MS showed an initial concentration of 5.54 $\mu g\ L^{-1}$ total As (Table 1). The lack of an initial As (III) peak in the acidified sample may be because ICP-MS determined As may have been in the electrochemically inactive As (V) form and therefore undetectable by LSV. This is quite likely considering this was a surface water and the As is more likely to be in a higher

oxidation state than in a ground water sample. The peak is broader and does not present the same shape as in the ultrapure water conditions. As can be observed through ICP analysis in Table 1 there are many commonly occurring ions in the sample which could be contributing to difference in the stripping characteristics of As from the Au nanofilm surface. Broadening could be due to co-adsorption or concentration gradient interferences, however studies which investigate the effects of individual ions present in common natural water matrices on As oxidation shape would be necessary to confirm this and could increase peak sensitivity and selectivity.

The electrode was able to detect at and below the 10 μg L^{-1} MCL in the water sample with the standard addition method. Figure 3.4B shows the charge density of As oxidation peaks versus As (III) standard additions concentrations (R^2 = 0.997). The linearity of the calibration curve was as good in the water sample as with the ultrapure water by using the difference in the area under the curve within the peak region and the baseline LSV data. However, the limit of detection was increased from 0.15 to 4.7 μg L^{-1}. The oxidation of As (III) at lower concentrations resulted in a small but broad increase above the baseline between 0.1 and 0.45 V vs. Ag/AgCl. The Au nanofilm could determine at and below the maximum contaminant level with strong linearity using the standard addition method in a source of drinking water for the people of Laguna.

3.5 Conclusions

This study shows that DC sputtering deposition of Au nanofilms on conductive substrates is a viable method for generating electrodes for effective As (III) detection with an ultralow loading of Au per electrode and uses current mass manufacturing technologies. The

nanofilm showed a strong linear correlation of charge density to As (III) concentration when using the standard additions method in both ultrapure and river water samples. The river water sample was analyzed using ICP MS and OES and IC and contained many common ions found in typical water samples such as alkalinity, nitrates, sulfates, and other metals. These other ions may have contributed to the broadening of the As oxidation peak in comparison to LSV performed in ultrapure conditions. However, further studies into the effects of individual ions on the peak shape would be necessary to come to definitive conclusions. There was not a detectable amount of As (III) in the river water sample, however statistically significant variance between 5, 10, and 15 $\mu g\ L^{-1}$ (Anova $p = 0.00021$) and an R^2 value of 0.997 suggest that the As present was likely in the oxidized and electrochemically inactive As (V) valence. The river water sample standard additions peak was broader and showed only one peak where the ultrapure water showed a peak with a shoulder. The two peaks in ultrapure conditions were attributed to the polycrystalline nature of the DC sputtered nanofilm surface, because there was no source of Cu (II) contamination and previous studies show that the crystallographic orientation can present multiple As stripping potentials when using nanostructures.

These results show the electrode is capable of detection below the 10 $\mu g\ L^{-1}$ MCL in drinking water using LSV. The use of sputter deposition allows for much lower Au loading films, which reduces the cost of Au as compared to screen-printed or wire electrodes. Physical vapor deposition also offers the ability to generate many electrodes at once in a facile and scalable manner. From an electrochemical standpoint DC sputtered films benefit from coating low surface area conductive substrates thus decreasing capacitive current. This was not the case for Au nanoparticles chemically deposited onto the high surface area carbon

support of XC 72R which suffered from excessive capacitive current masking.

Forward outlooks for the DC sputtered Au nanofilm electrodes are in preparing a selective and low Au consumption sensor for in-field use coupled with a handheld potentiostat/smartphone. Several studies have incorporated treatment of the samples to chemically reduce electrochemically inactive As (V) to As (III) which could be used to allow this method to determine total As in addition to As (III) in a river water sample. [22, 44, 80] Additionally, an in-field usability study comparing LSV and differential pulse voltammetry using the DC sputtered Au nanofilm electrodes would allow for determining and quantifying benefits and drawbacks of each method for in-situ use. A useability study would include performing the standard additions method in the field and assessing the impacts of deoxygenation. Physical vapor deposition of Au nanofilms offers an alternative method for fabricating low cost As (III) sensing electrodes. The sputtered Au thin film electrodes may also be effective for in field measurement of Cu, Cr, Fe and other ions of interest.

3.6 Acknowledgements

This material is based upon work supported by the National Science Foundation Graduate Research Fellowship under Grant No. (DGE-1418062), University of New Mexico Center for Water and the Environment, (CREST Grant Number 1345169 and 1914490) and the Center for Micro-Materials. Any opinion, findings, and conclusions or recommendations expressed in this material are those of the authors(s) and do not necessarily reflect the views of the National Science Foundation.

3.7 References

1. A. Basu, D. Saha, R. Saha, T. Ghosh, and B. Saha, Res. Chem. Intermed., 40 (2), 447-485 (2014).
2. M. M. Berg, Environ. Sci. Technol., 35 (13), 2621-2626 (2001).
3. WHO. World Health Organization, 2010.
4. USEPA, Vol. 40 CFR Part 423, Appendix A, 2014.
5. M. Simmler, Environ. Pollut., 231 722-731 (2017).
6. F.-A. Weber, A. F. Hofacker, A. Voegelin, and R. Kretzschmar, Environ. Sci. Technol., 44 (1), 116-122 (2010).
7. C. W. Neil, Environ. Sci. Technol., 48 (8), 4395-4405 (2014).
8. Z. Shi, S. Hu, J. Lin, T. Liu, X. Li, and F. Li, Environ. Sci. Technol., 54 (11), 6621-6631 (2020).
9. R. T. Wilkin, R. G. Ford, L. M. Costantino, R. R. Ross, D. G. Beak, and K. G. Scheckel, Environ. Sci. Technol., 53 (20), 11684-11693 (2019).
10. D. Renock and J. Voorhis, Environ. Sci. Technol., 51 (7), 3733-3741 (2017).
11. D. G. K. P.L. Smedley*, Appl. Geochem., 17 517-568 (2002).
12. D. Q. Hung, O. Nekrassova, and R. G. Compton, Talanta, 64 (2), 269-277 (2004).
13. K. D. Reid, F. Goff, and D. A. Counce, N. M. Geol., 25 (3), 75-82 (2003).
14. J. Das Joyati, P. Sarkar, J. Panda, and P. Pal, J. Environ. Sci. Health., A, 49 (1), 108-115 (2014).
15. Metrohm, (Metrohm, ed.), 2013.
16. Metrohm, (Metrohm, ed.), Vol. 416. Metrohm, Application Bulletin.
17. X. Dai, O. Nekrassova, M. E. Hyde, and R. G. Compton, Anal. Chem., 76 5924-5929 (2004).
18. J. C. Bullen, A. Torres-Huerta, P. Salaun, J. S. Watson, S. Majumdar, R. Vilar, and D. J. Weiss, Water Res, 175 115650 (2020).
19. J. A. Cox, I. A. Rutkowska, and P. J. Kulesza, J. Electrochem. Soc., 167 (3), 037565 (2020).
20. M. C. Welch Christine and R. G. Compton, Anal. Bioanal. Chem., 384 (3), 601-619.
21. L. D. Burke and P. F. Nugent, Gold Bull., 30 (2), 43-53 (1997).
22. E. Nunez-Bajo, M. C. Blanco-Lopez, A. Costa-Garcia, and M. T. Fernandez-Abedul, Anal. Chem., 89 (12), 6415-6423 (2017).
23. T. Gu, L. Bu, Z. Huang, Y. Liu, Z. Tang, Y. Liu, S. Huang, Q. Xie, S. Yao, X. Tu, X. Luo, and S. Luo, Electrochem. Commun., 33 43-46 (2013).
24. J.-F. Huang and H.-H. Chen, Talanta, 116 852-859 (2013).
25. B. K. Jena Bikash Kumar and C. R. Raj, Anal. Chem., 80 (13), 4836-4844 (2008).
26. X. Dai Xuan, G. G. Wildgoose, C. Salter, A. Crossley, and R. G. Compton, Anal. Chem., 78 (17), 6102-6108 (2006).
27. Y. Song and G. M. Swain, Anal. Chim. Acta., 593 (1), 7-12 (2007).
28. Z. L. L. Viltchinskaia E. A., Garcia D.M., Santos P.F., Electroanalysis, 9 633 - 640 (1996).
29. J. Wu, M. Yang, J. Xiao, X. Fu, J. Jin, L. Li, W. Chang, and C. Xie, J. Electrochem. Soc., 160 (11), B225-B230 (2013).

30. D. Kato, T. Kamata, D. Kato, H. Yanagisawa, and O. Niwa, Anal. Chem., 88 (5), 2944-2951 (2016).
31. S. A. Kumar, S.-F. Wang, and Y.-T. Chang, Thin Solid Films, 518 (20), 5832-5838 (2010).
32. Q. M. Mehran, M. A. Fazal, A. R. Bushroa, and S. Rubaiee, Crit. Rev. Solid State Mater. Sci., 43 (2), 158-175 (2017).
33. S. Shahidi, B. Moazzenchi, and M. Ghoranneviss, Eur. Phys. J. Appl. Phys., 71 (3), 31302 (2015).
34. M. Kim, W.-J. Ha, J.-W. Anh, H.-S. Kim, S.-W. Park, and D. Lee, J. Alloys Compd., 484 28-32 (2009).
35. A. K. Mo, V. L. Brown, B. K. Rugg, T. C. DeVore, H. M. Meyer, X. Hu, W. C. Hughes, and B. H. Augustine, Adv. Funct. Mater, 23 (11), 1431-1439 (2013).
36. S. Tanami, D. Ichida, S. Hashimoto, H. Seo, D. Yamashita, N. Itagaki, K. Koga, and M. Shiratani, Thin Solid Films, 641 59-64 (2017).
37. K. Kim, J. Park, H. Kim, G. Y. Jung, and M.-G. Kim, ACS Catal., 9 (10), 9206-9211 (2019).
38. J. van der Zalm, S. Chen, W. Huang, and A. Chen, J. Electrochem. Soc., 167 (3), 037532 (2020).
39. J. Jiang and C. Wang, J. Electrochem. Soc., 167 (3), 037521 (2020).
40. J. Thangphatthanarungruang, A. Lomae, O. Chailapakul, S. Chaiyo, and W. Siangproh, Electroanalysis, 33 (1), 226-232 (2020).
41. A. Pringkasemchai, F. Hoshyargar, B. Lertanantawong, and A. P. O'Mullane, Electroanalysis, 31 (11), 2095-2102 (2019).
42. N. R. Devi, M. Sasidharan, and A. K. Sundramoorthy, Journal of The Electrochemical Society, 165 (8), B3046-B3053 (2018).
43. M. Carmo, M. Linardi, and J. G. R. Poco, Appl. Catal. A Gen., 355 132-138 (2009).
44. L. Prati and G. Martra, Gold Bull., 32 (3), 96-101 (1999).
45. J. M. Blake, C. L. D. Vore, S. Avasarala, A.-M. Ali, C. Roldan, F. Bowers, M. N. Spilde, K. Artyushkova, M. F. Kirk, E. Peterson, L. Rodriguez-Freire, and J. M. Cerrato, Environ. Sci. Process Impacts, 19 605-621 (2017).
46. L. M. Fischer, M. Tenje, A. R. Heiskanen, N. Masuda, J. Castillo, A. Bentien, J. Émneus, M. H. Jakobsen, and A. Boisen, Microelectron. Eng., 86 (4-6), 1282-1285 (2009).
47. S. Palli and S. R. Dey, Adv. Mater. Sci., 2 (1), 1-6 (2017).
48. C. V. Thompson, Annu. Rev. Mater. Sci., 30 (1), 159 (2000).
49. P. Wei, F. Katmis, C. Z. Chang, and J. S. Moodera, Nano Lett., 16 (4), 2714-2719 (2016).
50. X. Luo, A. Morrin, A. J. Killard, and M. R. Smyth, Electroanalysis, 18 (4), 319-326 (2006).
51. D.-D. Han, S.-S. Li, Z. Guo, X. Chen, J.-H. Liu, and X.-J. Huang, RSC Adv., 6 (36), 30337-30344 (2016).
52. J. M. Feliu, A. Fernandez-Vega, A. Aldaz, and J. Clavilier, J Electroanal Chem Interfacial Electrochem, 256 (1), 149-163 (1988).
53. B. Ren, L. A. Jones, M. Chen, D. K. Oppedisano, D. Qiu, S. J. Ippolito, and S. K. Bhargava, J. Electrochem. Soc., 164 (14), H1121-H1128 (2017).

54. G. Forsberg, J. W. Olaughlin, R. G. Megargle, and S. R. Koirtyohann, Anal. Chem., 47 1586-1592 (1975).
55. T. K. Copeland, Anal. Chem., 45 2171-2174 (1973).
56. R. T. Kachoosangi and R. G. Compton, Sens. Actuators B Chem., 178 555-562 (2013).
57. F. T. Henry, Anal. Chem., 51 215-218 (1979).

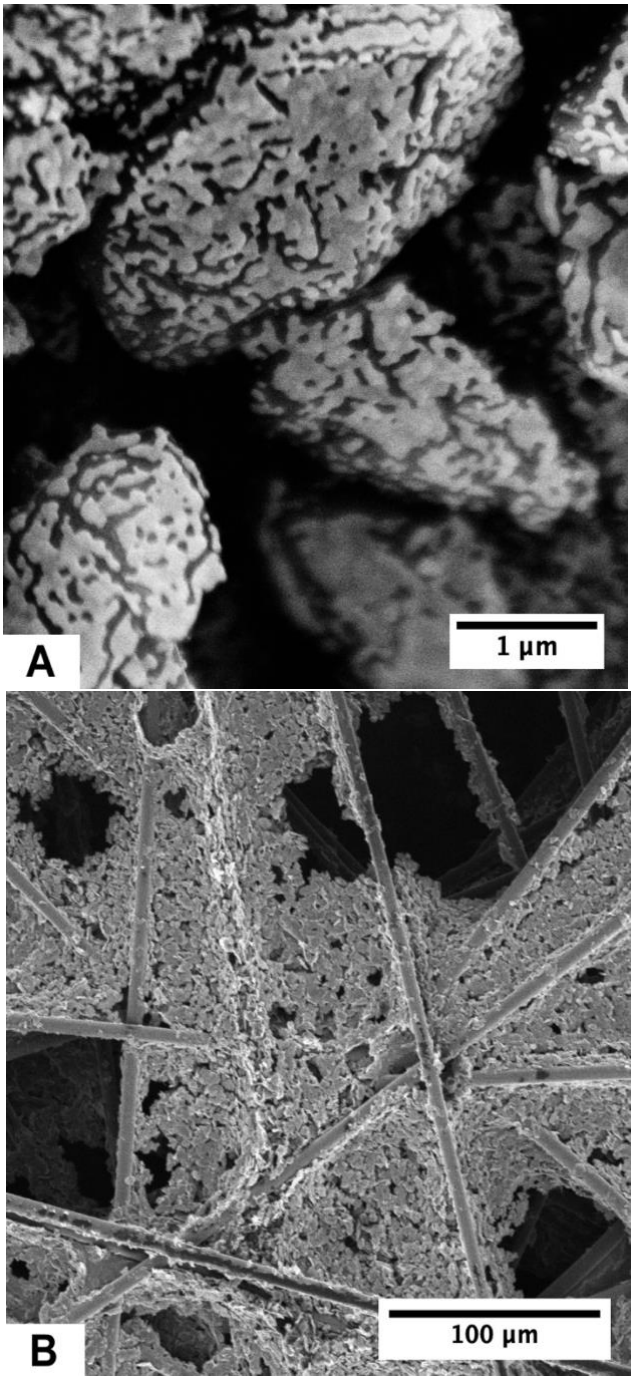

Figure 3.1 Gold nanofilm vapor deposited onto Sigracet 29AA. Scanning Electron Microscopy images SEM image at: (A) 10.0 kV x 20,100 and; (B) 10.0 kV x 300.

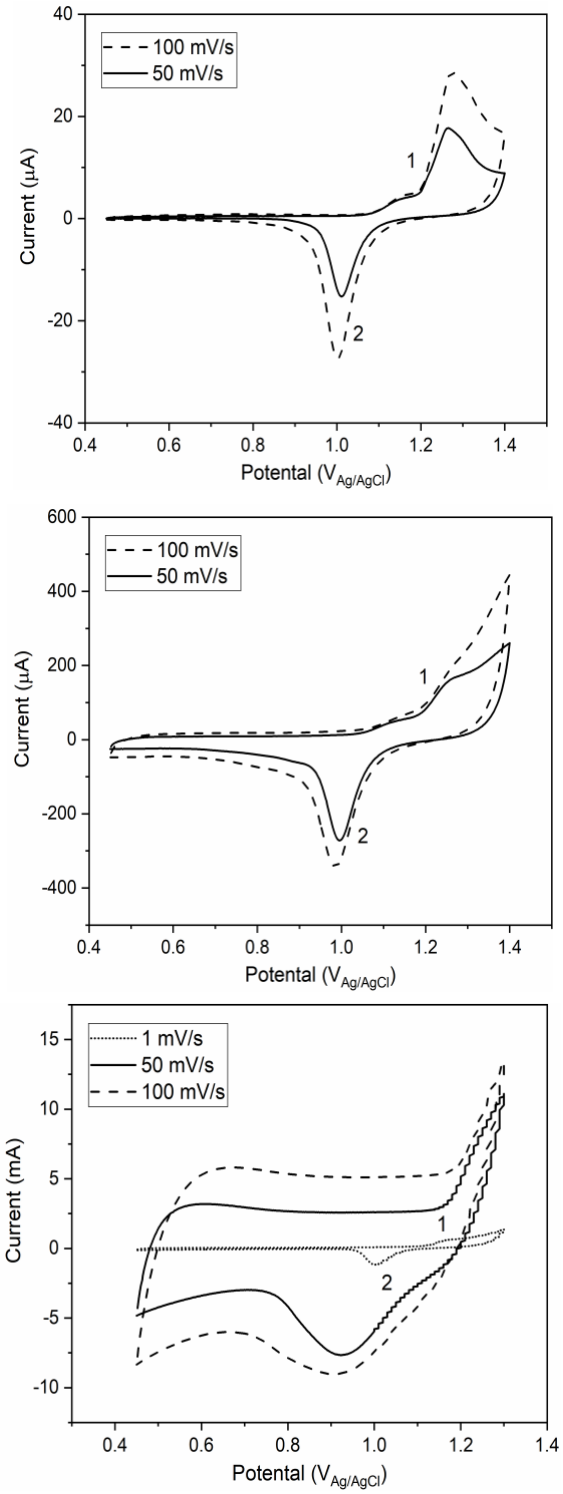

Figure 3.2 Cyclic voltammetry of Au surface oxidation [1] and reduction [2] in 0.5 M H_2SO_4: (A) Au wire, geometric surface area (GSA) = 1.2 cm^2 [50, 100 mV s^{-1}]; (B) Au nanofilm GSA = 2 cm^2 [50, 100 mV s^{-1}]; (C) Au nanoparticles GSA = 460 cm^2 [1, 50, 100 mV s^{-1}].

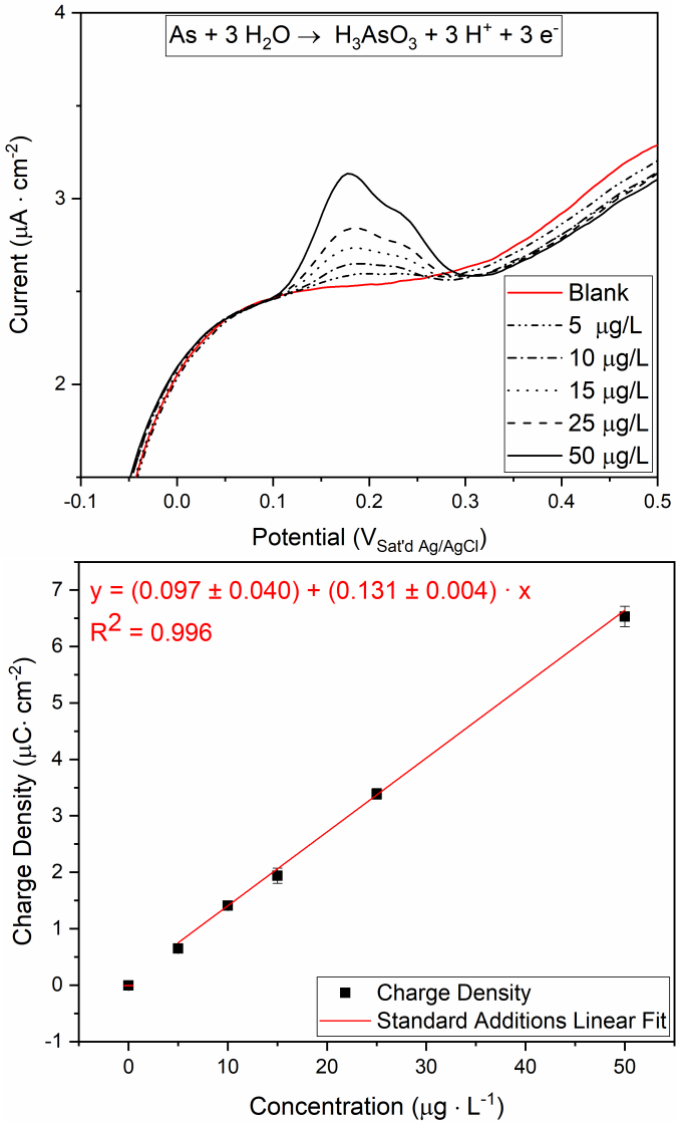

Figure 3.3 (A) Linear stripping voltammetry results for increasing As (III) concentrations of 5, 10, 25, and 50 $\mu g \cdot L^{-1}$ to ultrapure water with 0.5 M H_2SO_4 supporting electrolyte; (B) linear regression of area under curve between 0.14 and 0.3 V versus As (III) concentration. Average values are shown with error bars representing standard deviation of four replicate stripping processes.

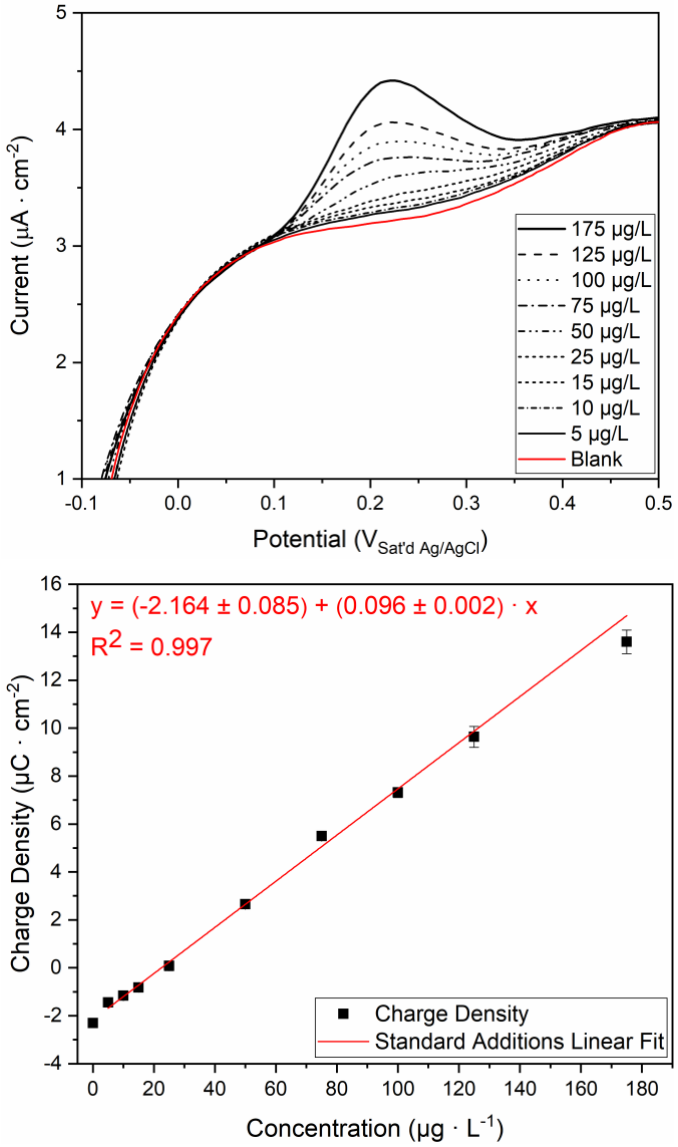

Figure 3.4 (A) Linear stripping voltammetry results for increasing As (III) concentrations of 5, 10, 15, 20, 25, 50, 75, 100, 125 and 175 $\mu g \cdot L^{-1}$ to Rio Paguate River water sample from Laguna NM, USA, with 0.5 M H_2SO_4 ; (B) linear regression of area between baseline between 0.1 and 0.4 V and standard additions curves.

Table 3-1 Inductively coupled plasma (ICP) mass spectroscopy and ICP optical emission spectroscopy analysis of Laguna, NM, USA groundwater sample.

	ICP – MS	**ICP – OES**
Analyte	**μ**g L^{-1}	mg L^{-1}
As	5.54	-
Pb	5.19	-
U	40.38	-
Cr	3.36	-
Al	-	0.01
K	-	16.32
Ca	-	269.21
Mg	-	122.52
Na	-	391.5
Cl	-	16.9
NO_3	-	1.2
SO_4	-	2028.1
Alkalinity as $CaCO_3$	-	247

Chapter 4. Increased Sensitivity and Selectivity for As (III) Detection at Au(111) Surface: Single Crystals and Ultraflat Thin Films Comparison

Tybur Q. Casuse[1,3*], Rubén Rizo,[2] Angelica Benavidez,[3] Adrian Brearly,[3,4] José M. Cerrato,[1,3] Fernando H. Garzon,[3*] Enrique Herrero,[2] Juan M. Feliu [2]

[z] Corresponding email addresses: garzon@unm.edu; tcasuse@unm.edu

Telephone: (001) 505-934-6971

Fax: (001) 505-277-1988

[1] Department of Civil, Construction & Environmental Engineering, 1 University of New Mexico, MSC01 1070, Albuquerque, NM, USA 87131

[2] Instituto de Electroquímica, Universidad de Alicante, Apdo. 99, E'0308, Alicante, Spain.

[3] Center for Micro-Engineered Materials, University of New Mexico, 1001 University Blvd SE, Albuquerque, NM, USA 87106

[4] Department of Earth & Planetary Sciences, MSC03 2040, 1 University of New Mexico, Albuquerque, New Mexico 87131, USA

Submitted to the *Journal of Physical Chemistry C* and published November 2023.

4.1 Abstract

Electrochemical stripping voltammetry electroanalysis sensitivity and selectivity is often times limited by wide variance in analyte electrode surface adsorption and desorption energies. The use of highly orientedAu(111) single crystal and thin film surfaces is shown to decrease this variance and improve detection for arsenic (As) in water. Cyclic voltammetry and linear stripping voltammetry (LSV) analysis on Au oriented and polyoriented electrode surfaces demonstrated that As deposition and oxidation is a complex surface structure dependent process. Electrochemical quartz microbalance indicated that As is deposited in multiple layers when in high concentrations and does not permanently reorganize the Au surface after stripping. LSV analysis of As (III) on the Au(111), Au(110), Au(100), and Au polyoriented single crystal, Au(Poly), model electrode surfaces showed that Au(111) had the highest peak to background ratio and narrowest peak width for As oxidative stripping. Furthermore, an ultraflat Au(111) thin film, Au(UTF), was then compared to the Au(111) and Au(Poly) single crystals and showed a bulk Au(111) single crystal-like response. The Au(UTF) was then used to perform a calibration curve to detect between 2.5 and 100 µg L^{-1} As (III) and resulted in a theoretical limit of detection of 0.0065 µg L^{-1} in 0.5 M H_2SO_4. The results from this study indicate that Au(UTF) provide the sensitivity necessary for detection of trace concentrations of As in water at or below the maximum contaminant level (MCL) of 10 µg L^{-1}.

SYNOPSIS: This study provides new insights into the effect of crystallographic surface orientation on electrochemical As deposition and stripping. Furthermore, our findings implement the increased sensitivity and selectivity of the Au(111) surface in an economically manufacturable and low Au consumption electrode by using ultrathinAu(111) films to detect

trace concentrations of As (III) in water. We expect to see similar enhanced trace metal detection for other suitable target metal ions,

Keywords: Arsenic, Electrochemical Detection, Gold Single Crystals, Gold Thin Films, Water

4.2 Introduction

The ability to detect arsenic (As) at part per billion (ppb) concentrations is essential to informing populations around the world with potential As contamination about the safety of their drinking water. [10, 12, 104] The maximum contaminant level (MCL) set by the World Health Organization and the United States Environmental Protection Agency for safe daily drinking water is 10 ppb or μg L^{-1}. [6, 64] Concentrations above this can lead to cancer in numerous organs, as well as adverse cardiovascular or neurological effects. Arsenite, As (III), is expected to be in the form of H_3AsO_3 in reducing and acidic condition. [105] Arsenite is considered to be the most toxic aqueous form of As in comparison to arsenate, As (V), and other methylated forms. [106] Although As (V) is considered to be electro-inactive it has been electrochemically determined by measuring the difference in concentration of As (III) before and after chemical reduction methods. [30] The growing overabundance of As in drinking water sources due to natural and anthropogenic mobilization calls for development of broadly available, portable, and highly sensitive and selective As sensing systems. [13, 16, 107-109]

Electrochemical detection of trace concentrations of As in water has been investigated using gold (Au) electrodes with a broad variety of morphologies and generation methods seeking to improve detection capabilities. [79, 109-111] Electrochemical sensing has several benefits over common laboratory methods, such as inductively coupled plasma (ICP) mass spectrometry, ICP atomic emission spectroscopy, and atomic absorption spectroscopy,

including the ability to provide in-situ quantitative analysis, decreased cost and portability. [44, 70, 72, 73, 92, 112] Sensing electrodes have been generated using electrodeposition, chemical nanoparticle deposition and physical vapor deposition to form macro and nanoscale structures capable of detecting well below the MCL in water. [35, 76, 77, 79, 94, 113-117] Recent developments have sought to understand the effects of surface orientation on the electrochemical detection of heavy metals including As and lead. [25, 37, 42, 51, 118] Identifying new electrode materials and factors affecting sensitivity and selectivity for As detection has been the focus of a growing body of research over the past two decades.

Single crystal electrochemical studies provide valuable insights into reaction mechanisms including electron transfer, [52, 53] adlayer adsorption and desorption, [54-59] and catalytic activity which are impacted by site geometry. [60, 61] The use of Au nanoparticles and nanostructured electrodes benefit from decreased precious metal consumption per electrode and have been shown to provide high sensitivity for As (III) detection. Pioneering work by Compton and others, identified the Au(111) surface orientation to present increased analytical sensitivity and selectivity when using single crystal and octahedral-shaped particles. [35, 37, 38, 42, 43, 51, 60, 79, 119] However, the use of nanoparticles with a three-dimensional structure inevitably includes imperfections in crystallographic orientation due to the edges of the nanoparticles and variation in size and shape during the synthesis processes. Single crystal surfaces with minimal imperfections provide clearer insight into structure-activity-selectivity relationships which directly benefits electroanalytical studies seeking to identify materials with high sensitivity and selectivity. [57, 120]

The objective of this study is to develop understanding of commercially available ultraflat Au(111) thin films, Au(UTF), capability to provide single crystal-like detection for

trace As (III) in water by identifying the impact of surface structure on As (III) redox at well-oriented Au surfaces. In this study we provide insight into the redox behavior of As (III) at single crystal surfaces with cyclic voltammetry (CV) and linear stripping voltammetry (LSV). A quartz crystal microbalance (QCM) was used to perform CV studies with an Au(111) oriented film to provide further insight into As (III) adlayer formation. The Au(UTF) was characterized using microscopy, diffraction techniques and electrochemical comparison to the model electrodes, and then utilized to detect trace concentrations of As (III) in 0.5 M sulfuric acid solution. This study provides new insights into the influence of surface structure on the selectivity and sensitivity for As (III) electrochemical detection at Au surfaces and implements our findings in a reproducible and commercially available electrode which can provide single crystal-like detection capabilities with ultralow Au loading per electrode.

4.3 Experimental

4.3.1 Materials Description and Characterization

4.3.1.1. Physical Characterization

Single Crystals. Clavilier's method was used to generate basal plane gold single crystal model surface electrodes for the Au(111), Au(110) and Au(100) orientations.[57, 121] A 0.5 mm gold wire was held vertically and melted using a controlled torch to form a bead at the end of the wire which was then slowly cooled to form a single crystal. The single crystal bead was then mounted in a four-cycle goniometer and oriented using the laser reflections form the surface facets. Then it was coated in epoxy for stabilization, cut with emery paper to a flat surface, which had the selected orientation and polished until a mirror finish with

diamond paste. The polyoriented Au single crystal, hereafter referred to as Au(Poly), was an uncut single crystal bead and represents the multiple orientations present in a single crystal.

Ultraflat Au(111) Thin Film. The Au(UTF) films (Platypus Technologies) were physically characterized using S/TEM, electron backscatter diffraction (EBSD), pole figures, atomic force microscopy (AFM) and XRD (Fig. S1 A-F, Fig. S2) and showed a strong Au(111) preferred orientation. Electron backscatter diffraction images were collected using a FIB Helios600 at the Nanoscale and Characterization Laboratory (NCFL) at Virginia Tech. A JEOL NEOARM 200 kV aberration corrected scanning transmission electron microscope (S/TEM) at UNM was used for film grain structure visualization. The films were highly (111) textured, polycrystalline materials with grains rotationally disordered parallel to the substrate surface. The manufacturer's data of thickness and grain size is reported as during EBSD analysis charging image distortion effects can be observed in Figures S1 A and B. Platypus Technologies quotes a film thickness near 100 nm and an average grain area of 3.64 ± 0.2 μm^2. [122] Figure S1B presents the EBSD data showing that the grains are predominantly oriented in the Au(111) direction as described in Figure S1E. The [100] pole figure displayed in S1C indicates that the grains in the thin film are randomly oriented in their in-plane directions. The inverse pole figure S1D shows that the vast majority of the domains are oriented in the Au(111) direction. Surface roughness was characterized by atomic force microscopy (AFM) using a WiTec Alpha300R. The AFM image of the Au(UTF) surface and shows that the surface is very flat with variations in a 30 nm range across the image (Fig. S1F). The root mean square (RMS) roughness is quoted by the manufacturer as 3.6 Å, however, our analysis found it to be 2.6 nm using Gwyddion measurements (Table S1). TEM

analysis Figure B-S1 illustrates the grain structure and grain size variation of the Au(UTF) materials.

Quartz Crystal Microbalance Electrode. Quartz Crystal Resonator QA-CL3 dip cells and a QCM943 oscillation circuit unit were obtained from Princeton Applied Research to collect electrochemical quartz crystal microbalance (EQCM) measurements. The surface normal orientation was determined using thin film Bragg diffraction (PanAnalytical X'Pert Pro) equipped with a multilayer X-ray mirror. The Au film on the EQCM showed strong (111) normal orientation (Fig. S2).

4.3.1.2. Electrochemical Characterization

Electrochemical experiments were carried out in a two-compartment electrochemical glass cell, using an Au wire as a counter electrode and a reversible hydrogen electrode (RHE) as a reference electrode. Voltammetric experiments were carried out at room temperature using a wave signal generator (EG&G PARC 175), potentiostat (eDAQ 161), and digital recorder (eDAQ e-corder 401) workstation. All solutions were made using ultrapure water (18.2 MΩ cm, Elga PureLab Ultra), concentrated sulfuric acid (VWR, 95 wt%), and As_2O_3 salt (Merck). A stock solution of 10^{-1} M As(III) in 0.5 M H_2SO_4 was used to prepare lower concentration solutions.

Single Crystals. The basal plane single crystals were connected to the solution using the hanging meniscus method so that the polished flat piece of the single crystal bead was the only surface touching the solution. The Au(Poly) electrode was submerged into the solution so that the wire was minimally interacting with the solution. The electrochemical surface area of the Au(Poly), QCM and Au(UTF) electrodes were determined using the charge of the Au reduction peak from cyclic voltammetry at 10 mV s^{-1} up to 1.7 V. The reference value used

was 660 μC cm^{-2}, which represents a three-electron transfer process per Au(111) surface atom with a specific current of 220 μC cm^{-2} per electron transferred. The surface area of the single crystal basal plane surfaces was determined using optical microscopy of the flat area prior to use. Prior to any electrochemical experiment, the electrode was annealed in a propane/oxygen flame to remove any organics that may have been adsorbed on the surface and to restore the surface order and quenched using ultrapure water. A protecting droplet of ultrapure water was left on the single crystal surface when the electrode was transported into the cell. After performing analysis in As-containing solutions the electrode was quenched and annealed using concentrated nitric acid to ensure all As was chemically stripped off of the electrode surface.

Ultraflat Au(111) Thin Film. The Au(UTF) electrodes were compared to single crystal model electrodes for their Au redox behavior using cyclic voltammetry (Fig. S1G). The Au(UTF) electrode was taken off from the substrate according to Platypus technologies instructions directly prior to use, and partially submerged in a solution of 0.5 M H_2SO_4. Figure S1G presents a comparison of the characteristic Au redox peaks for the Au(UTF) and the basal plane surfaces which are similar to expected peaks from previous research. [123] The Au redox profiles of Au(UTF) and Au(111) both begin with a shoulder in the positive sweep direction beginning at 1.4 V which leads to a peak at 1.6 V for Au oxidation, showing that the Au(UTF) has a Au(111) single crystal-like electrochemical response.

Quartz Crystal Microbalance Electrode. The QA-CL3 dip cell was used to perform cyclic voltammetry studies of As reduction and oxidation. The Sauerbrey equation [1] was used to convert between the frequency and mass.

$$\Delta F = -\frac{2f_0^2}{A\sqrt{\rho_q\,\mu_q}}\Delta m \qquad [1]$$

Where ΔF is the change in frequency, f_0 is the standard frequency of 9 MHz, A is the area of the electrode surface, 0.174 cm^2, ρ_q is the density of the quartz crystal, μ_q is the shear modulus of the quartz crystal, $2.947 \cdot 10^{11}$ g cm^{-1} s^{-2}, and Δm is the change in mass.

Statistical analysis was performed in EXCEL to determine average and standard deviation of three consecutive measurements where applicable. Linear stripping voltammetry was smoothed using a Lowess method with a span of 0.01 for clarity in the image. The raw data was used to calculate the calibration plot of concentration vs. charge density. Limits of detection were determined using the equation LOD = (k * Sb)/m, where k was equal to 3 for a 98.3% confidence level, Sb is the standard deviation for analysis of three blank curves, and m is the slope of the calibration curve.

4.4 Results and Discussion

4.4.1 Arsenite Deposition/Dissolution on Au electrodes.

Figure 4.1 shows the voltammetric profile of a polyoriented Au electrode immersed in a 10^{-3} M As(III) solution. As can be seen, in the deposition process up to -0.3 V vs. RHE (potential at which hydrogen evolution starts) several peaks can be detected in the negative scan direction which have been reported by previous studies as well.[124] The presence of several deposition peaks suggests the presence of a complex deposition process, in which the presence of a bare Au surface or a previous As adlayer alters the dynamics of the process. It should be noted that this voltammogram is stable upon cycling between these potential limits. Also, the deposition currents are significantly smaller than those expected for a diffusion-controlled process. In fact, currents recorded in 0.1 M As(III) solutions are similar to those

recorded here (Fig. S3 & Table S2), implying that the deposition is controlled by the kinetics of the process, explaining the presence of several deposition peaks. On the other hand, a main single peak is observed in the dissolution process of As. Since the deposition process is determined by the kinetics, the structure of the adlayers formed can have a significant impact on the dissolution process. To establish such an effect, voltammograms with different potential limits between 0.2 and -0.3 V were recorded (Fig. 4.1 & S4). As the lower potential limit is made more negative, the As stripping peak shifts progressively to higher potential values. The presence of a single peak, whose potential shifts to more positive values, clearly indicates that the dissolution of the As layer is governed by the topmost layer. The stability of this adlayer depends on the underneath layer and leads to increasing stability as the deposition progresses.

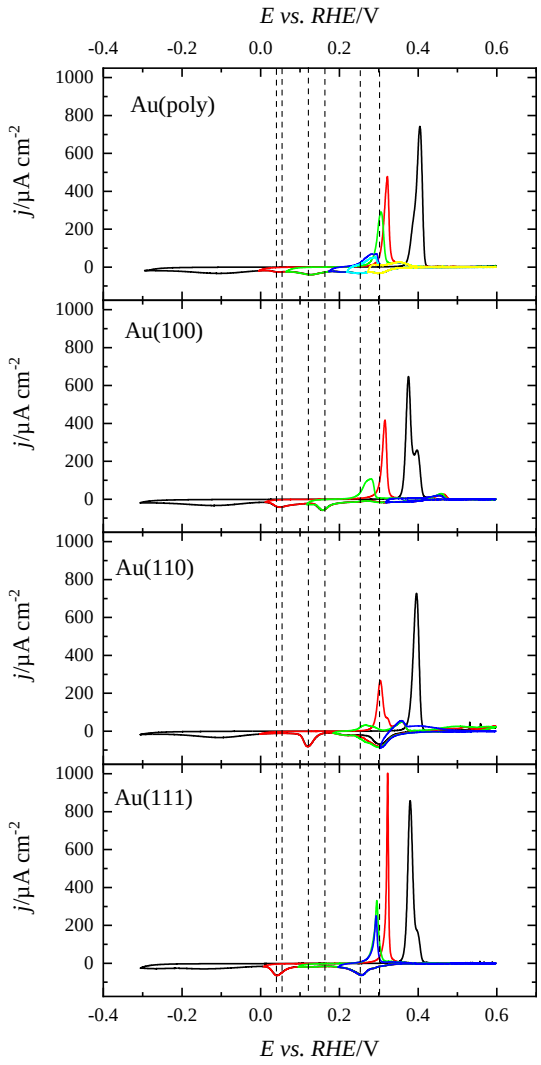

Figure 4.1 Cyclic voltammograms for the different Au electrodes in 0.5 M H_2SO_4 + 1 mM As (III) with different lower limits. Scan rate: 10 mV s^{-1}. The vertical lines mark the position of different deposition peaks on the electrodes.

This type of deposition/dissolution process, which is dependent on the nature of the underneath layer, is expected to depend also on the surface structure of the electrode. For this reason, As (III) deposition/ dissolution was studied on Au single crystal electrodes (Fig. 4.1). Although the qualitative behavior is the same as that observed for the Au polyoriented electrode, significant differences can be observed between the different surfaces. This fact

clearly indicates that the deposition process is a surface-sensitive process. At potentials higher than 0 V on the single crystal electrodes, two main peaks are observed for the deposition process, followed by a wider peak below this potential. Tentatively, the first two peaks can be assigned to the formation of the two first layers of As, and the peak at E<0 V represents the formation of a massive As film. As shown in Figure 4.2, which is an enlargement of the deposition scan of Figure 4.1, each of the peaks observed in the Au(111), Au(100), and Au(110) electrodes has its corresponding peak on the polyoriented electrode (in some cases, two of the peaks corresponding to the single crystal electrodes overlap in the polyoriented surfaces). Thus, it can be considered that the voltammogram of the polyoriented electrode is the result of the contributions of the different facets and ordered domains. In contrast, only one peak is observed in the dissolution. As happens in the polyoriented surface, the potential of the dissolution peak depends on the lower potential limit and the extension of the As deposition.

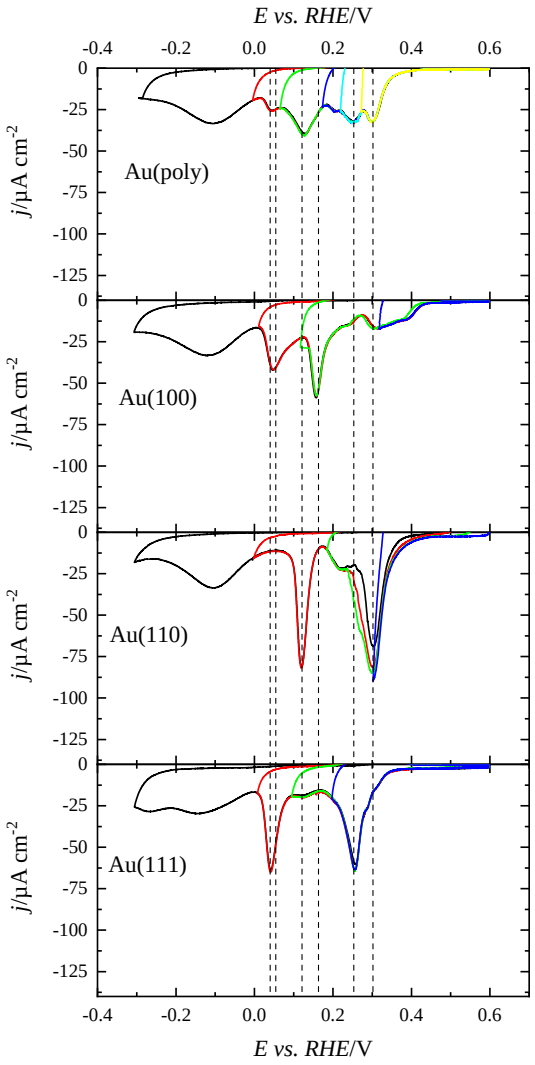

Figure 4.2 Cyclic voltammograms for the different Au electrodes in the deposition region in 0.5 M H_2SO_4 + 1 mM As (III) with different lower limits. Scan rate: 10 mV s^{-1}. The vertical lines mark the position of different deposition peaks on the electrodes.

It should be noted that the standard potential of H_3AsO_3 reduction to As(0) is 0.248 V vs SHE, which means that the equilibrium potential of this redox couple in this medium is ca. 0.24 V. This fact implies that any deposition process taking place at higher potentials is an underpotential deposition (UPD) process. [125, 126] As can be observed in Figures 4.1 and 4.2, the onset for As deposition is higher than this value for all the surfaces. However, clear peaks related to the As UPD deposition are only observed for Au(110) and Au(100) single crystal

electrodes. Underpotential deposition of As (III) onto Au electrodes has been observed and utilized by other researchers in detection.[60] Figure S4 shows an enlargement of this region for cycles with lower limits larger than 0 V. Clearly dissolution peaks at 0.36 and 0.45 V for the Au(110) and Au(100) electrodes respectively are observed, which corresponds to the dissolution of the UPD processes and confirms previous studies findings.[127] For the Au(111) electrode, although the deposition starts at a higher potential, there is no well-defined deposition peak below this potential and the main peak potential is ca. 0.25 V, which suggests that it contains contributions only from the normal deposition process. For the Au(Poly) electrode, the UPD dissolution process is observed due to the presence of (100) and (110) domains in the polyoriented surface.

Charge curves for the deposition process are shown in Figure 4.3. As can be seen, total charges at -0.3 V (the lower limit for the deposition process) are very similar for all the electrodes, standing for ca. 1700 μC cm^{-2}. For the Au(111) surface, the measured charge at 0.125 V, just after the first deposition peak stands for ca. 624 μC cm^{-2}. Taking into account that a process transferring 1 electron per Au(111) surface atom exchanges 220 μC cm^{-2}, and 3 electrons are exchanged in the As (III) deposition process, it can be proposed that after the first deposition peak a pseudomorphic (1×1) As layer has been formed. After the second deposition peak centered at 0.045 V, the deposition charge at 0 V is ca. 1000 μC cm^{-2}, which would suggest that this second peak is related to the formation of the second layer. From that point, multilayer deposition would occur in the third and broad peak. For the Au(100) and Au(110) surfaces, the situation is similar to that observed for the Au(111) electrode, and thus, each peak should correspond to the deposition of the first and second layers. It should be noted that the final charge is very similar for all the electrodes, although at intermediate

potentials they differ. This implies that in the deposition of the third and subsequent layers the underneath gold structure does not affect the deposition process and only the deposition of the first two layers depends on the Au structure.

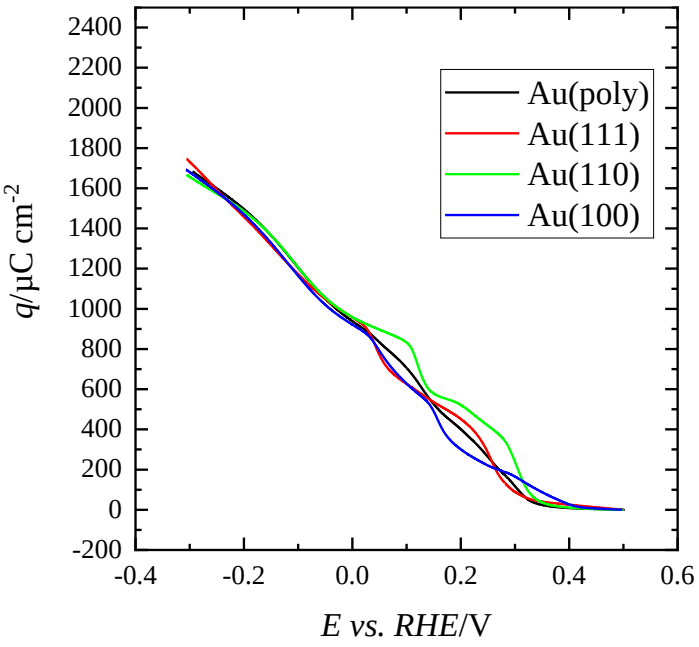

Figure 4.3 Integrated charges measured during the deposition scan for the different Au electrodes using the voltammetric curves in Figure 4.1.

Electrochemical QCM experiments were carried out to determine the nature of the deposited adlayer, Figure 4.4 presents the evolution of the QCM frequency and current density during the cyclic voltammetry of an Au film electrode in 10^{-3} M As (III). The QCM surface showed a highly Au(111) preferred surface orientation in XRD analysis (Fig. S1) and the Au redox prior to introduction of As to solution also showed a degree of preferred Au(111) orientation due to the primary Au oxidation peak being at 1.6 V (Fig. S5). [123] As shown in Figure 4.4A, the frequency returns at the initial value after one complete cycle, indicating that the only process occurring is related to the As deposition/dissolution. The mass of the deposition species can therefore be determined from the ratio between the

frequency change and the charge. Figure 4.4B the comparison between the deposition current, the integrated charge density, and the mass adsorbed onto the Au surface. The mass changes and the integrated charge curves overlap, which implies that the stoichiometry of the deposition process is the same in the whole potential window. Additionally, the ratio between the deposition change and mass is 15 g $(mol\ e^-)^{-1}$. Since, in the reduction process of As, 3 electrons are exchanged, this value implies that the molar mass of the depositing species is 45 g mol^{-1}. This value is lower than the atomic mass of As (75 g mol^{-1}), which suggests that in the deposition process adsorbed water molecules have been displaced from the interface. Considering the difference between the measured molar mass and the As molar mass (75-45=30 g mol^{-1}), approximately two water molecules have been displaced from the interface per As atom deposited.

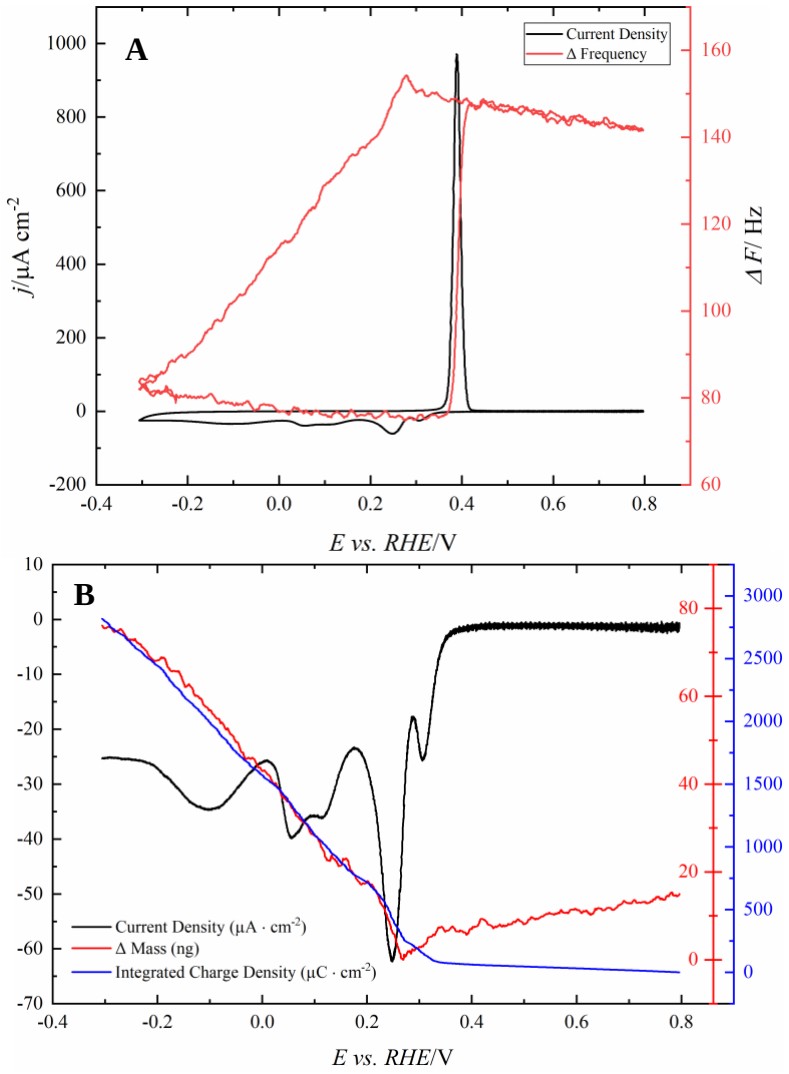

Figure 4.4 Electrochemical Quartz microbalance during cyclic voltammetry in 0.5 M H_2SO_4 + 1 mM As (III) with supporting electrolyte. A) Current density and change in crystal frequency vs. potential during CV at 10 mV s^{-1}; B) Current density, charge density and change in mass vs potential during deposition of As (III) at the QCM surface.

Now that the electrochemical behavior of As on Au electrodes was established, the possible use of these electrodes for chemical analysis of As (III) in solution can be tested. For that, the different electrodes were held at different potentials for 60 s and the stripping curve was recorded for 10^{-5} M As (III) in 0.5 M H_2SO_4 (Fig. 4.5). Two potentials were chosen for the basal planes, each one after the first two deposition peaks, and three potentials were

evaluated for the polyoriented Au electrode. Important differences have been observed between the profiles of the four electrodes. While the Au(111) electrode showed a single sharp peak the Au(110), Au(100) and polyoriented electrodes showed more complex oxidation processes. Table 4-1 summarizes the main data for the experiment. For Au(100) three peaks are observed whereas for Au(110) two peaks can be distinguished. In fact, the observed behavior for the stripping peaks is very similar to that obtained for the positive scan direction of the voltammetric experiments in 10^{-3} M As(III) solution using a similar lower limit for the scan (Fig. 4.1 & S3). The only notable difference is the small shift in the peak potentials due to the difference in concentration of the solution. Using this information, we can assign the peaks at 0.450 V for the Au(100) electrode and at 0.360 V for the Au(110) electrode to the dissolution of the UPD layer, since these peaks are still visible when the lower limit of the scan is above 0.3 V, that is, when bulk As deposition is still not thermodynamically favorable. Thus, the observed difference between the Au(111) electrode and the rest of the surfaces is that no UPD phenomenon is observed on the Au(111). In the case of the polyoriented Au electrode, the observed behavior is the weighted combination of the electrochemical behavior of the different sites present on the surface. Thus, as observed for 10^{-3} M As (III) solutions, the different peaks can be correlated with the peaks in the single crystal electrodes. Regarding the possibility of using the stripping signals for the chemical determination of As (III) in solution, it is clear that the best surface is the Au(111) electrode because a single sharp peak is obtained, which can provide a higher amperometric signal than the rest of the surfaces with minimal peak overlap from interference species.

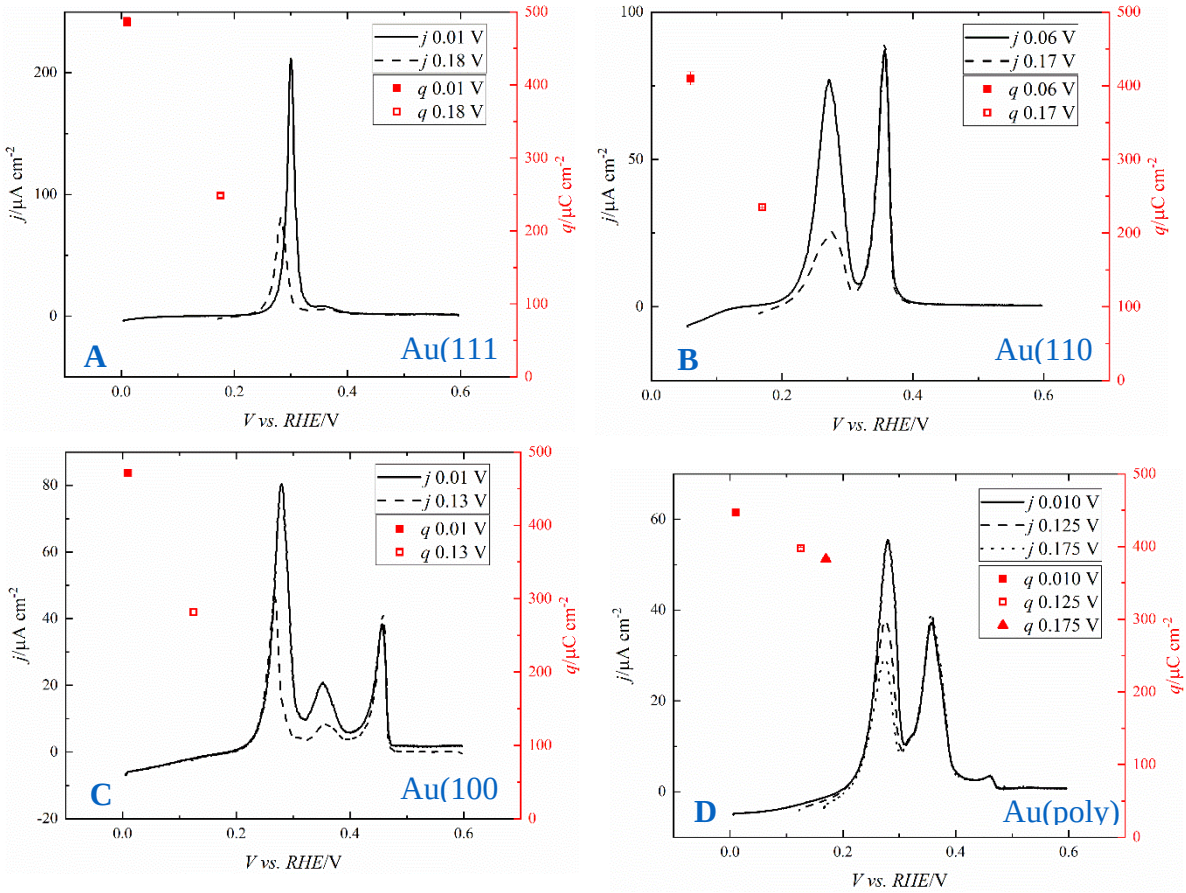

Figure 4.5 As stripping voltammograms for the different electrodes A) Au(111); B) Au(110); C) Au(100); and D) Au(poly), in 0.5 M H_2SO_4 + 10^{-5} M As (III). The electrode potential was held for 60 s at the depositing potentials shown in the legends. The scan rate is 10 mV s^{-1}. The red dots in the figure represent the integrated charge (right-hand axis).

Table 4-1 Summary of the main characteristics of the stripping peaks obtained after the deposition of As on the different gold electrodes in in 0.1 M H_2SO_4+ 10^{-5} M As(III).

Electrode	Deposition potential	Stripping peak potential	Stripping peak charge	Total Stripping charge
Au(111)	0.175 V	0.280 V	248±3 µC cm^{-2}	248±3 µC cm^{-2}
	0.010 V	0.300 V	487±6 µC cm^{-2}	487±6 µC cm^{-2}
Au(110)	0.160 V	0.270 V	149±2 µC cm^{-2}	443±3 µC cm^{-2}
		0.360 V	294±3 µC cm^{-2}	
	0.060 V	0.270 V	278±3 µC cm^{-2}	572±6 µC cm^{-2}
		0.360 V	294±3 µC cm^{-2}	
Au(100)	0.125 V	0.275 V	***	443± 2.6 cm^{-2}
		0.350 V	***	
		0.450 V	100±1 µC cm^{-2}	
	0.010 V	0.275 V	***	572± 6 µC cm^{-2}
		0.350 V	***	
		0.450 V	100±1 µC cm^{-2}	
Au(poly)	0.170 V,	0.280 V	***	382± 2 µC cm^{-2}
		0.360 V	***	
		0.460 V	176±1 µC cm^{-2}	
	0.125 V	0.280 V	***	397± 2 µC cm^{-2}
		0.360 V	***	
		0.460 V	176±1 µC cm^{-2}	
	0.02 V	0.280 V	***	447± 2 µC cm^{-2}
		0.360 V	***	
		0.460 V	176±1 µC cm^{-2}	

Au(UTF) comparison to single crystals

Linear stripping voltammetry was used to compare the electrochemical detection of As (III) for the Au(111), Au(Poly) and Au(UTF) electrode surfaces. Figure 4.6 presents the LSV of the Au(111) and Au(Poly) single crystals compared to the Au(UTF). The Au(UTF) performed similarly to the Au(111) in 10^{-5} M As (III) solution + 0.5 M H_2SO_4. Table 4-2 presents a comparison of the maximum peak current potential, full width half max (FWHM), and charge density. The peak potential for the Au(111) and Au(UTF) are 0.337 and 0.338, respectively, showing that the binding energy for the stripping process was by and large the same. The maximum peak potential for the Au(poly) electrode was a slightly lower energy at 0.324 V. This may be associated with increased underpotential deposition activity for deposition at Au geometries besides Au(111) which are included in the Au(Poly) electrode. The FWHM was determined to identify the capacity for selectivity when other redox active metals may be present in the water matrix. The Au(UTF) and Au(111) surfaces showed FWHM below 20 mV while the Au(Poly) electrode was 48 mV wide which shows that the Au(111) and Au(UTF) have a narrower potential window for detection which may lead to higher selectivity when other metals or electrochemically active species are also present in the water matrix. The peak potential intensity and width of the Au(UTF) electrode is very similar to that of the Au(111) surface, which implies that both surfaces are almost equivalent for this reaction, and that the defects present in the Au(UTF) do not significantly alter the response for this reaction, which is mainly dominated by the presence of (111) grain boundary domains in the Au(UTF).

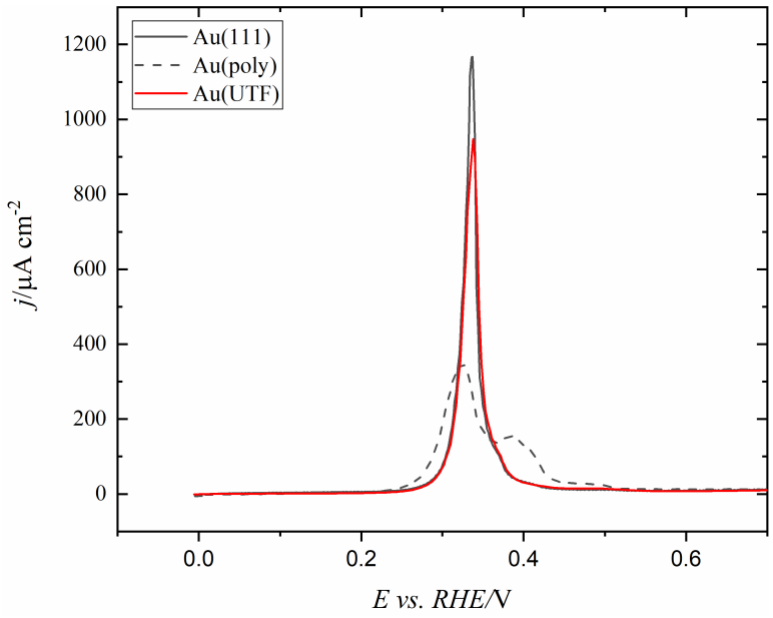

Figure 4.6 As stripping voltammograms for the different electrodes in 0.5 M H_2SO_4 + 10^{-5} M As (III). The electrode potential was held for 5 minutes at 0 V vs RHE. The scan rate is 50 mV s^{-1}.

Table 4-2 Summary of the main characteristics of the stripping peaks obtained after the deposition of As on the different Au electrodes in 0.5 M H_2SO_4 + 10^{-5} M As(III)

Electrode	Stripping peak potential	Full Width Half Max	Total Stripping Charge Density
	V vs. RHE	V vs. RHE	μC cm^{-2}
Au(111)	0.337	0.0155	589
Au(poly)	0.324	0.0480	541
Au(UTF)	0.338	0.0206	570

4.4.2 Au(UTF) thin film calibration curve

The standard additions method was used to detect trace As (III) in 0.5 M H_2SO_4 and the linear range was determined to be between 2.5 and 50 μg L^{-1} showing the capability to detect at and below the MCL of 10 μg L^{-1}. For reference, the statistical limit of detection was

0.0065 µg L^{-1}. The blue curve in Figure 4.7A is the baseline in 0.5 M sulfuric acid. There is a peak near 0.55 V in the baseline that has been observed on other Au(111) surfaces,[55] which disappears upon addition of As (III) even in small concentrations. At concentrations between 2.5 and 17.5 µg L^{-1} the peak is quite broad beginning near 0.25 V and ends near 0.6 V (Fig. 4.7A). However, at 50 µg L^{-1} the current increases sharply at 0.25 presenting a peak at 0.35 with a shoulder that ends near 0.6 V. The 100 µg L^{-1} LSV follows a similar peak shape as the 50 µg L^{-1} concentration, however with a larger increase in the peak area at 0.35 V than in the broad region that the lower concentration analysis had. This peak shape changes with concentration impacted the linearity when plotting the peak area vs. the concentration and resulted in an adjusted R^2 of 0.983 between 2.5 and 50 µg L^{-1} (Fig. 4.7B). Additionally, the R^2 value is increased to 0.998 between 2.5 and 17.5 µg L^{-1} As (III) (Fig. S6) showing higher linearity within ± 7.5 µg L^{-1} of the 10 µg L^{-1} MCL. Zhang et. al [60] have shown R^2 values of 0.991 and 0.990 with bulk Au and 5 nm Au nanoparticle electrodes between 0.75 and 7.5 µg L^{-1}. As shown in the voltammetric profiles of the single crystal electrodes, the region above 0.3 V should be related to the stripping of the As UPD. Since the Au(111) electrode does not show any characteristic peak in this region, the signal appearing for low concentrations should be related to the presence of defects on the surface, mainly composed of (110) and (100) steps. Those sites are generally more reactive and thus, they are occupied in the early stages of the deposition, giving rise to the formation of a wide wave.

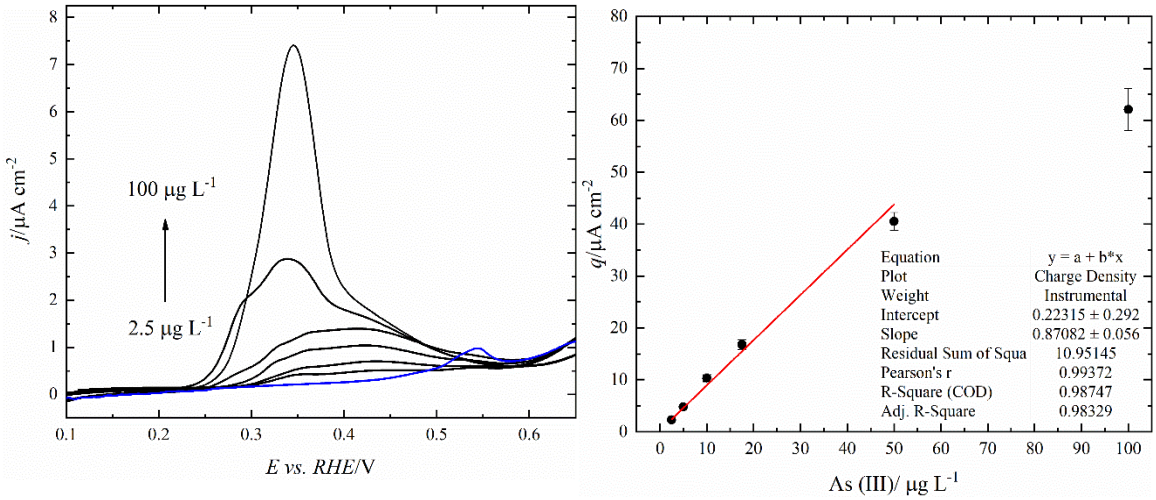

Figure 4.7 Linear Stripping voltammetry analysis curves of baseline 0.5 M H_2SO_4 and standard additions between 2.5 and 100 µg L^{-1} of As (III) solution, B) Calibration curve of charge density calculated from the area under the curve and a linear regression curve for data between 2.5 and 50 µg L^{-1}.

4.5 Conclusions

The results of this study show that the Au(111) single crystal surface has the highest sensitivity and selectivity for As (III) stripping analysis and can be implemented as an optimized sensing electrode through the use of ultraflat Au(111) texture thin films for trace As (III) detection in water. The deposition and stripping process was investigated using single crystal model electrodes and QCM. Cyclic voltammetry using the Au(Poly) surface with high concentrations of As (III) in solution showed that As (III) redox has a complex deposition process, is kinetically controlled, and the oxidation process was dependent on the stability of the adlayers formed during deposition. [128] Deposition on the basal plane surfaces showed that there were two peaks above 0 V which corresponded to the first and second adlayer and had varying peak potentials with each surface orientation. Stripping of As from the basal plane surfaces showed that the Au(111) model electrode had the highest sensitivity and selectivity as evidenced by having the highest maximum peak current compared to the

other surfaces and a single stripping peak while the other surfaces had multiple peaks which were spread out along a broader potential region. Electrochemical QCM data showed that the deposition of As (III) onto the Au surface occurs in multiple layers and for each As atom adsorbed approximately two water molecules are displaced from the surface. The QCM also showed that the stripping of the layers returns the surface to the original state without restructuring or irreversible adsorption of As onto the Au surface. Ultraflat Au(111) thin films were then compared to the Au(111) and Au(Poly) electrodes, which found that the Au(UTF)s preformed highly similar to the Au(111) model electrode for As (III) stripping during LSV analysis. Finally, the Au(UTF) was used to detect linearly between 2.5 and 50 µg L^{-1} As (III) in ultrapure water with 0.5 M H_2SO_4 supporting electrolyte and found a theoretical limit of detection of 0.0065 µg L^{-1}. This work provides a single crystal model study of the effects of surface structure on electrochemical As (III) detection at Au surfaces and applies the findings by implementing the benefits of the Au(111) surface in ultraflat Au(111) thin films, which can provide high sensitivity and selectivity. Note that single crystal-like detection capabilities are achievable with minimal (~2µg) quantities of Au on glass substrates, thus in an economically viable electrode. The use ofAu(111) texture thin film electrodes with sub-nanometer roughness, may impact many other areas of electroanalysis as Au electrodes are very commonly used for a large variety of electrochemical investigations.

4.6 Acknowledgments

This material is based upon work supported by the National Science Foundation (NSF) Graduate Research Fellowship Program (GRFP) under Grant No. (DGE-1418062), University of New Mexico Center for Water and the Environment, (NSF CREST Grant

Number 1345169 and 1914490) and the Center for Micro-Engineered Materials (NSF MRI Award 1828731, We would like to thank NanoEarth's Multicultural and Underserved Nanoscience Initiative and the Nanoscale Characterization and Fabrication Laboratory at Virginia Tech (NSF ECCS 1542100 and ECCS 2025151) along with Ya Peng Yu for their aid in providing the SEM, EBSD and pole figure data for the Au(UTF) thin films. Thanks to the Fulbright U.S. Scholar Senior Research Award to Spain for Professor Cerrato to collaborate with the Universidad de Alicante. The authors would also like to thank all our colleagues at the Universidad de Alicante for their guidance, generosity and friendship. Any opinion, findings, and conclusions or recommendations expressed in this material are those of the authors(s) and do not necessarily reflect the views of the National Science Foundation.

4.7 References

Uncategorized References

(1) Ng, J. C.; Wang, J.; Shraim, A. A global health problem caused by arsenic

from natural sources. Pergamon: Chemosphere, 2003.
(2) Shankar, S.; Shanker, U.; Shikha. Arsenic contamination of groundwater: a review of sources, prevalence, health risks, and strategies for mitigation. *ScientificWorldJournal* **2014**, *2014*, 304524. DOI: 10.1155/2014/304524.
(3) Bencko, V.; Yan Li Foong, F. The history of arsenical pesticides and health risks related to the use of Agent Blue. *Ann Agric Environ Med* **2017**, *24* (2), 312-316. DOI: 10.26444/aaem/74715 From NLM.
(4) Berg, M. M. Arsenic contamination of groundwater and drinking water in Vietnam: a human health threat. *Environ. Sci. Technol.* **2001**, *35* (13), 2621-2626. DOI: https://doi.org/10.1021/es010027y.
(5) Rahman, A. H. S. E. O. L. M. Contamination of drinking-water by arsenic in Bangladesh: a public health emergency. *Bulletin of the World Health Organization* **2000**, *78*.
(6) USEPA. Priority Pollutant List. 2014; Vol. 40 CFR Part 423, Appendix A.
(7) Kurttio, P.; Hirose , A.; Fawell, J. WHO Guidelines for Drinking-water Quality. World Health Organization: 2010.
(8) Organization, W. H. *Exposure to Arsenic: A Major Public Health Concern*; 2010.
(9) Rahaman, M. S.; Rahman, M. M.; Mise, N.; Sikder, M. T.; Ichihara, G.; Uddin, M. K.; Kurasaki, M.; Ichihara, S. Environmental arsenic exposure and its contribution to human diseases, toxicity mechanism and management. *Environmental Pollution* **2021**, *289*, 117940. DOI: https://doi.org/10.1016/j.envpol.2021.117940.
(10) Podgorski, J. Global threat of arsenic in groundwater. *Science* **2020**, *368* (6493), 845-850. DOI: https://doi.org/10.1126/science.aba1510.
(11) Simmler, M. Reductive solubilization of arsenic in a mining-impacted river floodplain: Influence of soil properties and temperature. *Environ. Pollut.* **2017**, *231*, 722-731. From http://worldcat.org /z-wcorg/.
(12) Blake, J. M.; Avasarala, S.; Artyushkova, K.; Ali, A.-M. S.; Brearley, A. J.; Shuey, C.; Robinson, W. P.; Nez, C.; Bill, S.; Lewis, J.; et al. Elevated Concentrations of U and Co-occurring Metals in Abandoned Mine Wastes in a Northeastern Arizona Native American Community. *Environ. Sci. Technol.* **2015**, *49* (14), 8506-8514. DOI: https://doi.org/10.1021/acs.est.5b01408.
(13) Smedley, P. L. K., D.G. . A review of the source, behaviour and distribution of arsenic in natural waters. *Appl. Geochem.* **2002**, *17*, 517-568. DOI: https://doi.org/10.1016/S0883-2927(02)00018-5.
(14) Basu, A.; Saha, D.; Saha, R.; Ghosh, T.; Saha, B. A review on sources, toxicity and remediation technologies for removing arsenic from drinking water. *Res. Chem. Intermed.* **2014**, *40* (2), 447-485, Article. DOI: https://doi.org/10.1007/s11164-012-1000-4.
(15) Raqib, R.; Ahmed, S.; Sultana, R.; Wagatsuma, Y.; Mondal, D.; Hoque, A. W.; Nermell, B.; Yunus, M.; Roy, S.; Persson, L. A. Effects of in utero arsenic exposure on child immunity and morbidity in rural Bangladesh. *Toxicology letters* **2009**, *185* (3), 197-202.

(16) Komorowicz Izabela, I.; Baralkiewicz, D. Arsenic and its speciation in water samples by high performance liquid chromatography inductively coupled plasma mass spectrometry--last decade review. *Talanta* **2011**, *84* (2), 247-261. From http://worldcat.org /z-wcorg/.
(17) Profumo, A.; Merli, D.; Pesavento, M. Voltammetric determination of inorganic As(III) and total inorganic As in natural waters. *Analytica Chimica Acta* **2005**, *539* (1), 245-250. DOI: https://doi.org/10.1016/j.aca.2005.02.062.
(18) Song, Y.; Swain, G. M. Development of a Method for Total Inorganic Arsenic Analysis Using Anodic Stripping Voltammetry and a Au-Coated, Diamond Thin-Film Electrode. *Analytical Chemistry* **2007**, *79* (6), 2412-2420. DOI: 10.1021/ac061543f.
(19) Henry, F. T. Determination of trace level arsenic (III), arsenic(V), and total inorganic arsenic by differential pulse polarography. *Anal. Chem.* **1979**, *51*, 215-218. From http://worldcat.org /z-wcorg/.
(20) USEPA. METHOD 7063: ARSENIC IN AQUEOUS SAMPLES AND EXTRACTS

BY ANODIC STRIPPING VOLTAMMETRY (ASV). 1996.
(21) Dai, X.; Nekrassova, O.; Hyde, M. E.; Compton, R. G. Anodic Stripping Voltammetry of Arsenic(III) Using Gold Nanoparticle-Modified Electrodes. *Anal. Chem.* **2004**, *76*, 5924-5929.
(22) Dai, X.; Compton, R. G. Determination of Copper in the Presence of Various Amounts of Arsenic withL-Cysteine Modified Gold Electrodes. *Electroanalysis* **2005**, *17* (20), 1835-1840. DOI: 10.1002/elan.200503310.
(23) Jia, Z.; Simm, A. O.; Dai, X.; Compton, R. G. The electrochemical reaction mechanism of arsenic deposition on an Au(111) electrode. *J. Electroanal. Chem.* **2006**, *587* (2), 247-253. DOI: https://doi.org/10.1016/j.jelechem.2005.11.017.
(24) Zhang, Y.; Li, D.; Compton, R. G. Arsenic (III) Detection with Underpotential Deposition and Anodic Stripping Voltammetry. *ChemElectroChem* **2021**, *8* (19), 3707-3715. DOI: https://doi.org/10.1002/celc.202101022.
(25) Stanković, A.; Kajinić, Ž.; Turkalj, J. V.; Romić, Ž.; Sikirić, M. D.; Asserghine, A.; Nagy, G.; Medvidović-Kosanović, M. Voltammetric Determination of Arsenic with Modified Glassy Carbon Electrode. *Electroanalysis* **2020**, *32* (5), 1043-1051. DOI: 10.1002/elan.201900666.
(26) Yamada, D.; Ivandini, T. A.; Komatsu, M.; Fujishima, A.; Einaga, Y. Anodic stripping voltammetry of inorganic species of As3+ and As5+ at gold-modified boron doped diamond electrodes. *Journal of Electroanalytical Chemistry* **2008**, *615* (2), 145-153. DOI: https://doi.org/10.1016/j.jelechem.2007.12.004.
(27) Bu, L.; Liu, J.; Xie, Q.; Yao, S. Anodic stripping voltammetric analysis of trace arsenic(III) enhanced by mild hydrogen-evolution at a bimetallic Au–Pt nanoparticle modified glassy carbon electrode. *Electrochemistry Communications* **2015**, *59*, 28-31. DOI: https://doi.org/10.1016/j.elecom.2015.06.015.
(28) Han, D.-D.; Li, S.-S.; Guo, Z.; Chen, X.; Liu, J.-H.; Huang, X.-J. Shape dependent stripping behavior of Au nanoparticles toward arsenic detection: evidence of enhanced sensitivity on the Au (111) facet. *RSC Adv.* **2016**, *6* (36), 30337-30344. DOI: https://doi.org/10.1039/c5ra27778g.
(29) Babar, N. U.; Joya, K. S.; Tayyab, M. A.; Ashiq, M. N.; Sohail, M. Highly Sensitive and Selective Detection of Arsenic Using Electrogenerated Nanotextured Gold Assemblage. *ACS Omega* **2019**, *4* (9), 13645-13657. DOI: https://doi.org/10.1021/acsomega.9b00807.

(30) Kanido Camerun Kastro, M. J. S., Hwakyeung Jeong, and Joongwon Kim. Effect of Nanostructures of Au Electrodes on the Electrochemical Detection of As. *J. Electrochem. Sci. Technol* **2019**. DOI: https://doi.org/10.5229/JECST.2019.10.2.206.
(31) Pourbaix, M. Atlas of electrochemical equilibria in aqueous solution. *Corrosion Science* **1966**, *10*, 343.
(32) Vanysek, P. Electrochemical series. *CRC handbook of chemistry and physics* **2000**, *8*.
(33) Karimov, K. A.; Rogozhnikov, D. A.; Kuzas, E. A.; Shoppert, A. A. Leaching Kinetics of Arsenic Sulfide-Containing Materials by Copper Sulfate Solution. *Metals* **2019**, *10* (1). DOI: 10.3390/met10010007.
(34) Shishin, D.; Jak, E. Critical assessment and thermodynamic modeling of the Cu-As system. *Calphad* **2018**, *60*, 134-143. DOI: https://doi.org/10.1016/j.calphad.2017.12.005.
(35) Kishioka, S.-y.; Nishino, J.; Sakaguchi, H. Fabrication of Stable, Highly Flat Gold Film Electrodes with an Effective Thickness on the Order of 10 nm. *Analytical Chemistry* **2007**, *79* (17), 6851-6856. DOI: 10.1021/ac070603u.
(36) Kim, M.; Ha, W.-J.; Anh, J.-W.; Kim, H.-S.; Park, S.-W.; Lee, D. Fabrication of nanoporous gold thin films on silicon substrate by multilayer deposition of Au and Ag. *J. Alloys Compd.* **2009**, *484*, 28-32. DOI: 10.1016/j.jallcom.2009.05.067.
(37) WHO. *Arsenic Fact Sheet*. World Health Organization, 2010. https://www.who.int/news-room/fact-sheets/detail/arsenic (accessed 2022 07/21).
(38) Weber, F.-A.; Hofacker, A. F.; Voegelin, A.; Kretzschmar, R. Temperature Dependence and Coupling of Iron and Arsenic Reduction and Release during Flooding of a Contaminated Soil. *Environ. Sci. Technol.* **2010**, *44* (1), 116-122. DOI: 10.1021/es902100h.
(39) Neil, C. W. Water Chemistry Impacts on Arsenic Mobilization from Arsenopyrite Dissolution and Secondary Mineral Precipitation: Implications for Managed Aquifer Recharge. *Environ. Sci. Technol.* **2014**, *48* (8), 4395-4405. From http://worldcat.org /z-wcorg/.
(40) Shi, Z.; Hu, S.; Lin, J.; Liu, T.; Li, X.; Li, F. Quantifying Microbially Mediated Kinetics of Ferrihydrite Transformation and Arsenic Reduction: Role of the Arsenate-Reducing Gene Expression Pattern. *Environ. Sci. Technol.* **2020**, *54* (11), 6621-6631. DOI: 10.1021/acs.est.9b07137.
(41) Wilkin, R. T.; Ford, R. G.; Costantino, L. M.; Ross, R. R.; Beak, D. G.; Scheckel, K. G. Thioarsenite Detection and Implications for Arsenic Transport in Groundwater. *Environ. Sci. Technol.* **2019**, *53* (20), 11684-11693. DOI: 10.1021/acs.est.9b04478.
(42) Renock, D.; Voorhis, J. Electrochemical Investigation of Arsenic Redox Processes on Pyrite. *Environ. Sci. Technol.* **2017**, *51* (7), 3733-3741. DOI: 10.1021/acs.est.6b06018.
(43) Hung, D. Q.; Nekrassova, O.; Compton, R. G. Analytical methods for inorganic arsenic in water: a review. *Talanta* **2004**, *64* (2), 269-277, Periodical. From EBSCOhost edsbl.
(44) Reid, K. D.; Goff, F.; Counce, D. A. Arsenic concentration and mass flow rate in natural waters of the Valles caldera and Jemez Mountains region, New Mexico. *N. M. Geol.* **2003**, *25* (3), 75-82.
(45) Das Joyati, J.; Sarkar, P.; Panda, J.; Pal, P. Low-cost field test kits for arsenic detection in water. *J. Environ. Sci. Health., A* **2014**, *49* (1), 108-115. DOI: https://doi.org/10.1080/10934529.2013.824764.
(46) Metrohm. *scTRACE Gold*. 2013. https://www.metrohm.com/en-us/products-overview/61258000 (accessed.
(47) *Determination of arsenic in water with the scTRACE Gold*; 416; Metrohm.

(48) Bullen, J. C.; Torres-Huerta, A.; Salaun, P.; Watson, J. S.; Majumdar, S.; Vilar, R.; Weiss, D. J. Portable and rapid arsenic speciation in synthetic and natural waters by an As(V)-selective chemisorbent, validated against anodic stripping voltammetry. *Water Res* **2020**, *175*, 115650. DOI: https://doi.org/10.1016/j.watres.2020.115650.
(49) Cox, J. A.; Rutkowska, I. A.; Kulesza, P. J. Critical Review—Electrocatalytic Sensors for Arsenic Oxo Species. *J. Electrochem. Soc.* **2020**, *167* (3), 037565. DOI: https://doi.org/10.1149/1945-7111/ab697d.
(50) Welch Christine, M. C.; Compton, R. G. The use of nanoparticles in electroanalysis: a review. *Anal. Bioanal. Chem.* *384* (3), 601-619. From http://worldcat.org /z-wcorg/.
(51) Burke, L. D.; Nugent, P. F. The electrochemistry of gold: I the redox behaviour of the metal in aqueous media. *Gold Bull.* **1997**, *30* (2), 43-53.
(52) Nunez-Bajo, E.; Blanco-Lopez, M. C.; Costa-Garcia, A.; Fernandez-Abedul, M. T. Electrogeneration of Gold Nanoparticles on Porous-Carbon Paper-Based Electrodes and Application to Inorganic Arsenic Analysis in White Wines by Chronoamperometric Stripping. *Anal. Chem.* **2017**, *89* (12), 6415-6423. DOI: https://doi.org/10.1021/acs.analchem.7b00144.
(53) Gu, T.; Bu, L.; Huang, Z.; Liu, Y.; Tang, Z.; Liu, Y.; Huang, S.; Xie, Q.; Yao, S.; Tu, X.; et al. Dual-signal anodic stripping voltammetric determination of trace arsenic(III) at a glassy carbon electrode modified with internal-electrolysis deposited gold nanoparticles. *Electrochem. Commun.* **2013**, *33*, 43-46. DOI: https://doi.org/10.1016/j.elecom.2013.04.019.
(54) Huang, J.-F.; Chen, H.-H. Gold-nanoparticle-embedded nafion composite modified on glassy carbon electrode for highly selective detection of arsenic(III). *Talanta* **2013**, *116*, 852-859, Article. DOI: https://doi.org/10.1016/j.talanta.2013.07.063.
(55) Jena Bikash Kumar, B. K.; Raj, C. R. Gold nanoelectrode ensembles for the simultaneous electrochemical detection of ultratrace arsenic, mercury, and copper. *Anal. Chem.* **2008**, *80* (13), 4836-4844. From http://worldcat.org /z-wcorg/.
(56) Dai Xuan, X.; Wildgoose, G. G.; Salter, C.; Crossley, A.; Compton, R. G. Electroanalysis using macro-, micro-, and nanochemical architectures on electrode surfaces. Bulk surface modification of glassy carbon microspheres with gold nanoparticles and their electrical wiring using carbon nanotubes. *Anal. Chem.* **2006**, *78* (17), 6102-6108. DOI: https://doi.org/10.1021/ac060582o.
(57) Song, Y.; Swain, G. M. Total inorganic arsenic detection in real water samples using anodic stripping voltammetry and a gold-coated diamond thin-film electrode. *Anal. Chim. Acta.* **2007**, *593* (1), 7-12. DOI: 10.1016/j.aca.2007.04.033.
(58) Viltchinskaia E. A., Z. L. L., Garcia D.M., Santos P.F. Simultaneous determination of Mercury and Arsenic by Anodic Stripping Voltammetry. *Electroanalysis* **1996**, *9*, 633 - 640.
(59) Wu, J.; Yang, M.; Xiao, J.; Fu, X.; Jin, J.; Li, L.; Chang, W.; Xie, C. Gold Nanoparticle Dropped Titania Microsphere Hybrids as an Enhanced Sensitive Material for Stripping Voltammetry Determination of As (III). *J. Electrochem. Soc.* **2013**, *160* (11), B225-B230. DOI: 10.1149/2.103311jes.
(60) Kato, D.; Kamata, T.; Kato, D.; Yanagisawa, H.; Niwa, O. Au Nanoparticle-Embedded Carbon Films for Electrochemical As(3+) Detection with High Sensitivity and Stability. *Anal. Chem.* **2016**, *88* (5), 2944-2951. DOI: 10.1021/acs.analchem.6b00136.
(61) Kumar, S. A.; Wang, S.-F.; Chang, Y.-T. Poly(BCB)/Au-nanoparticles hybrid film modified electrode: Preparation, characterization and its application as a non-enzymatic

sensor. *Thin Solid Films* **2010**, *518* (20), 5832-5838. DOI: https://doi.org/10.1016/j.tsf.2010.05.076.
(62) Mehran, Q. M.; Fazal, M. A.; Bushroa, A. R.; Rubaiee, S. A Critical Review on Physical Vapor Deposition Coatings Applied on Different Engine Components. *Crit. Rev. Solid State Mater. Sci.* **2017**, *43* (2), 158-175. DOI: 10.1080/10408436.2017.1320648.
(63) Shahidi, S.; Moazzenchi, B.; Ghoranneviss, M. A review-application of physical vapor deposition (PVD) and related methods in the textile industry. *Eur. Phys. J. Appl. Phys.* **2015**, *71* (3), 31302. DOI: 10.1051/epjap/2015140439.
(64) Mo, A. K.; Brown, V. L.; Rugg, B. K.; DeVore, T. C.; Meyer, H. M.; Hu, X.; Hughes, W. C.; Augustine, B. H. Understanding the Mechanism of Solvent-Mediated Adhesion of Vacuum Deposited Au and Pt Thin Films onto PMMA Substrates. *Adv. Funct. Mater* **2013**, *23* (11), 1431-1439. DOI: 10.1002/adfm.201201955.
(65) Tanami, S.; Ichida, D.; Hashimoto, S.; Seo, H.; Yamashita, D.; Itagaki, N.; Koga, K.; Shiratani, M. Low temperature rapid formation of Au-induced crystalline Ge films using sputtering deposition. *Thin Solid Films* **2017**, *641*, 59-64. DOI: 10.1016/j.tsf.2017.02.067.
(66) Kim, K.; Park, J.; Kim, H.; Jung, G. Y.; Kim, M.-G. Solid-Phase Photocatalysts: Physical Vapor Deposition of Au Nanoislands on Porous TiO2 Films for Millimolar H2O2 Production within a Few Minutes. *ACS Catal.* **2019**, *9* (10), 9206-9211. DOI: 10.1021/acscatal.9b02269.
(67) van der Zalm, J.; Chen, S.; Huang, W.; Chen, A. Review—Recent Advances in the Development of Nanoporous Au for Sensing Applications. *J. Electrochem. Soc.* **2020**, *167* (3), 037532. DOI: https://doi.org/10.1149/1945-7111/ab64c0.
(68) Jiang, J.; Wang, C. Review—Electrolytic Metal Atoms Enabled Manufacturing of Nanostructured Sensor Electrodes. *J. Electrochem. Soc.* **2020**, *167* (3), 037521. DOI: 10.1149/2.0212003jes.
(69) Thangphatthanarungruang, J.; Lomae, A.; Chailapakul, O.; Chaiyo, S.; Siangproh, W. A Low-cost Paper-based Diamond Electrode for Trace Copper Analysis at On-site Environmental Area. *Electroanalysis* **2020**, *33* (1), 226-232. DOI: https://doi.org/10.1002/elan.202060305.
(70) Pringkasemchai, A.; Hoshyargar, F.; Lertanantawong, B.; O'Mullane, A. P. Lightweight ITO Electrodes Decorated with Gold Nanostructures for Electrochemical Applications. *Electroanalysis* **2019**, *31* (11), 2095-2102. DOI: 10.1002/elan.201900152.
(71) Devi, N. R.; Sasidharan, M.; Sundramoorthy, A. K. Gold Nanoparticles-Thiol-Functionalized Reduced Graphene Oxide Coated Electrochemical Sensor System for Selective Detection of Mercury Ion. *J. Electrochem. Soc.* **2018**, *165* (8), B3046-B3053. DOI: https://doi.org/10.1149/2.0081808jes.
(72) Carmo, M.; Linardi, M.; Poco, J. G. R. Characterization of nitric acid functionalized carbon black and its evaluation as electrocatalyst support for direct methanol fuel cell applications. *Appl. Catal. A Gen.* **2009**, *355*, 132-138, Article. DOI: 10.1016/j.apcata.2008.12.010 From EBSCOhost edselp.
(73) Prati, L.; Martra, G. New gold catalysts for liquid phase oxidation. *Gold Bull.* **1999**, *32* (3), 96-101. DOI: Doi 10.1007/Bf03216617.
(74) Blake, J. M.; Vore, C. L. D.; Avasarala, S.; Ali, A.-M.; Roldan, C.; Bowers, F.; Spilde, M. N.; Artyushkova, K.; Kirk, M. F.; Peterson, E.; et al. Uranium mobility and accumulation along the Rio

Paguate, Jackpile Mine in Laguna Pueblo, NM. *Environ. Sci. Process Impacts* **2017**, *19*, 605-621.
(75) Fischer, L. M.; Tenje, M.; Heiskanen, A. R.; Masuda, N.; Castillo, J.; Bentien, A.; Émneus, J.; Jakobsen, M. H.; Boisen, A. Gold cleaning methods for electrochemical detection applications. *Microelectron. Eng.* **2009**, *86* (4-6), 1282-1285. DOI: 10.1016/j.mee.2008.11.045.
(76) Palli, S.; R. Dey, S. Thermal stability of pulse electroplated gold films: SEM-EBSD studies. *Adv. Mater. Sci.* **2017**, *2* (1), 1-6. DOI: 10.15761/ams.1000118.
(77) Thompson, C. V. Structure Evolution During Processing of Polycrystalline Films. *Annu. Rev. Mater. Sci.* **2000**, *30* (1), 159, Article. DOI: 10.1146/annurev.matsci.30.1.159 From EBSCOhost bth.
(78) Wei, P.; Katmis, F.; Chang, C. Z.; Moodera, J. S. Induced Superconductivity and Engineered Josephson Tunneling Devices in Epitaxial (111)-Oriented Gold/Vanadium Heterostructures. *Nano Lett.* **2016**, *16* (4), 2714-2719. DOI: 10.1021/acs.nanolett.6b00361.
(79) Luo, X.; Morrin, A.; Killard, A. J.; Smyth, M. R. Application of Nanoparticles in Electrochemical Sensors and Biosensors. *Electroanalysis* **2006**, *18* (4), 319-326. DOI: 10.1002/elan.200503415.
(80) Feliu, J. M.; Fernandez-Vega, A.; Aldaz, A.; Clavilier, J. New observations of a structure sensitive electrochemical behaviour of irreversibly adsorbed arsenic and antimony from acidic solutions on Pt (111) and Pt (100) orientations. *J. Electroanal. Chem. Interfacial Electrochem.* **1988**, *256* (1), 149-163. DOI: https://doi.org/10.1016/0022-0728(88)85014-9.
(81) Ren, B.; Jones, L. A.; Chen, M.; Oppedisano, D. K.; Qiu, D.; Ippolito, S. J.; Bhargava, S. K. The Effect of Electrodeposition Parameters and Morphology on the Performance of Au Nanostructures for the Detection of As (III). *J. Electrochem. Soc.* **2017**, *164* (14), H1121-H1128. DOI: https://doi.org/10.1149/2.1261714jes.
(82) Forsberg, G.; Olaughlin, J. W.; Megargle, R. G.; Koirtyohann, S. R. Determination of arsenic by anodic stripping voltammetry and differential pulse anodic stripping voltammetry. *Anal. Chem.* **1975**, *47*, 1586-1592. DOI: https://doi.org/10.1021/ac60359a057.
(83) Copeland, T. K. Analytical applications of pulsed voltammetric stripping at thin film mercury electrodes. *Anal. Chem.* **1973**, *45*, 2171-2174. From http://worldcat.org /z-wcorg/.
(84) Kachoosangi, R. T.; Compton, R. G. Voltammetric determination of Chromium(VI) using a gold film modified carbon composite electrode. *Sens. Actuators B Chem.* **2013**, *178*, 555-562. DOI: 10.1016/j.snb.2012.12.122.
(85) Sikdar, S.; Kundu, M. A Review on Detection and Abatement of Heavy Metals. *ChemBioEng Rev.* **2017**, *5* (1), 18-29. DOI: https://doi.org/10.1002/cben.201700005.
(86) Ferguson, J. F.; Gavis, J. Review of the arsenic cycle in natural waters. *Water Res.* **1972**, *6*, 1259-1274, Article. DOI: https://doi.org/10.1016/0043-1354(72)90052-8.
(87) Korte, N. E. Q., Fernando. A review of arsenic (III) in groundwater. *Crit. rev. environ. control* **1991**, *21*, 1-39. DOI: https://doi.org/10.1080/10643389109388408.
(88) Stuckey, Jason W.; Schaefer, Michael V.; Kocar, Benjamin D.; Benner, Shawn G.; Fendorf, S. Arsenic release metabolically limited to permanently water-saturated soil in Mekong Delta. *Nat. Geosci.* **2016**, *9* (1), 70-76. DOI: https://doi.org/10.1038/ngeo2589.
(89) LeMonte, J. J.; Stuckey, J. W.; Sanchez, J. Z.; Tappero, R.; Rinklebe, J.; Sparks, D. L. Sea Level Rise Induced Arsenic Release from Historically Contaminated Coastal Soils. *Environ. Sci. Technol.* **2017**, *51* (11), 5913-5922. DOI: https://doi.org/10.1021/acs.est.6b06152.

(90) deLemos, J. L.; Bostick, B. C.; Renshaw, C. E.; StÜrup, S.; Feng, X. Landfill-Stimulated Iron Reduction and Arsenic Release at the Coakley Superfund Site (NH). *Environ. Sci. Technol.* **2006**, *40* (1), 67-73. DOI: https://doi.org/10.1021/es051054h.
(91) He, C.; Tao, M.; Zhang, C.; He, Y.; Xu, W.; Liu, Y.; Zhu, W. Microelectrode-Based Electrochemical Sensing Technology for in Vivo Detection of Dopamine: Recent Developments and Future Prospects. *Crit. Rev. Environ. Control* **2022**, *52*, 544-554, Periodical. DOI: https://doi.org/10.1080/10408347.2020.1811946.
(92) Fleischmann, M.; Pons, S. The behavior of microelectrodes. *Anal. Chem.* **1987**, *59* (24), 1391A-1399A. DOI: https://doi.org/10.1021/ac00151a001.
(93) Compton, R. G.; Wildgoose, G. G.; Rees, N. V.; Streeter, I.; Baron, R. Design, fabrication, characterisation and application of nanoelectrode arrays. *Chem. Phys. Lett.* **2008**, *459* (1), 1-17. DOI: https://doi.org/10.1016/j.cplett.2008.03.095.
(94) Borrill, A. J.; Reily, N. E.; Macpherson, J. V. Addressing the practicalities of anodic stripping voltammetry for heavy metal detection: a tutorial review. *Analyst* **2019**, *144* (23), 6834-6849. DOI: https://doi.org/10.1039/c9an01437c.
(95) Buffa, A.; Mandler, D. Arsenic(III) detection in water by flow-through carbon nanotube membrane decorated by gold nanoparticles. *Electrochim. Acta* **2019**, *318*, 496-503. DOI: https://doi.org/10.1016/j.electacta.2019.06.114.
(96) Garcia-Gonzalez, R.; Fernandez-Abedul, M. T.; Costa-Garcia, A. Nafion(R) modified-screen printed gold electrodes and their carbon nanostructuration for electrochemical sensors applications. *Talanta* **2013**, *107*, 376-381. DOI: https://doi.org/10.1016/j.talanta.2013.01.034.
(97) Hamilton, E. T. W. J.; Florence, T. M. Determination of arsenic and antimony in electrolytic copper by anodic stripping voltammetry at a gold film electrode. *Anal. Chim. Acta* **1980**, *119* (2), 225-233, Article. DOI: https://doi.org/10.1016/S0003-2670(01)93621-9.
(98) Casuse, T. Q.; Benavidez, A.; Plumley, J. B.; Tsui, L.-k.; Ali, A.-M.; Cerrato, J. M.; Garzon, F. H. DC Sputtered Ultralow Loading Gold Nanofilm Electrodes for Detection of As (III) in Water. *ECS Sens. Plus* **2022**, *1* (1), 014602. DOI: https://doi.org/10.1149/2754-2726/ac6d67.
(99) Udayan, A. P. M.; Kachwala, B.; Karthikeyan, K. G.; Gunasekaran, S. Ultrathin quasi-hexagonal gold nanostructures for sensing arsenic in tap water. *RSC Adv.* **2020**, *10* (34), 20211-20221. DOI: https://doi.org/10.1039/d0ra02750b.
(100) Jiang, X.; Ma, J.; Jiang, G.; Xu, M.; Huang, X.; Gao, G.; Dai, X. Preparation of Gold Nanoplates Using Ortho Carbonyl Compounds as Capping Agents for Electrochemical Sensing of Lead Ions. *Nanoscale Res. Lett.* **2021**, *16* (1), 57. DOI: https://doi.org/10.1186/s11671-021-03521-2.
(101) Kuzume, A.; Herrero, E.; Feliu, J. M. Oxygen reduction on stepped platinum surfaces in acidic media. *J. Electroanal. Chem.* **2007**, *599* (2), 333-343. DOI: https://doi.org/10.1016/j.jelechem.2006.05.006.
(102) Rizo, R.; Pastor, E.; Koper, M. T. M. CO electrooxidation on Sn-modified Pt single crystals in acid media. *J. Electroanal. Chem.* **2017**, *800*, 32-38, Article. DOI: https://doi.org/10.1016/j.jelechem.2016.10.014.
(103) Fang, Y.; Ding, S. Y.; Zhang, M.; Steinmann, S. N.; Hu, R.; Mao, B. W.; Feliu, J. M.; Tian, Z. Q. Revisiting the Atomistic Structures at the Interface of Au(111) Electrode-Sulfuric Acid Solution. *J. Am. Chem. Soc.* **2020**, *142* (20), 9439-9446. DOI: https://doi.org/10.1021/jacs.0c02639.

(104) Gisbert-González, J. M.; Oliver-Pardo, M. V.; Sarabia, F. J.; Climent, V.; Feliu, J. M.; Herrero, E. On the behavior of CTAB/CTAOH adlayers on gold single crystal surfaces. *Electrochim. Acta* **2021**, *391*. DOI: https://doi.org/10.1016/j.electacta.2021.138947.
(105) Rodes, A.; Herrero, E.; Feliu, J. M.; Aldaz, A. Structure sensitivity of irreversibly adsorbed tin on gold single-crystal electrodes in acid media. *J. Chem. Soc. Faraday Trans.* **1996**, *92* (20), 3769-3776, 10.1039/FT9969203769. DOI: https://doi.org/10.1039/FT9969203769.
(106) Hamelin, A. Underpotential deposition of lead on single crystal faces of gold: Part I. The influence of crystallographic orientation of the substrate. *J. Electroanal. Chem. Interfacial Electrochem.* **1984**, *165* (1), 167-180. DOI: https://doi.org/10.1016/S0022-0728(84)80095-9.
(107) Hamelin, A.; Lipkowski, J. Underpotential deposition of lead on gold single crystal faces: Part II. General discussion. *J. Electroanal. Chem. Interfacial Electrochem.* **1984**, *171* (1), 317-330. DOI: https://doi.org/10.1016/0022-0728(84)80123-0.
(108) Zhang, Y.; Li, D.; Compton, R. G. Arsenic (III) detection with underpotential deposition on gold. *J. Electroanal. Chem.* **2022**, *909*. DOI: https://doi.org/10.1016/j.jelechem.2022.116154.
(109) Lebedeva, N. P.; Rodes, A.; Feliu, J. M.; Koper, M. T. M.; van Santen, R. A. Role of Crystalline Defects in Electrocatalysis: CO Adsorption and Oxidation on Stepped Platinum Electrodes As Studied by in situ Infrared Spectroscopy. *J. Phys. Chem. B* **2002**, *106* (38), 9863-9872. DOI: https://doi.org/10.1021/jp0203806.
(110) Salinas, S.; Mosquera, N.; Luis, Y.; Emerson, C.; Germán, Y.; Edgar, G. Surface Plasmon Resonance Nanosensor for the Detection of Arsenic in Water. *Sens. Transducers* **2014**, *183* (12), 97-102, article. DOI: https://doaj.org/article/4f3c21b9962f414cae3b42938e984c77.
(111) Bentley, C. L.; Kang, M.; Unwin, P. R. Nanoscale Surface Structure–Activity in Electrochemistry and Electrocatalysis. *J. Am. Chem. Soc.* **2019**, *141* (6), 2179-2193. DOI: https://doi.org/10.1021/jacs.8b09828.
(112) Clavilier, J.; Faure, R.; Guinet, G.; Durand, R. Preparation of monocrystalline Pt microelectrodes and electrochemical study of the plane surfaces cut in the direction of the {111} and {110} planes. *J. Electroanal. Chem. Interfacial Electrochem.* **1980**, *107* (1), 205-209. DOI: https://doi.org/10.1016/S0022-0728(79)80022-4.
(113) Technologies, P. *Ultra-Flat Gold Surfaces*. https://www.platypustech.com/gold-thin-films/ultra-flat-gold-films (accessed 10/25/2021).
(114) Hamelin, A. Cyclic voltammetry at gold single-crystal surfaces. Part 1. Behaviour at low-index faces. *J. Electroanaly. Chem.* **1996**, *407* (1/2), 1-11. DOI: https://doi.org/10.1016/0022-0728(95)04499-X.
(115) Dinan, T. E.; Jou, W. F.; Cheh, H. Y. Arsenic Deposition onto a Gold Substrate. *J. Electrochem. Soc.* **1989**, *136* (11), 3284-3287. DOI: https://doi.org/10.1149/1.2096439.
(116) Orozco, J.; Fernández-Sánchez, C.; Jiménez-Jorquera, C. Underpotential Deposition−Anodic Stripping Voltammetric Detection of Copper at Gold Nanoparticle-Modified Ultramicroelectrode Arrays. *Environ. Sci. Technol.* **2008**, *42* (13), 4877-4882. DOI: https://doi.org/10.1021/es8005964.
(117) Desimoni, E.; Palmisano, F.; Sabbatini, L. Simultaneous determination of tin and lead at the parts-per-billion level by coupling differential pulse anodic stripping voltammetry with

a matrix exchange method. *Anal. Chem.* **1980**, *52* (12), 1889-1892. DOI: https://doi.org/10.1021/ac50062a026.
(118) Villegas, I.; Stickney, J. L. PRELIMINARY STUDIES OF GAAS DEPOSITION ON AU(100), (110), AND (111) SURFACES BY ELECTROCHEMICAL ATOMIC LAYER EPITAXY. *J. Electrochem. Soc.* **1992**, *139* (3), 686-694. DOI: https://doi.org/10.1149/1.2069285.
(119) Blum, L.; Huckaby, D. A. Underpotential deposition of Cu on Au(111): implications of the HB model. *J. Electroanal. Chem.* **1994**, *375* (1), 69-77. DOI: https://doi.org/10.1016/0022-0728(94)03336-6.

Chapter 5. Electrochemical Redox of Arsenic (III) and Cu (II) Mixtures with Ultraflat Au(111) Thin Films in Water

Tybur Q. Casuse-Driovínto,[1,2] Angelica Benavidez,[2] Noah Jemison,[2] José M. Cerrato,[1,2] Juan Feliu,[3] Fernando H. Garzon,[2z]

[z] Corresponding email addresses: garzon@unm.edu

Telephone: (001) 505-934-6971

Fax: (001) 505-277-1988

[1] Gerald May Department of Civil, Construction & Environmental Engineering, 1 University of New Mexico, MSC01 1070, Albuquerque, NM, USA 87131

[2] Center for Micro-Engineered Materials, University of New Mexico, 1001 University Blvd SE, Albuquerque, NM, USA 87106

[3] Instituto de Electroquímica, Universidad de Alicante, Apdo. 99, E'0308, Alicante, Spain.

Prepared for Submission to *Physical Chemistry Chemical Physics*

5.1 Abstract

The ability to detect trace concentrations of Arsenite, As (III), in real water solutions is impacted by co-contamination of other metals and co-occurring ions. The presence of copper ions, specifically Cu (II), is the most concerning common co-contaminant in natural waters due to the close proximity of the Cu (II) oxidation potential to that of As (III). The use of well oriented ultraflatAu(111) thin film electrodes provided increased peak separation and sensitivity for electrochemical deposition and oxidation of Cu (II) and As (III) in 0.5 M sulfuric acid compared to an Au wire electrode. However, mixtures of As (III) and Cu (II) yielded new electrochemical properties during both cyclic voltammetry (CV) and linear stripping voltammetry (LSV) analysis. Sweeping deposition during CV in As & Cu mixtures resulted in a sequential deposition condition where a layer of Cu blocked effective deposition of As to the electrode. In contrast rapid shifting of potential to 0 V where As and Cu will deposit produced a peak profile different from Cu and As alone, and a significantly larger oxidation peak due to an increase in coulombic efficiency during. Ex-situ analysis using X-ray photoelectron spectroscopy showed that a mixture of approximately 6% As to 94% Cu was adsorbed onto the surface after 60 seconds of deposition at 0 V, suggesting an alloying process is occurring. Trace analysis calibration curves using the standard additions method were conducted for Cu, As, and Cu + As solutions. This study provides detailed insights into the deposition of co-occurring Cu and As at Au(111) electrode surfaces during LSV and provides new insights into the impacts of Cu-As alloying on trace As (III) detection in 0.5 M H_2SO_4 solutions.

SYNOPSIS: Analysis of Cu (II), As (III) and As (III) + Cu (II) mixtures suggests that a Cu_3As phase is formed during LSV which impacts trace As detection even in trace Cu conditions.

This has important implications for the ability to determine As concentrations near the MCL of 10 µg L^{-1} in natural water systems which may contain Cu (II) as a co-contaminant.

Keywords: Arsenic, Copper, Electrochemical Detection, Gold Single Crystals, Gold Thin Films, Water

5.2 Introduction

The electrochemical detection of Arsenite, As (III), in complex water matrices is an essential tool for identifying unsafe concentrations and assessing remediation efficacy in natural water samples. [72, 104, 129] Methods such as linear stripping voltammetry have been proven to be accurate at part per billion (µg L^{-1}) concentrations, capable of detecting multiple co-occurring species simultaneously, and cost effective. [130] These capabilities make electrochemical detection a highly valuable tool for identifying if a drinking water source contains more than 10 µg L^{-1} As (III) and considered dangerous by the World Health Organization and United States Environmental Protection Agency. [6, 64] A significant portion of the U.S. and Global population obtain their daily drinking water directly from surface or groundwater sources which may contain unsafe As concentrations and are not protected by municipal water treatment systems. [10, 131, 132] Electrochemical sensors for heavy metals in water can be a lifesaving, portable, and rapid tool for supporting rural community health. [48, 70, 92, 133]

The most concerning form of Arsenic is its trivalent state Arsenite, As (III), and is the focus of many electrochemical sensing studies due to its electrochemical activity and high bioavailability. [9, 13, 105] Arsenate, As (V) is the second most concerning form and can be chemically reduced to As (III) for determination of total As after initial determination of As

(III). [22, 30, 40, 80] Electrochemical detection on gold (Au) electrodes is beneficial due to its high nobility, reversible As (III) redox reaction, and broad region of stability. Seminal works provided a foundation for development of electrodes with a variety of morphologies, methods, and investigations. [22, 26, 35, 79, 129, 134] Thin Au films, nanoparticles, and microarrays on a variety of substrates have been investigated to identify low-cost and highly effective electrode materials. [29, 41, 44, 80, 83, 135, 136] Recent works have begun to identify controlled Au surface morphology as a potential path to increased sensitivity and selectivity for As (III) detection. [25, 37, 38, 42, 43, 51, 118]

Arsenic is commonly mobilized into water with many other anions such as sulfate and cations such as uranium, lead, iron and copper. [12, 14] Copper (II) is the most commonly cited cation interference with electrochemical As (III) detection and are used as an example interferant to determine the selectivity of novel electrodes. [36, 38, 78, 137, 138] Several studies have identified the mechanisms for sulfate assisted electrochemical Cu (II) reduction and oxidation at Au(111) surfaces which contribute to a characteristic three peak cyclic voltammogram. [128, 139-142] During Cu (II) deposition, an ordered sub monolayer structure $(\sqrt{3}\,x\,\sqrt{3})\,R30°$ stabilized by sulfate co-adsorption forms with underpotential deposition. [143] This is followed by peaks associated with the filling of a $(1\,x\,1)$ Cu to Au monolayer and a multilayer as potential decreases. Oxidation of Cu results in three peaks associated with the reversal of these three processes. [140, 144] The formation of Cu-As intermetallic species during deposition and overlapping oxidation peaks impeded our ability to detect trace concentrations of As. [32, 145] The Cu-As system has received interest in recent years due to increased copper production and several researchers have reassessed older thermodynamic research for

modelling phase diagrams. [47, 146, 147] However, observing the impacts of Cu-As alloying on electrochemical response at Au(111) ordered surfaces has yet to be systematically studied.

The objective of this work is to assess the capability of a well oriented and ultraflat Au(111) thin film, Au(UTF) to selectively detect As (III) in the presence of Cu (II) using linear stripping voltammetry (LSV). In previous work from our group we compared the Au(UTF) to single crystal model electrode surfaces, and found that it performed very similarly to the Au(111) single crystal surface and had increased selectivity and sensitivity for As detection compared to the other basal planes. [148] In this study, linear stripping voltammetry (LSV) and cyclic voltammetry (CV) were used to systematically identify the impacts of Cu (II) co-contamination on As (III) detection in both high and trace concentration mixtures. The formation of an As-Cu intermetallic during LSV was confirmed with x-ray photoelectron spectroscopy (XPS) and chemical modelling using thermodynamic data. In both high and trace concentrations of As & Cu mixtures the peak potential and shape were shifted significantly and the ability to detect As (III) at the MCL was diminished. This study provides new insights into electrochemical Cu-As alloying as an important As detection interference mechanism. Our work shows the drastic impacts co-occurring Cu can have on electrochemical As detection with even trace concentrations of Cu. This work has implications for detection of natural waters which may have Cu and As such as mining legacy impacts and suggests Cu removal may be necessary for accurate trace As detection.

A core value of this study is to identify a highly sensitive and selective As (III) detection system which is also accessible to communities from a cost and usability perspective. In consideration of consumer economic accessibility, we are utilizing a commercially available film which is ~100 nm thick to limit the amount of Au consumed in

each electrode and focusing. In consideration of consumer usability, we are using a portable potentiostat and linear stripping voltammetry which is more automatable than capacitive current separating methods such as pulse voltammetry. The authors of this study hope that this highly effective and portable technology will one day be readily available to communities around the world who are in need of accurate detection of As (III).

5.3 Experimental

5.3.1 Materials description and characterization

Ultraflat Au(111) Thin Film. Ultraflat Au(111) thin films used in this study were purchased from Platypus Technologies. Physical characterization of the films are available at the purchasing website and have been reported in our previous work with the Au(UTF)s. [122, 148] The website quotes a film thickness near 100 nm and an average grain area of 3.64 ± 0.2 μm^2 with predominantly Au(111) surface orientation.

5.3.2 Electrochemical Characterization

Electrochemical experiments were carried out in a 200 ml five port glass cell, using an Au wire as a counter electrode and a reversible hydrogen electrode (RHE) as a reference electrode with a fritted glass tube to separate the RHE from the solution. Voltammetric experiments were carried out at room temperature using a PalmSens 4 PALM-PS4.F2.05 portable potentiostat. All solutions were made using ultrapure water (18.2 MΩ cm, Elga PureLab OptionQ), concentrated sulfuric acid (VWR, 95 wt%), As_2O_3 salt (Merck), and $CuSO_4$ salt. Fresh As (III) stock solution were prepared by adding 1.229 g of $NaAs_2O_3$ to 100 ml of 0.5 M H_2SO_4 in 18 MΩ water to generate a 7.5 g/L (10^{-1} M) As(III) stock solution. One ml of this solution was then used to prepare 100 mL of 75 mg/L (10^{-1} M) As (III) in 0.5 M H_2SO_4 solutions. This was then used with a micropipette to perform the standard additions

methods for trace As (III) detection and experiments with 750 ug/L (10^{-5} M) As (III). A 1 g/L (1.57 mM) Cu (II) solution was prepared and used as the stock solution for standard additions and 10 mg/L (15.7 μM) Cu (II) experiments.

Ultraflat Au(111) Thin Film. The Au(UTF) electrodes were purchased from Platypus Technologies, [122] and were analyzed in previously published research. Our previous study showed that the Au(UTF) performed similarly toAu(111) single crystal electrodes for electrochemical oxidation and reduction of Au and As (III) and provided increased sensitivity and selectivity for As redox compared to a Au(Poly) and other basal plane electrodes. [148] The Au(UTF) electrode is an Au(111) thin film with a thickness around 100 nm. An alligator clip which was DC sputtered with Au on each side for 2 minutes using a Polaron sputtering system with a voltage 1.7 kV, current 18 mA to decrease potential contamination when clipped to the Au(UTF)s. The clip was attached near one end of the 5 x 20 mm glass slide and 18 MΩ ultrapure water was used to rinse the lower portion of the electrode before inserting it into the cell. A new Au(UTF) electrode was used for each experiment. A CV from 0.7 to 1.7 V vs. RHE at 10 mV/s was performed at the begginning of each experiment to assess surface orientation and electrochemical surfae area for current density normalization of the Au(UTF) and a Au(wire) electrodes. As can be seen in Figure C-S1, the Au(UTF) surface oxidation begins with a shoulder in the positive sweep direction beginning at 1.4 V which leads to a single sharp peak at 1.6 V in 0.5 M H2SO4. This shows that the Au surface is predomininantly Au(111) oriented as compared to the Au(wire) electrode which presents a broad set of peaks from 1.4 to 1.6 for Au oxidation indicating multiple surface orientations. [123] The area of the Au reduction peak occuring at 1.2 V vs. RHE was determined and a value of 660 uC/cm^2 was used to convert the area of the peak to cm^2 and

the result was used to normalize experimental results. The reference value used represents a three-electron transfer process per Au(111) surface atom with a specific current of 220 μC cm^{-2} per electron transferred was 660 μC cm^{-2}.

5.3.3 Physical Characterization

X-ray Photoelectron Spectroscopy. XPS measurements were performed on a Kratos Ultra DLD spectrometer using a monochromatic Al Kα source operating at 150 W (1486.6 eV). The operating pressure was 2 x 10^{-9} Torr. High-resolution spectra were acquired at a pass energy of 20 eV. XPS data was processed using Casa XPS software. The analysis was performed at six locations along the length of the Au(UTF) electrode; three in the submerged area and three on the area which was not submerged. An area which was submerged was then used to perform slow scans at 0°, 20°, 40°, 60°, and 80° to observe variance in concentrations of As and Cu due to depth of the electrochemically adsorbed layer during 60 seconds of deposition in 10 mg L^{-1} (157 μM) Cu (II) and 750 ug/L (10.0 μM) As (III) with 0.5 M H_2SO_4 supporting electrolyte.

5.3.4 Statistical Analysis.

Statistical analysis was performed in EXCEL to determine average and standard deviation of three consecutive measurements where applicable. The raw data was used to calculate the calibration plot of concentration vs. charge density. Limits of detection were determined using the equation LOD = (k * Sb)/m, where k was equal to 3 for a 98.3% confidence level, Sb is the standard deviation for analysis of three blank curves, and m is the slope of the calibration curve.

5.4 Results & Discussion

5.4.1 Increased Sensitivity and Selectivity for As & Cu at Au(UTF) compared to Au(Wire) Electrodes.

The use of the Au(UTF) increased sensitivity for As (III) and Cu (II) redox processes over an Au wire electrode. The Au(UTF) thin films were compared to an Au(Wire) in 750 μg L^{-1} As (III) and 10 mg L^{-1} Cu in 0.5 M H_2SO_4. Figure 5.1 presents CV between 0 and 0.7 V vs. RHE with a scan rate of 10 mV s starting in the negative direction. In 750 μg L^{-1} As (III) the Au(Wire) electrode shows a broad peak beginning at approximately 0.45 V and a maximum reduction peak potential at 0.25 V followed by a plateau near -9 μA cm^{-2} until 0 V (Fig. 5.1A). The Au(UTF) deposition for the same solution conditions begins at a lower potential, 0.325 V, and consists of a broad maximal peak potential of 0.15 V with a smaller shoulder peak at 0.26 V. During the positive sweep the oxidation potential for the Au(Wire) occurs at 0.33 V and has a broad bell shape. Whereas the Au(UTF) has a sharp peak at 0.31 V with a sharp fall off until a shoulder begins at 0.35 V. Figure 5.1B presents the comparison of the Au(UTF) to the Au(Wire) in 10 mg L^{-1} Cu (II) with 0.5 M H_2SO_4. The Au(Wire) deposition begins near 0.6 V and has a broad wave followed by a larger peak at 0.16 V. The Au(UTF) shows more distinctive deposition peaks at 0.42 V and 0.22 V followed by a wave from 0.15 to 0 V. The positive sweep shows that the Au(Wire) has a crown shape with 3 major peaks which are not well resolved from each other. However, the Au(UTF) shows sharp peaks at 0.25, 0.35, and 0.46 V. The charge density for the oxidation peaks at the Au(UTF) surface are 275, 270, and 183 μC cm^{-2}, respectively.

The results of Cu redox on the Au(UTF) is similar to studies observing Cu underpotential deposition and structure during cyclic voltammetry on Au(111) surfaces. [140,

[144, 149] Each peak was assigned a potential range which was chosen by identifying the lowest current between the peaks during the potential sweep. The charge density of the redox peaks were analyzed as three separate processes with the half wave potential occurring at approximately 0.2, 0.3, and 0.4 V for peaks 1, 2, and 3, respectively. Reduction peaks at 0.42, 0.22, and 0.15 V were termed R1, R2, and R3, respectively. Oxidation peaks at 0.25, 0.35, and 0.46 V were termed O1, O2, and O3, respectively. Similar charge density for each reduction and oxidation of the redox processes showed that the peaks are correlated and reversible. The oxidation charge density for O1, O2, and O3 were 275, 270, and 183 μC cm^{-2} (Table 5-1). The O3 peak is often cited as the formation of a 2/3 monolayer structure which takes a honeycomb structure on the Au(111) surface, while O2 is determined to be the filling of a full 1:1 Cu to Au monolayer and O1 is associated with the formation of a bulk layer. [149] The combined charge for O2 and O3 is 453 μC cm^{-2} which aligns well with the expected specific current from a two-electron process at the Au(111) surface being 440 μC cm^{-2}. However, the ratio of O3 accounts for only 2/5 of the total charge associated with the formation of a full 1x1 monolayer of Cu. This variance from expected ratios may be due to the presence of multiple randomly rotated Au(111) crystals with grain boundaries in the film resulting in various Au(111) terrace sizes. [140] However, the charge ratios for the peaks cannot be relied upon for conclusive evidence of surface structure due to influence from co-adsorbed sulfate. [144, 150] The current density correlation to theoretical values and the ability to observe these processes in sharp and mostly separated peaks shows the quality of the Au(111) surface of the Au(UTF) for observing electrochemical processes with increased sensitivity and selectivity.

5.4.2 Cu Limitation of As Deposition for As-Cu Mixtures during Cyclic Voltammetry

During cyclic voltammetry the sequential deposition of Cu followed by As + Cu during deposition limited the adsorption of As (III). Cyclic voltammetry analysis in 750 μg L^{-1} As (III) + 10 mg L^{-1} Cu in was compared to CVs in As alone and Cu alone between 0 and 0.7 V vs. RHE (Fig. 5.2). During the negative going sweep deposition in 10 mg L^{-1} Cu alone begins at 0.55 V while As (III) deposition begins at 0.325 V. The deposition sweep in the mixture begins at 0.55 V and shows deposition peaks similar to 10 mg L^{-1} Cu alone. However, the current between 0.15 and 0 V is increased in comparison to Cu alone but is not increased to match the current passed for deposition of As alone.

The mixture deposition profile indicates that there is a period of time where Cu is being deposited before As, and the charge passed for deposition of As was reduced in comparison to As alone. The charge passed for the deposition process in Cu alone, As alone and Cu & As mixtures was 788, 752, and 960 $\mu C\ cm^{-2}$. Upon the sweeping positively the oxidation process for the Cu & As mixture resembles that of Cu alone more closely than As alone. However, the first oxidation peak at 0.25 V shows increased peak current from 30 to 50 $\mu A\ cm^{-2}$ and the second oxidation peak is shifted from 0.35 V to 0.325 V between the Cu alone and mixture profiles. The total charge passed for the oxidation processes for Cu alone, As alone, and Cu & As mixtures were 613, 710, and 727 $\mu C\ cm^{-2}$ (Table 5-2).

The deposition of As onto the Au(UTF) electrode is inhibited by the presence of Cu in solution. The deposition process in the Cu & As mixture did not show an additive increase in charge density as would be expected if Cu and As adsorbed in the same quantity when individually present. If the Cu and As were depositing at the same rate in the mixture as

when they were alone, we would expect the current to be closer to 1540 μC cm^{-2} rather than 960 μC cm^{-2} (Table 5-2). Additionally, the oxidation process peaks during the positive going sweep of the CV for the mixture more closely resembled that of Cu alone with slight shifts. This can be explained by the sweeping condition results in a semi-charge transfer limited condition for As & Cu co-deposition during sweeping. Due to the higher deposition onset potential of Cu a layer of Cu is adsorbed during sweeping before potentials which would allow for both Cu and As to adsorb are reached. The co-deposition of As with Cu has been determined to occur primarily in the early stages of deposition and a change in the surface overpotential when a Cu layer adsorbed may be contributing to the limitation of As deposition under cyclic voltammetry conditions. [151]

It is important to note that the separation of Cu (II) and As (III) deposition processes is increased at the Au(UTF) surface in comparison to an Au wire, which may have implications for a sensing system with two Au(UTF) working electrodes. Using a single electrode, the sequential deposition of a Cu layer prior to As deposition blocked the deposition of As. However, chronoamperometry with a secondary Au(UTF) electrode held at a potential below the Cu sub-monolayer peak, but above the As deposition peak (~0.325 V vs. RHE) could electrochemically remove Cu (II) from solution without removing As (III). This would be ideal for in-situ detection because it would limit the amount of chemical alteration necessary for trace As (III) detection.

5.4.3 Increased Deposition and Oxidation Charge Transfer for As-Cu Mixtures During Linear Stripping Voltammetry

Linear stripping voltammetry analysis of the same solution conditions was performed and compared to results from CV experiments. Figure 5.3 A shows the LSV stripping peak

for 10 mg L^{-1} Cu alone, 750 μg L^{-1} As alone, and the 10 mg L^{-1} Cu + 750 μg L^{-1} As mixture with a scan rate of 10 mV s^{-1} and deposition time of 60 s at 0 V vs. SHE. The LSV analysis was performed directly after each CV study without removing the Au(UTF) electrode from section 3.2 for consistency.

The LSV oxidation process for 10 mg L^{-1} Cu (II) alone resembles that of the CV in figure 5.1B, however the lowest oxidation peak, O1, is broader and larger than peak O2. During LSV the charge densities for O1, O2, and O3 were 412, 210, and 147 μC cm^{-2}. The charge associated with the filling of the full monolayer (O2 + O3) decreased from 453 to 415 μC cm^{-2} when comparing the oxidation process peaks in section 3.1. Peak O1 is the only peak which increased from 275 to 338 μC cm^{-2} between CV and LSV, respectively. The oxidation process for 750 μg L^{-1} As (III) LSV shows a similar peak shape and position with a peak area increase from 710 to 857 μC cm^{-2}. When both 10 mg L^{-1} Cu (II) and 750 μg L^{-1} As (III) were present the LSV analysis resulted in a drastically increased charge from 727 to 4921 μC cm^{-2} (Table 5-3). To further assess the drastic increase an LSV experiment where chronoamperometry data was collected during the deposition step was performed for 750 μg L^{-1} As (III) and the 10 mg L^{-1} Cu (II) + 750 μg L^{-1} As (III) mixture solutions (Fig. C-S2A, B). The total charge during deposition of As alone and the As + Cu mixture were 1454 and 3143 μC cm^{-2}, respectively. When compared to the stripping charge of As alone and the As + Cu mixture (459 and 3110 μC cm^{-2}, respectively) the deposition efficiency was increased from 32% for As alone to 99% in the As + Cu mixture. In addition to an increase in peak current the shape of the peak is shifted and the maximal peak potential for the As + Cu

mixture is 0.325 V with a shoulder peak at 0.375 V vs. RHE. These peak potentials do not align with the peak potential for As or Cu alone and suggest a new phase has been formed.

The LSV analysis further develops understanding of the three phase Cu redox system and introduces evidence of Cu-As alloy formation at the Au(UTF) surface. The three step Cu oxidation process for 10 mg L^{-1} Cu (II) alone is maintained for LSV with an increase in charge for O1 and relatively similar charges for peaks O2 and O3. The increase in the multilayer oxidation peaks and stability of monolayer oxidation peaks aligns well with the three-phase mechanism for formation of multiple Cu layers discussed in section 3.2. There is a decrease in peak current for O3 and O2 during LSV which may be due to restructuring of the Au(111) facets from adsorption during LSV or CV studies. [152, 153] LSV in 750 μg L^{-1} As (III) shows a primary peak at 0.34 V with a slope to the right extending to 0.425 V. Considering that the onset of the As oxidation peak is near 0.325 V the total width of the As detection peak is 100 mV, which is a small potential region compared to unoriented electrodes at similar concentrations of As even when pulse voltammetry techniques are utilized. [26, 35, 38, 129] The LSV of the Cu + As mixture indicates that an intermetallic is being formed due to increased deposition efficiency resulting in increased peak current, and a positive shift in peak potential and shape when both As and Cu are present.

Analysis of linear stripping voltammetry was conducted with 175 μg L^{-1} (2.34 μM) As (III) and (23.6 μM) 1500 μg L^{-1} Cu (II) to observe impacts of co-occurring Cu + As at trace concentrations (Fig. 5.3B). LSV was performed under with the same electrochemical parameters as in section 3.3. The charge of oxidation peaks during LSV for 175 μg L^{-1} As (III) alone, 1500 μg L^{-1} Cu (II) alone and a 175 μg L^{-1} As (III) + 1500 μg L^{-1} Cu (II) mixture

were 125, 358, and 462 μC cm^{-2}, respectively (Table 5-3). The oxidation profile for Cu (II) alone shows only two peaks at 0.35 V and 0.45 V which are the same as O2 and O3 from section 3.1. The lower potential peak for Cu oxidation due to multilayer deposition, O1, is not expected to be present at this concentration because the charge associated with 1500μg L^{-1} Cu (II) alone is significantly less than the expected value of 440 μC cm^{-2} for a 1x1 monolayer. Since the peak at 0.35 accounts for 125 μC cm^{-2} and the peak at 0.45 is associated with 192 μC cm^{-2} of the charge we can assume that the full (1x1) monolayer is not being filled. The maximal peak for 175 μg L^{-1} As (III) alone was at 0.275 V with a shoulder with a maximum current at 0.32 V. For the 175 μg L^{-1} As (III) + 1500μg L^{-1} Cu (II) mixture the maximal peak potential during LSV was at 0.36 V with sloped shoulder peaks at 0.28 and 0.44 V.

The LSV comparison of high and trace concentrations shows that the Cu-As intermetallic is forming for both multiple layer and monolayer conditions. The sum of As alone and Cu alone would be 483 μC cm^{-2} which is close to what was observed when both Cu + As were present (462 μC cm^{-2}). The specific charge expected for As (III) reduction, a 3-electron process, on an Au(111) surface would be 660 μC cm^{-2}. Taking the specific charge of each reaction as an estimation the charge passed for Cu alone would be equal to about 81% of a monolayer, and the charge passed for As would correlate to about 19% of a monolayer which is what may be expected for a 1x1 monolayer.

5.4.4 Formation of As-Cu Intermetallic Alloy Influences Linear Stripping Voltammetry for As-Cu Mixtures

X-ray photoelectron spectroscopy (XPS) and thermodynamic modelling provide evidence that a Cu-As intermetallic is being formed during the deposition phase of LSV

analysis. Figure 5.4A presents the angle resolved XPS analysis of elemental composition on the surface of the Au(UTF) directly after deposition and before stripping. The elemental percentage of As increases from 6 to 18 % elemental (8-26 wt%) as the angle of the film is tilted from 0 to 60 ° during analysis. Increase in concentration with tilt angle indicates that As is more concentrated towards the surface of the adlayer than towards the Au(111) surface. The concentration range determined is well within the range where Cu_3As and other Cu-As intermetallic species are formed according to metallurgical modelling. [47, 146, 147] Thermodynamic modelling for an aqueous electrolyte containing 0.5 M H_2SO_4, 1 mg L^{-1} Cu (II), and 750 μg L^{-1} As (III) indicates that at the concentrations of interest Cu_3As is likely to be formed at a slightly higher potential than As alone (Fig 5.4B). Chen et al found that the co-deposition As with Cu increases deposition of Cu and forms a Cu_3As intermetallic alloy. [154] Although the thermodynamic characteristics of a bulk solid metal are different from those in solution, the co-deposition phenomena cited in metallurgical studies may explain increased deposition efficiency and peak charge density for the 10 mg L^{-1} Cu (II) + 750 μg L^{-1} As (III) mixture compared the individual species at the Au(UTF) surface during LSV. A limitation of this study is that XPS and electrochemical data are not capable of discerning the structure of the intermetallic. Further studies using electron diffraction or atomic imaging are needed to determine if electrochemical deposition of the Cu-As intermetallic is forming a solid solution, or an ordered phase. The Au(UTF) was then tested with lower concentrations to identify if there are impacts on detection of trace As from Cu-As intermetallic formation.

3.5 Co-occurrence of Cu Limits Selectivity for As Detection

The Au(UTF) was highly effective at detecting trace concentrations of As (III) and Cu (II) near 1 mg L^{-1}. The Au(UTF) was used to generate LSV standard additions method calibration curves for 5, 10, 15, 25, 50, 75, 100, 125, and 175 μg L^{-1} (0.07, 0.13, 0.20, 0.33, 0.67, 1, 1.34, 1.67, and 2.3 μM) As (III) and 250, 500, 1000, and 1500 μg L^{-1} (3.9, 7.9, 15.7 and 23.6 μM) Cu (II) in 0.5 M H_2SO_4 , Figure 5.5 A and C, respectively. Linear regression analysis showed that the adjusted R^2 for Cu (II) and As (III) detection were 0.999 and 0.901, respectively (Fig. 5.5 B & D). This results in theoretical limits of detection (LOD) of 0.6 μg L^{-1} (0.01 μM) As (III) and 45 μg L^{-1} (0.7 μM) Cu (II) for the Au(UTF) electrode while using linear stripping voltammetry. Sub part per billion detection of As (III) with a portable potentiostat shows portable and accurate detection below the MCL while using LSV which can be automated and applied to a large set of electrodes. This avoids usability issues inherent to differential pulse techniques such as individual electrode optimization for detection.

The LSV curves for trace As (III) alone show a peak at 0.54 V which is consistent throughout all curves and commonly associated with the dissolution of an ordered sulfate layer on Au(111) electrodes. [55, 155] The addition of increments of As (III) to achieve between 5 and 25 μg L^{-1} result in an increasing peak with a bell shape at 0.35 V. At 50 μg L^{-1} As (III) a second peak at 0.27 begins and continues to increase and becomes the dominant peak with increasing concentrations up to 175 μg L^{-1} As (III). The initial peak at low concentrations becomes a shoulder of the lower energy peak and continues to have a maximum peak current near 6 μA with concentrations at and above 50 μg L^{-1}. This may be due to saturation of imperfections at the surface of the Au(UTF) which are not Au(111) oriented such as grain

boundaries which are adsorbing As (III) through underpotential deposition and thus require a higher energy to strip from the surface. [148]

Concentrations of Cu alone from 250 to 1500 μg L^{-1} Cu (II) show that a peak at 0.45 V initially increases and then a peak at 0.35 V begins to increase upon increasing concentration (Fig. 5.5C). This is consistent with previous sections showing that there is a maximal potential for the highest peak energy peak due to the formation of an ordered sub-monolayer of Cu followed by the filling of a 1x1 monolayer at an Au(111) surface.

When mixtures of trace As (III) in the presence of Cu (II) were analyzed, it was found that Cu (II) concentrations as low at 250 μg L^{-1} can impact the peak shape and detection of trace As (III) at an Au(111) surface. The Au(UTF) was used to generate LSV standard additions method calibration curves for 5, 10, 15, 25, 50, 75, 100, 125, and 175 μg L^{-1} As (III) in the presence of 1500 μg L^{-1} Cu (II) (Fig. 5.6A & B). The initial peaks associated with 1500 μg L^{-1} Cu (II) are at 0.34 and 0.45 V. With increasing As (III) concentrations the lower potential peak shifts from 0.34 to 0.37 V and the higher potential peak decreases in current from 37 to 19 μA, becoming a shoulder to the lower energy peak. The amount of error for each concentration of As (III) was increased when 1500 μg L^{-1} Cu (II) was in solution, and the limit of detection was increased to 43.7 μg L^{-1} (0.58 μM) for As (III). This high of a limit of detection effectively eliminates the ability to detect As at the maximum contaminant level with 1500 μg L^{-1} Cu (II) present. [24]

Additions of Cu (II) from 250, 500, 1000, and 1500 μg L^{-1} Cu (II) were added to a solution containing 175 μg L^{-1} As (III) in 0.5 M H_2SO_4 (Fig. 5.6 C & D). With the addition of 250 μg L^{-1} Cu (II) the peak for 175 μg L^{-1} As (III) at 0.25 V shifts positively to 0.3 V and a

second peak at 0.44 V is introduced. Further additions of Cu (II) to 1500 μg L^{-1} continue to shift the primary peak potential to 0.35 V and increase the higher energy peak at 0.44 until it becomes a shoulder. The resulting peak shape for additions of Cu (II) to As (III) and vice versa are similar with a predominant peak near 0.35 V and a shoulder at 0.45 V. The limit of detection by analyzing the area under the curve for Cu (II) in the presence of 175 μg L^{-1} As (III) was 13 μg L^{-1} (0.2 μM) Cu (II). The impacts of As on Cu detection have been found to be minimal, [36] and in our findings aided in decreasing the limit of detection for Cu (II) from 45 to 13 μg L^{-1}.

The trace concentration mixtures show shifts in peak potentials and heights when Cu (II) is added to a solution containing As (III) and vice versa. When approaching 175 μg L^{-1} As (III) and 1500 μg L^{-1} Cu (II) by adding As or Cu the final peak shape is quite similar regardless of which species is being added. This raises an interesting prospect of implementing a machine learning system by analyzing a large set of experiments with a range of concentrations and Cu:As ratio mixtures to teach a neural network to identify Cu and As concentrations based on peak shape and intensity.

5.5 Conclusions

The results of this study show that even though the use of a highly oriented and ultraflat Au(111) surface provided increased sensitivity to surface redox processes it was not able to selectively detect As (III) in the presence of Cu (II) with 0.5 M H_2SO_4 supporting electrolyte due to Cu-As alloy formation. We observed that the formation of a Cu-As intermetallic during LSV at both high and trace concentrations of As & Cu mixtures impacted the ability to detect As (III) at the Au(UTF) surface. The deposition process was

characterized through CV and LSV studies, as well as XPS analysis. Cyclic voltammetry showed that if deposition in a mixture of Cu and As is performed by sweeping negatively the sequential deposition of Cu then As results in limited As deposition. However, when deposition is performed by a rapid step to a potential where both As and Cu are likely to form there is a drastic increase in deposition efficiency and oxidation peak charge density compared to As or Cu alone. At the concentrations studied modelling showed that a stable Cu_3As species is formed which is likely the cause for increased deposition efficiency. The standard additions method was used to detect As (III) with a LOD of 0.6 $\mu g\ L^{-1}$ in 0.5 M H_2SO_4 showing highly sensitive detection using a nanofilm of Au and the readily automatable LSV method. However, when 1500 g μL^{-1} Cu (II) was present the LOD was increased to 43.7 $\mu g\ L^{-1}$, making the electrode ineffective for detection at the 10 $\mu g\ L^{-1}$ MCL for As (III). The limit of detection for standard additions of Cu (II) in 0.5 M H_2SO_4 was 4.5 $\mu g\ L^{-1}$ and was decreased to 1.3 $\mu g\ L^{-1}$ when 175 $\mu g\ L^{-1}$ As (III) was present in solution. This work provides a systematic analysis of the impacts of Cu-As intermetallic formation on As (III) detection at an Au(111) oriented surface and shows that the presence of Cu (II) can have significant impacts on As (III) detection at Au(111) surfaces. This work provides insights into electrochemical Cu-As alloy formation at highly oriented Au(111) electrodes and highlights the importance of Cu (II) removal before direct analysis of As (III). However, increased peak separation and sensitivity for As and Cu redox can benefit the use of machine learning and neural network analysis as a potential path towards deconvoluting As detection in the presence of Cu without the need for removal. The application of Au(UTF) for heavy metals analysis encourages an exciting and accessible path towards the use of Au(111) electrodes surfaces for a multitude of electrochemistry applications.

5.6 Acknowledgments

This material is based upon work supported by the National Science Foundation (NSF) Graduate Research Fellowship Program (GRFP) under Grant No. (DGE-1418062), University of New Mexico Center for Water and the Environment, (NSF CREST Grant Number 1345169 and 1914490) and the Center for Micro-Engineered Materials (NSF MRI Award 1828731). Any opinion, findings, and conclusions or recommendations expressed in this material are those of the authors(s) and do not necessarily reflect the views of the National Science Foundation.

Tables and Figures

Table 5-1 Reduction and oxidation charge densities at the Au(UTF) electrode for three phase Cu redox peaks 1, 2, and 3 in 10 mg L^{-1} Cu during cyclic voltammetry and linear stripping voltammetry.

Peak	Potential Range V vs. RHE	CV Reduction Charge Density μC cm^{-2}	Peak	Potential Range V vs. RHE	CV Oxidation Charge Density μC cm^{-2}	LSV Oxidation Charge Density μC cm^{-2}
R3	0.3- 0.6	185	**O3**	0.4 - 0.6	183	151
R2	0.15 - 0.3	250	**O2**	0.3 - 0.4 V	270	264
R1	0 - 0.15	286	**O1**	0.2 - 0.3 V	275	338

Table 5-2 Total oxidation and reduction charge during CV at the Au(UTF) electrode in 750 μg L^{-1} As (III), 10 mg L^{-1} Cu, and 750 μg L^{-1} As (III) + 10 mg L^{-1} Cu mixture with 0.5 M H_2SO_4 supporting electrolyte.

Solution	Reduction Charge Density $\mu C\ cm^{-2}$	Oxidation Charge Density $\mu C\ cm^{-2}$
Blank (0.5 M H_2SO_4)	34	3
750 ug L^{-1} As	752	710
10 mg L^{-1} Cu	788	613
750 ug L^{-1} As + 10 mg L^{-1} Cu	960	727

Table 5-3 Oxidation peak charge density during LSV for Au(UTF) in high and trace concentration analysis of individual species and mixtures with 0.5 M H_2SO_4 supporting electrolyte.

Solution	Oxidation Charge Density μC cm^{-2}
Blank (0.5 M H_2SO_4)	7
750 ug L^{-1} As	857
10 mg L^{-1} Cu	768
750 ug L^{-1} As + 10 mg L^{-1} Cu	4921
175 μg L^{-1} As	125
1500 μg L^{-1} Cu	358
175 μg L^{-1} As + 1500 μg L^{-1} Cu	462

Table 5-4 Concentration conversion table for As and Cu concentrations used.

As Concentration ($\mu g\ L^{-1}$)	As Concentration (μM)	Cu Concentration ($\mu g\ L^{-1}$)	Cu Concentration (μM)
750	10.0	10000	157
175	2.34	1500	23.6
125	1.67	1000	15.7
100	1.34	500	7.9
75	1.00	250	3.9
50	0.67		
25	0.33		
15	0.20		
10	0.13		
5	0.07		

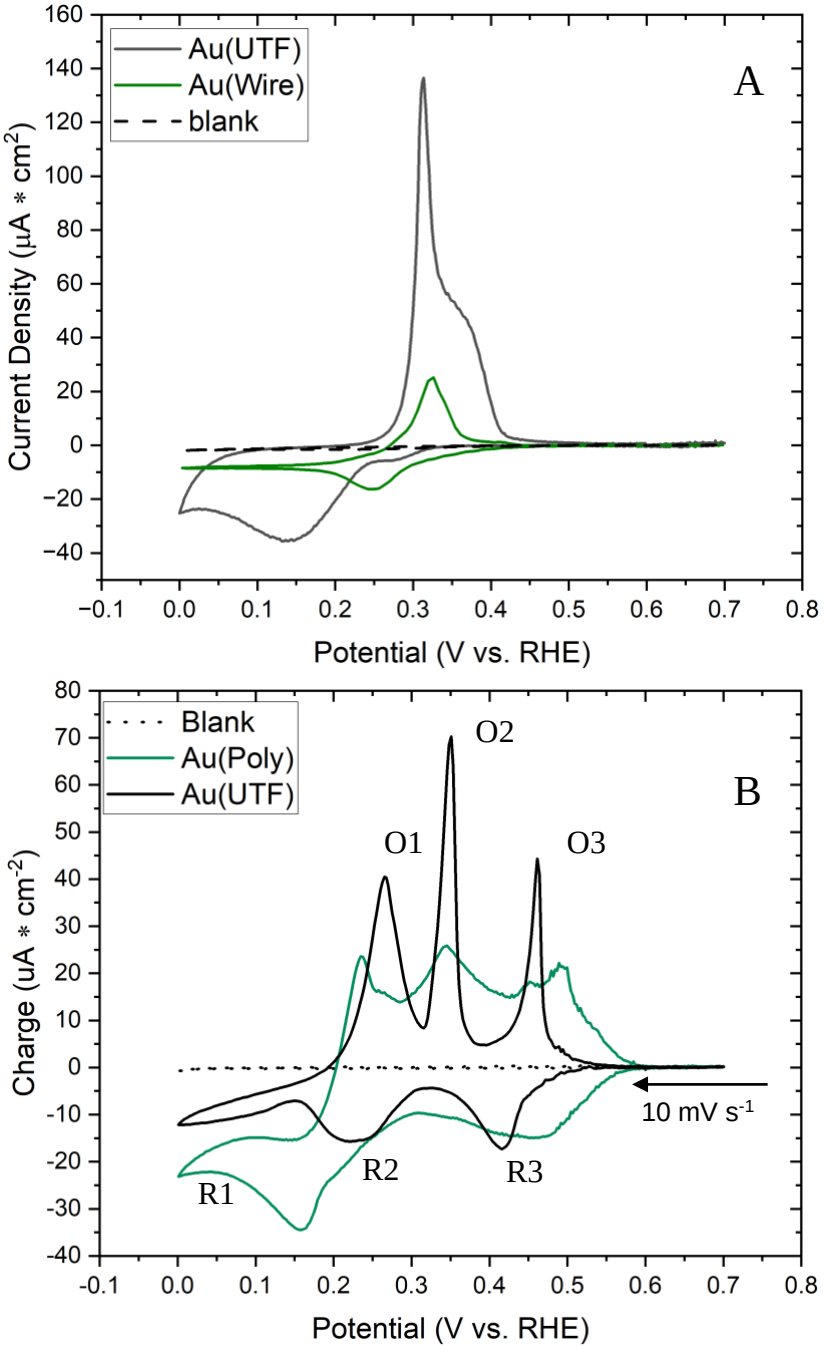

Figure 5.1 Cyclic voltammograms comparing an ultraflat Au(111) thin film, Au(UTF), electrode compared to an Au wire, Au(Wire), electrode in **A)** 750 μg L^{-1} As (III) and **B)** 10 mg L^{-1} Cu (II) with 0.5 M H_2SO_4 supporting electrolyte.

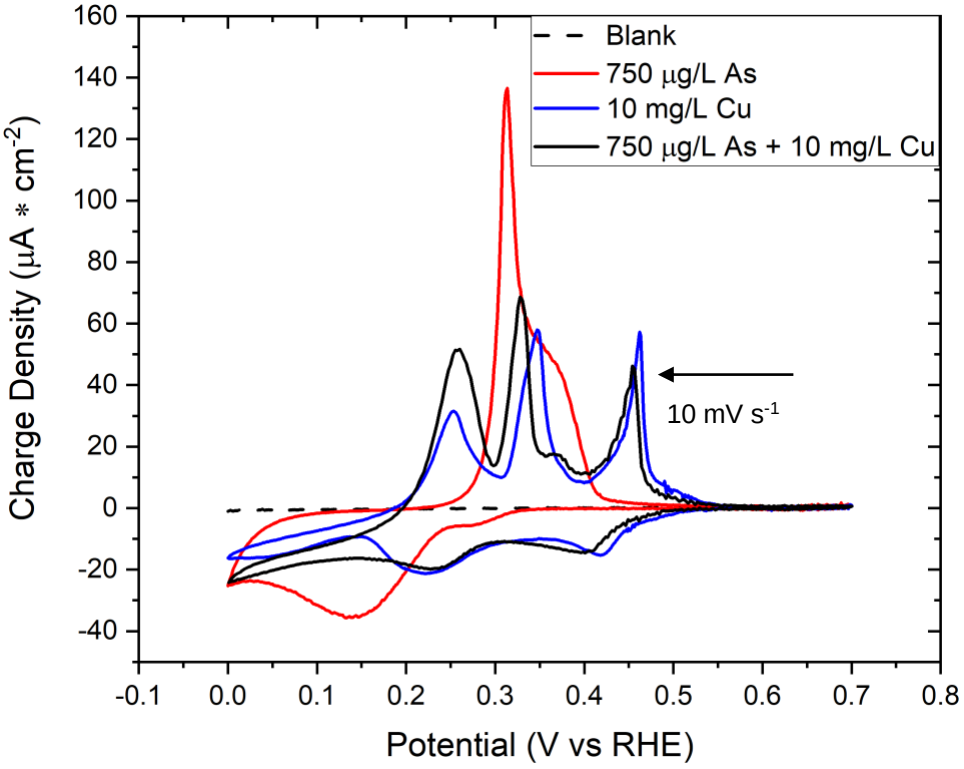

Figure 5.2 Cyclic voltammetry at the Au(UTF) electrode in 750 μg L^{-1} As (III), 10 mg L^{-1} Cu, and 750 μg L^{-1} As (III) + 10 mg L^{-1} Cu mixture with 0.5 M H_2SO_4 supporting electrolyte. Scan rate of 10 mV s^{-1} negative starting sweep.

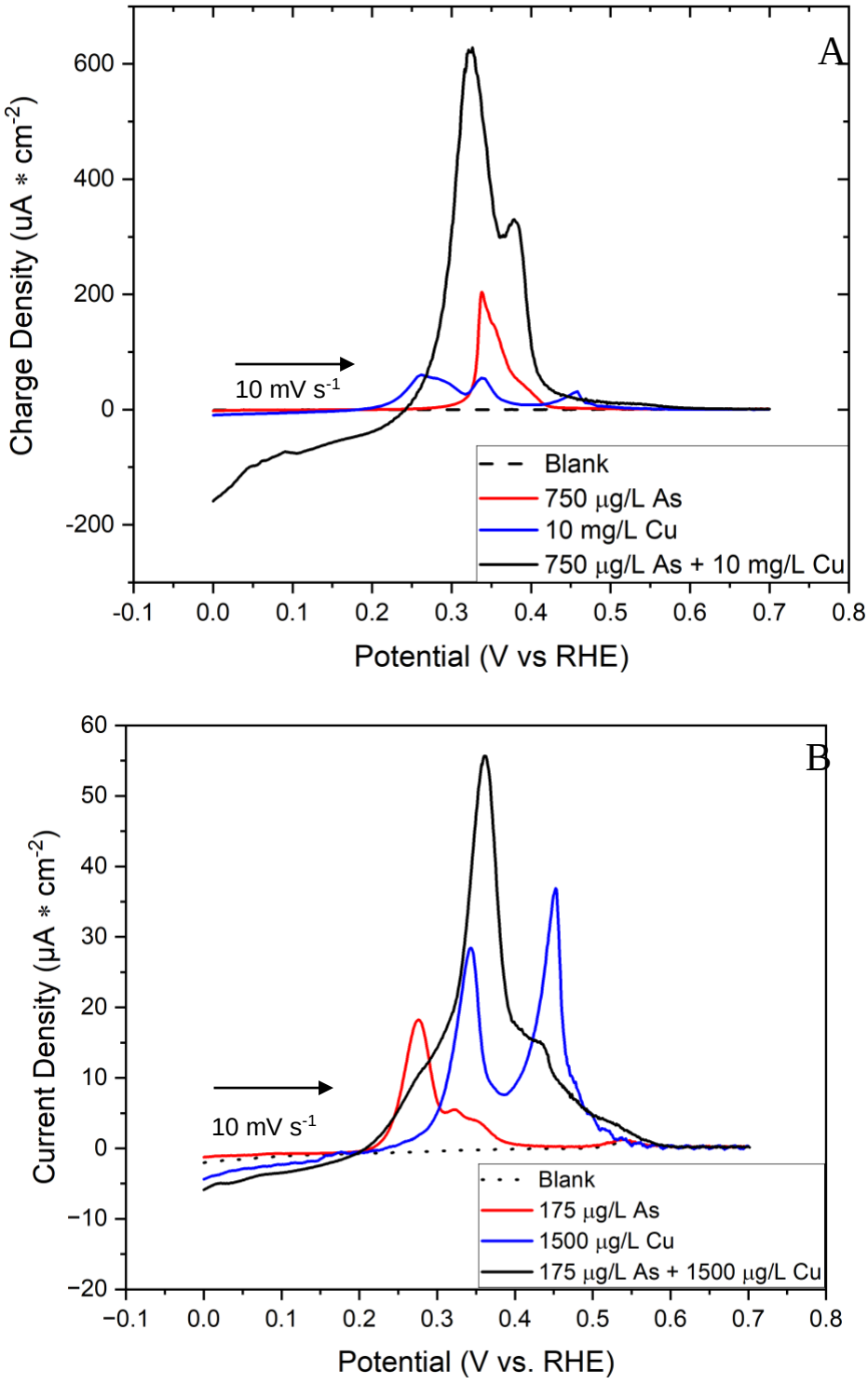

Figure 5.3 Linear stripping voltammetry at the Au(UTF) electrode in **A)** 750 μg L^{-1} As (III), 10 mg L^{-1} Cu, and 750 μg L^{-1} As (III) + 10 mg L^{-1} Cu mixture and **B)** 175 μg L^{-1} As (III), 1500 μg L^{-1} Cu (II), and 175 μg L^{-1} As (III) + 1500 μg L^{-1} Cu (II) mixture, with 0.5 M H_2SO_4 supporting electrolyte. Deposition for 60 s at 0 V vs. RHE and a scan rate of 10 mV s^{-1}.

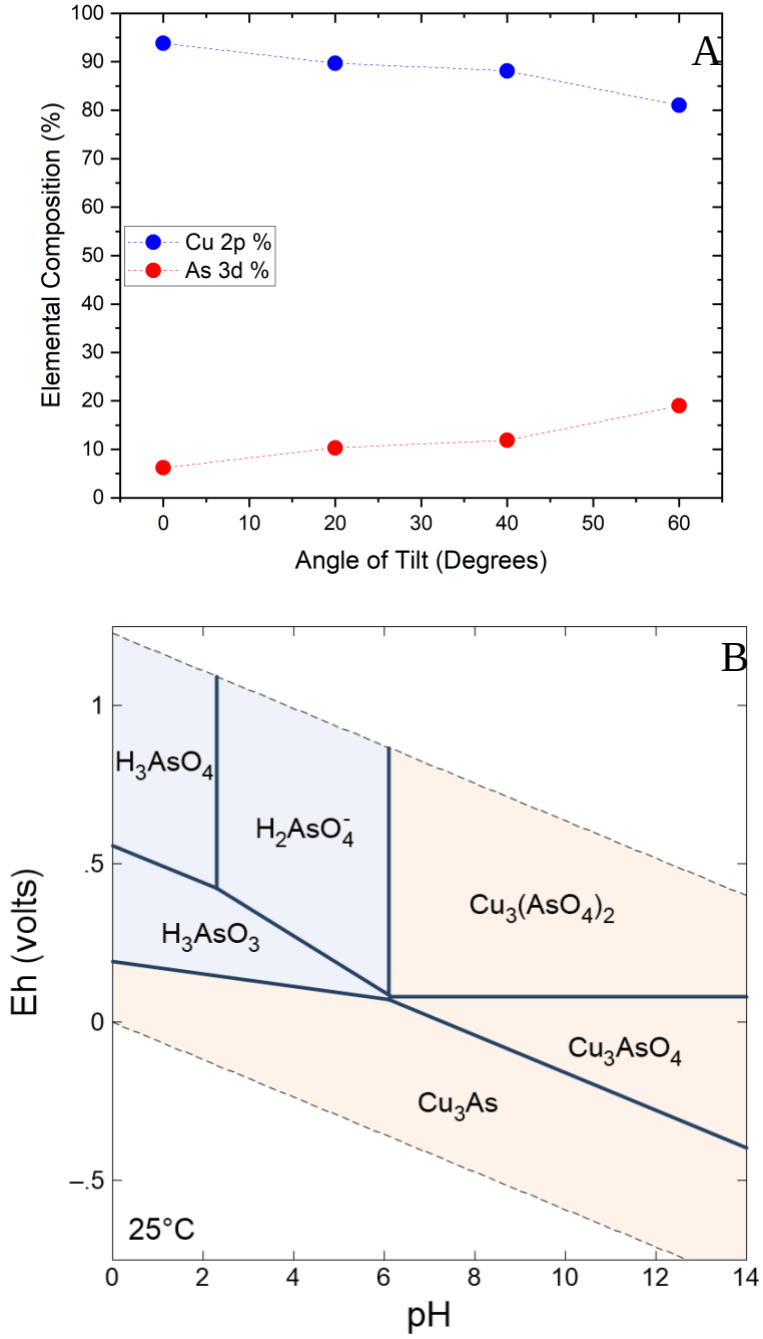

Figure 5.4 A) Angle resolved x-ray photoelectron spectroscopy showing the elemental composition at the Au(UTF) surface after 60 s of deposition at 0 V vs. RHE in 750 $\mu g \cdot L^{-1}$ As (III) and 10 mg $\cdot L^{-1}$ Cu (II) mixture **B)** Eh vs. pH diagram for 750 $\mu g \cdot L^{-1}$ As (III), 1 mg $\cdot L^{-1}$ Cu (II) at 25 ° C and 1.013 bars, generated using geochemist's workbench.

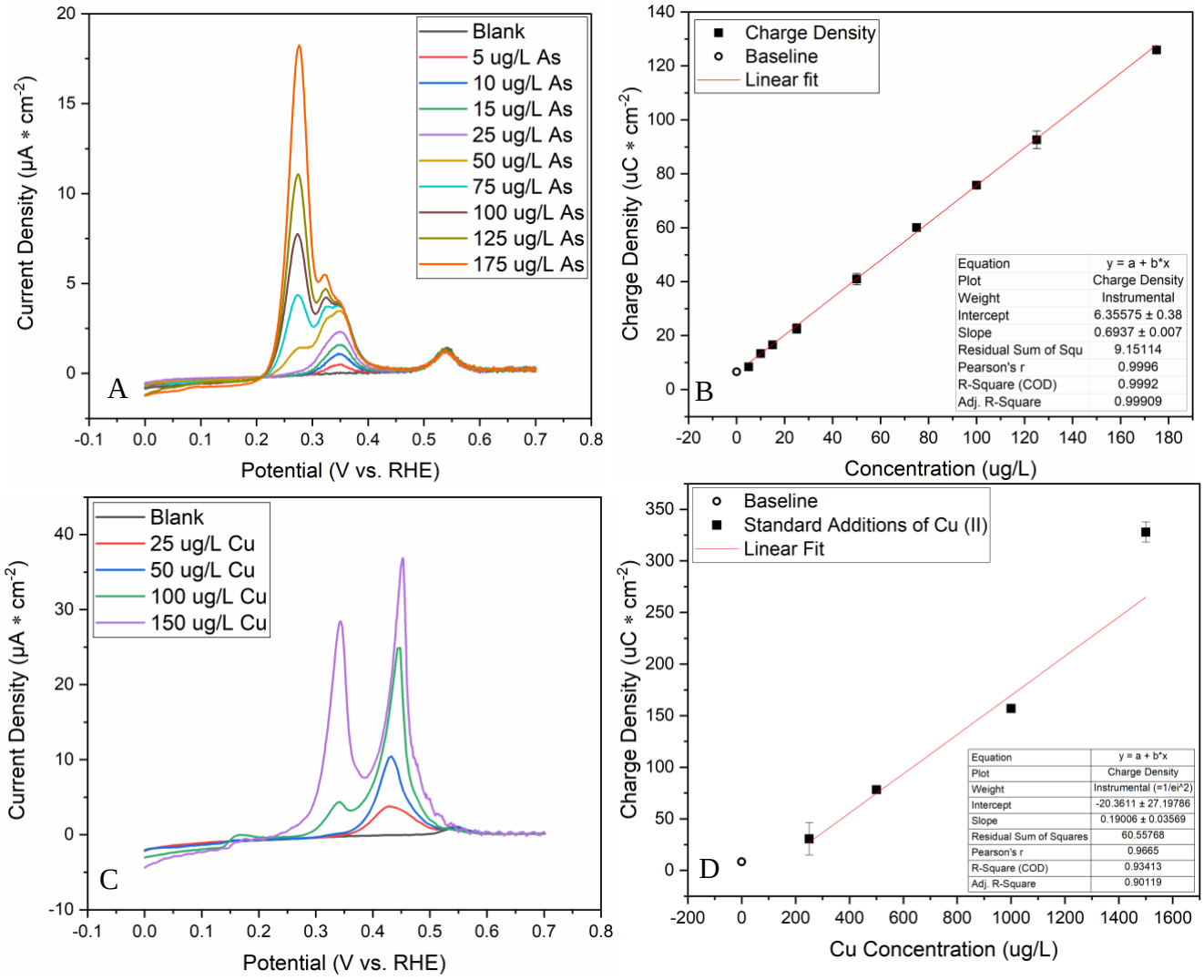

Figure 5.5 Linear stripping voltammetry curves produced by standard additions method for trace detection of **A)** 5, 10, 15, 25, 50, 75, 100, 125, and 175 µg L^{-1} As (III) with **B)** associated As (III) calibration curve and **C)** 250, 500, 1000, and 1500 µg L^{-1} Cu (II) with **D)** associated Cu (II) calibration curve.

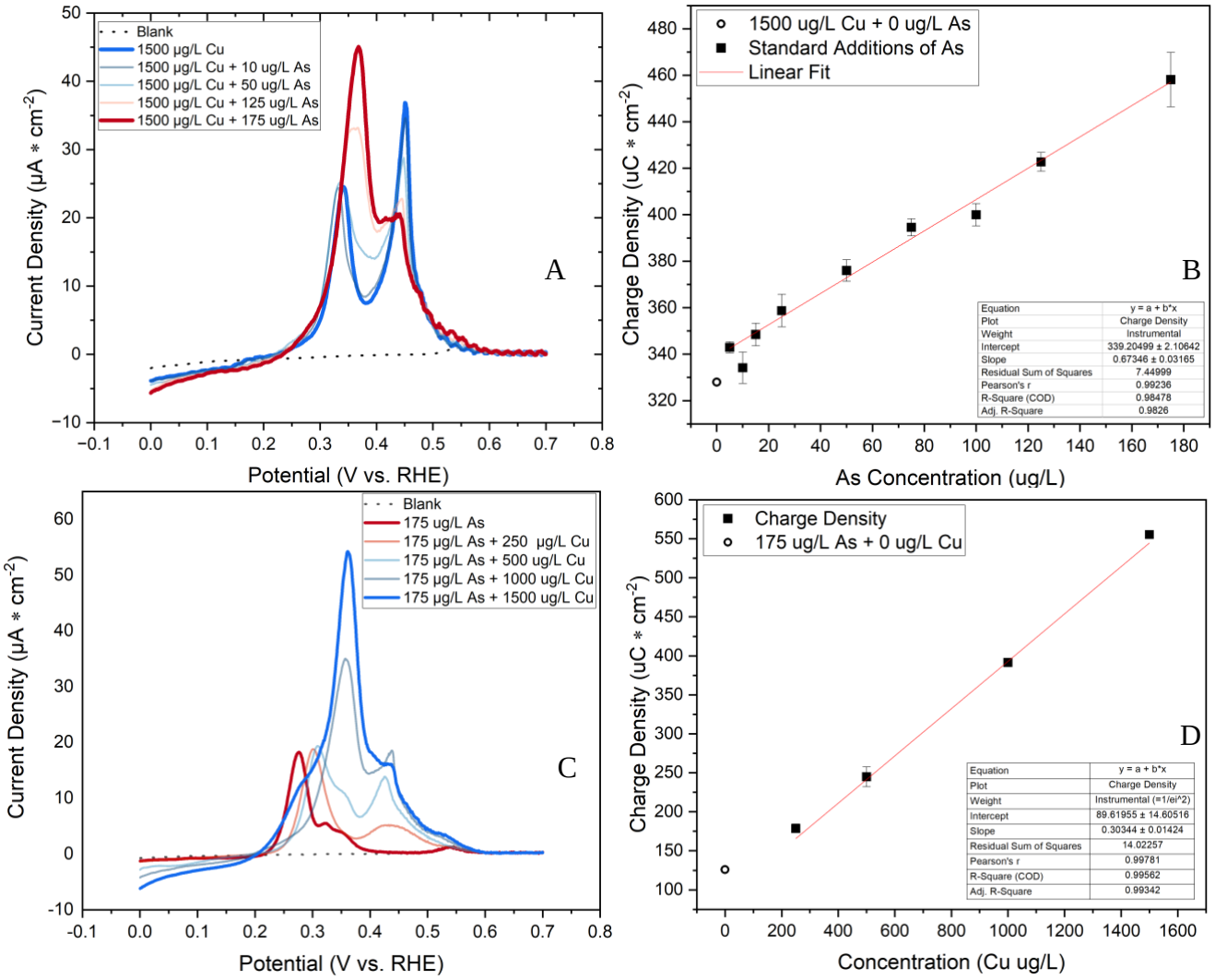

Figure 5.6 Selected LSV curves produced by standard additions method for trace detection of **A)** 5, 10, 15, 25, 50, 75, 100, 125, and 175 µg L^{-1} As (III) to a solution containing 1500 µg L^{-1} Cu (II) with **B)** associated As (III) calibration curve, and **C)** 250, 500, 1000, and 1500 µg L^{-1} Cu (II) to a solution containing 175 µg L^{-1} As (III) with **D)** associated Cu (II) calibration curve.

5.7 References

Uncategorized References

(1) Ng, J. C.; Wang, J.; Shraim, A. A global health problem caused by arsenic

from natural sources. Pergamon: Chemosphere, 2003.
(2) Shankar, S.; Shanker, U.; Shikha. Arsenic contamination of groundwater: a review of sources, prevalence, health risks, and strategies for mitigation. *ScientificWorldJournal* **2014**, *2014*, 304524. DOI: 10.1155/2014/304524.
(3) Bencko, V.; Yan Li Foong, F. The history of arsenical pesticides and health risks related to the use of Agent Blue. *Ann Agric Environ Med* **2017**, *24* (2), 312-316. DOI: 10.26444/aaem/74715 From NLM.
(4) Berg, M. M. Arsenic contamination of groundwater and drinking water in Vietnam: a human health threat. *Environ. Sci. Technol.* **2001**, *35* (13), 2621-2626. DOI: https://doi.org/10.1021/es010027y.
(5) Rahman, A. H. S. E. O. L. M. Contamination of drinking-water by arsenic in Bangladesh: a public health emergency. *Bulletin of the World Health Organization* **2000**, *78*.
(6) USEPA. Priority Pollutant List. 2014; Vol. 40 CFR Part 423, Appendix A.
(7) Kurttio, P.; Hirose , A.; Fawell, J. WHO Guidelines for Drinking-water Quality. World Health Organization: 2010.
(8) Organization, W. H. *Exposure to Arsenic: A Major Public Health Concern*; 2010.
(9) Rahaman, M. S.; Rahman, M. M.; Mise, N.; Sikder, M. T.; Ichihara, G.; Uddin, M. K.; Kurasaki, M.; Ichihara, S. Environmental arsenic exposure and its contribution to human diseases, toxicity mechanism and management. *Environmental Pollution* **2021**, *289*, 117940. DOI: https://doi.org/10.1016/j.envpol.2021.117940.
(10) Podgorski, J. Global threat of arsenic in groundwater. *Science* **2020**, *368* (6493), 845-850. DOI: https://doi.org/10.1126/science.aba1510.
(11) Simmler, M. Reductive solubilization of arsenic in a mining-impacted river floodplain: Influence of soil properties and temperature. *Environ. Pollut.* **2017**, *231*, 722-731. From http://worldcat.org /z-wcorg/.
(12) Blake, J. M.; Avasarala, S.; Artyushkova, K.; Ali, A.-M. S.; Brearley, A. J.; Shuey, C.; Robinson, W. P.; Nez, C.; Bill, S.; Lewis, J.; et al. Elevated Concentrations of U and Co-occurring Metals in Abandoned Mine Wastes in a Northeastern Arizona Native American Community. *Environ. Sci. Technol.* **2015**, *49* (14), 8506-8514. DOI: https://doi.org/10.1021/acs.est.5b01408.
(13) Smedley, P. L. K., D.G. . A review of the source, behaviour and distribution of arsenic in natural waters. *Appl. Geochem.* **2002**, *17*, 517-568. DOI: https://doi.org/10.1016/S0883-2927(02)00018-5.
(14) Neil, C. W. Water Chemistry Impacts on Arsenic Mobilization from Arsenopyrite Dissolution and Secondary Mineral Precipitation: Implications for Managed Aquifer Recharge. *Environ. Sci. Technol.* **2014**, *48* (8), 4395-4405. From http://worldcat.org /z-wcorg/.
(15) Indika Herath, M. V., Saman Seneweera, Jochen Bundschuh. Thiolated arsenic in natural systems: What is current, what is new and what needs to be known. *Environmental International* **2018**, *115*, 370-386.

(16) LeMonte, J. J.; Stuckey, J. W.; Sanchez, J. Z.; Tappero, R.; Rinklebe, J.; Sparks, D. L. Sea Level Rise Induced Arsenic Release from Historically Contaminated Coastal Soils. *Environ. Sci. Technol.* **2017**, *51* (11), 5913-5922. DOI: https://doi.org/10.1021/acs.est.6b06152.
(17) Basu, A.; Saha, D.; Saha, R.; Ghosh, T.; Saha, B. A review on sources, toxicity and remediation technologies for removing arsenic from drinking water. *Res. Chem. Intermed.* **2014**, *40* (2), 447-485, Article. DOI: https://doi.org/10.1007/s11164-012-1000-4.
(18) Raqib, R.; Ahmed, S.; Sultana, R.; Wagatsuma, Y.; Mondal, D.; Hoque, A. W.; Nermell, B.; Yunus, M.; Roy, S.; Persson, L. A. Effects of in utero arsenic exposure on child immunity and morbidity in rural Bangladesh. *Toxicology letters* **2009**, *185* (3), 197-202.
(19) Komorowicz Izabela, I.; Baralkiewicz, D. Arsenic and its speciation in water samples by high performance liquid chromatography inductively coupled plasma mass spectrometry--last decade review. *Talanta* **2011**, *84* (2), 247-261. From http://worldcat.org /z-wcorg/.
(20) Profumo, A.; Merli, D.; Pesavento, M. Voltammetric determination of inorganic As(III) and total inorganic As in natural waters. *Analytica Chimica Acta* **2005**, *539* (1), 245-250. DOI: https://doi.org/10.1016/j.aca.2005.02.062.
(21) Song, Y.; Swain, G. M. Development of a Method for Total Inorganic Arsenic Analysis Using Anodic Stripping Voltammetry and a Au-Coated, Diamond Thin-Film Electrode. *Analytical Chemistry* **2007**, *79* (6), 2412-2420. DOI: 10.1021/ac061543f.
(22) Henry, F. T. Determination of trace level arsenic (III), arsenic(V), and total inorganic arsenic by differential pulse polarography. *Anal. Chem.* **1979**, *51*, 215-218. From http://worldcat.org /z-wcorg/.
(23) Dugo, G.; La Pera, L.; Lo Turco, V.; Di Bella, G. Speciation of inorganic arsenic in alimentary and environmental aqueous samples by using derivative anodic stripping chronopotentiometry (dASCP). *Chemosphere* **2005**, *61* (8), 1093-1101. DOI: https://doi.org/10.1016/j.chemosphere.2005.03.049.
(24) USEPA. METHOD 7063: ARSENIC IN AQUEOUS SAMPLES AND EXTRACTS

BY ANODIC STRIPPING VOLTAMMETRY (ASV). 1996.
(25) Babar, N. U.; Joya, K. S.; Tayyab, M. A.; Ashiq, M. N.; Sohail, M. Highly Sensitive and Selective Detection of Arsenic Using Electrogenerated Nanotextured Gold Assemblage. *ACS Omega* **2019**, *4* (9), 13645-13657. DOI: https://doi.org/10.1021/acsomega.9b00807.
(26) Xiao, L.; Wildgoose, G. G.; Compton, R. G. Sensitive electrochemical detection of arsenic (III) using gold nanoparticle modified carbon nanotubes via anodic stripping voltammetry. *Analytica Chimica Acta* **2008**, *620* (1), 44-49. DOI: https://doi.org/10.1016/j.aca.2008.05.015.
(27) Li, C.-Y.; Wei, Y.-Y.; Shen, W.; Dong, X.; Yang, M.; Wei, J. Ultrahigh sensitivity electroanalysis of trace As(III) in water and human serum via gold nanoparticles uniformly anchored to Co3O4 porous microsheets. *Electrochimica Acta* **2021**, *368*, 137605. DOI: https://doi.org/10.1016/j.electacta.2020.137605.
(28) Mardegan, A.; Scopece, P.; Lamberti, F.; Meneghetti, M.; Moretto, L. M.; Ugo, P. Electroanalysis of Trace Inorganic Arsenic with Gold Nanoelectrode Ensembles. *Electroanalysis* **2012**, *24* (4), 798-806. DOI: https://doi.org/10.1002/elan.201100555.
(29) Buffa, A.; Mandler, D. Arsenic(III) detection in water by flow-through carbon nanotube membrane decorated by gold nanoparticles. *Electrochimica Acta* **2019**, *318*, 496-503. DOI: https://doi.org/10.1016/j.electacta.2019.06.114.

(30) Forsberg, G.; Olaughlin, J. W.; Megargle, R. G.; Koirtyohann, S. R. Determination of arsenic by anodic stripping voltammetry and differential pulse anodic stripping voltammetry. *Anal. Chem.* **1975**, *47*, 1586-1592. DOI: https://doi.org/10.1021/ac60359a057.
(31) Metrohm. *Two, Three and Four Electrode Experiments*. https://www.gamry.com/application-notes/electrodes-cells/two-three-and-four-electrode-experiments/ (accessed 01/16/19).
(32) Vanysek, P. Electrochemical series. *CRC handbook of chemistry and physics* **2000**, *8*.
(33) Pourbaix, M. Atlas of electrochemical equilibria in aqueous solution. *Corrosion Science* **1966**, *10*, 343.
(34) Bard, A. J.; Faulkner, L. R. Chapter 7: Polarography and Pulse Voltammetry. In *Electrochemical Methods: Fundamentals and Applications*, John Wiley & sons, 2001; pp 275-301.
(35) Dai, X.; Nekrassova, O.; Hyde, M. E.; Compton, R. G. Anodic Stripping Voltammetry of Arsenic(III) Using Gold Nanoparticle-Modified Electrodes. *Anal. Chem.* **2004**, *76*, 5924-5929.
(36) Dai, X.; Compton, R. G. Determination of Copper in the Presence of Various Amounts of Arsenic withL-Cysteine Modified Gold Electrodes. *Electroanalysis* **2005**, *17* (20), 1835-1840. DOI: 10.1002/elan.200503310.
(37) Jia, Z.; Simm, A. O.; Dai, X.; Compton, R. G. The electrochemical reaction mechanism of arsenic deposition on an Au(111) electrode. *J. Electroanal. Chem.* **2006**, *587* (2), 247-253. DOI: https://doi.org/10.1016/j.jelechem.2005.11.017.
(38) Zhang, Y.; Li, D.; Compton, R. G. Arsenic (III) Detection with Underpotential Deposition and Anodic Stripping Voltammetry. *ChemElectroChem* **2021**, *8* (19), 3707-3715. DOI: https://doi.org/10.1002/celc.202101022.
(39) Stanković, A.; Kajinić, Ž.; Turkalj, J. V.; Romić, Ž.; Sikirić, M. D.; Asserghine, A.; Nagy, G.; Medvidović-Kosanović, M. Voltammetric Determination of Arsenic with Modified Glassy Carbon Electrode. *Electroanalysis* **2020**, *32* (5), 1043-1051. DOI: 10.1002/elan.201900666.
(40) Yamada, D.; Ivandini, T. A.; Komatsu, M.; Fujishima, A.; Einaga, Y. Anodic stripping voltammetry of inorganic species of As3+ and As5+ at gold-modified boron doped diamond electrodes. *Journal of Electroanalytical Chemistry* **2008**, *615* (2), 145-153. DOI: https://doi.org/10.1016/j.jelechem.2007.12.004.
(41) Bu, L.; Liu, J.; Xie, Q.; Yao, S. Anodic stripping voltammetric analysis of trace arsenic(III) enhanced by mild hydrogen-evolution at a bimetallic Au–Pt nanoparticle modified glassy carbon electrode. *Electrochemistry Communications* **2015**, *59*, 28-31. DOI: https://doi.org/10.1016/j.elecom.2015.06.015.
(42) Han, D.-D.; Li, S.-S.; Guo, Z.; Chen, X.; Liu, J.-H.; Huang, X.-J. Shape dependent stripping behavior of Au nanoparticles toward arsenic detection: evidence of enhanced sensitivity on the Au (111) facet. *RSC Adv.* **2016**, *6* (36), 30337-30344. DOI: https://doi.org/10.1039/c5ra27778g.
(43) Kanido Camerun Kastro, M. J. S., Hwakyeung Jeong, and Joongwon Kim. Effect of Nanostructures of Au Electrodes on the Electrochemical Detection of As. *J. Electrochem. Sci. Technol* **2019**. DOI: https://doi.org/10.5229/JECST.2019.10.2.206.
(44) Nunez-Bajo, E.; Blanco-Lopez, M. C.; Costa-Garcia, A.; Fernandez-Abedul, M. T. Electrogeneration of Gold Nanoparticles on Porous-Carbon Paper-Based Electrodes and Application to Inorganic Arsenic Analysis in White Wines by Chronoamperometric

Stripping. *Anal. Chem.* **2017**, *89* (12), 6415-6423. DOI: https://doi.org/10.1021/acs.analchem.7b00144.
(45) Salaun, P.; Planer-Friedrich, B.; van den Berg, C. M. Inorganic arsenic speciation in water and seawater by anodic stripping voltammetry with a gold microelectrode. *Anal Chim Acta* **2007**, *585* (2), 312-322. DOI: 10.1016/j.aca.2006.12.048.
(46) Karimov, K. A.; Rogozhnikov, D. A.; Kuzas, E. A.; Shoppert, A. A. Leaching Kinetics of Arsenic Sulfide-Containing Materials by Copper Sulfate Solution. *Metals* **2019**, *10* (1). DOI: 10.3390/met10010007.
(47) Shishin, D.; Jak, E. Critical assessment and thermodynamic modeling of the Cu-As system. *Calphad* **2018**, *60*, 134-143. DOI: https://doi.org/10.1016/j.calphad.2017.12.005.
(48) Reid, K. D.; Goff, F.; Counce, D. A. Arsenic concentration and mass flow rate in natural waters of the Valles caldera and Jemez Mountains region, New Mexico. *N. M. Geol.* **2003**, *25* (3), 75-82.
(49) Metrohm. *scTRACE Gold*. 2013. https://www.metrohm.com/en-us/products-overview/61258000 (accessed.
(50) Fischer, L. M.; Tenje, M.; Heiskanen, A. R.; Masuda, N.; Castillo, J.; Bentien, A.; Émneus, J.; Jakobsen, M. H.; Boisen, A. Gold cleaning methods for electrochemical detection applications. *Microelectron. Eng.* **2009**, *86* (4-6), 1282-1285. DOI: 10.1016/j.mee.2008.11.045.
(51) Ren, B.; Jones, L. A.; Chen, M.; Oppedisano, D. K.; Qiu, D.; Ippolito, S. J.; Bhargava, S. K. The Effect of Electrodeposition Parameters and Morphology on the Performance of Au Nanostructures for the Detection of As (III). *J. Electrochem. Soc.* **2017**, *164* (14), H1121-H1128. DOI: https://doi.org/10.1149/2.1261714jes.
(52) Kuzume, A.; Herrero, E.; Feliu, J. M. Oxygen reduction on stepped platinum surfaces in acidic media. *J. Electroanal. Chem.* **2007**, *599* (2), 333-343. DOI: https://doi.org/10.1016/j.jelechem.2006.05.006.
(53) Feliu, J. M.; Fernandez-Vega, A.; Aldaz, A.; Clavilier, J. New observations of a structure sensitive electrochemical behaviour of irreversibly adsorbed arsenic and antimony from acidic solutions on Pt (111) and Pt (100) orientations. *J. Electroanal. Chem. Interfacial Electrochem.* **1988**, *256* (1), 149-163. DOI: https://doi.org/10.1016/0022-0728(88)85014-9.
(54) Rizo, R.; Pastor, E.; Koper, M. T. M. CO electrooxidation on Sn-modified Pt single crystals in acid media. *J. Electroanal. Chem.* **2017**, *800*, 32-38, Article. DOI: https://doi.org/10.1016/j.jelechem.2016.10.014.
(55) Fang, Y.; Ding, S. Y.; Zhang, M.; Steinmann, S. N.; Hu, R.; Mao, B. W.; Feliu, J. M.; Tian, Z. Q. Revisiting the Atomistic Structures at the Interface of Au(111) Electrode-Sulfuric Acid Solution. *J. Am. Chem. Soc.* **2020**, *142* (20), 9439-9446. DOI: https://doi.org/10.1021/jacs.0c02639.
(56) Gisbert-González, J. M.; Oliver-Pardo, M. V.; Sarabia, F. J.; Climent, V.; Feliu, J. M.; Herrero, E. On the behavior of CTAB/CTAOH adlayers on gold single crystal surfaces. *Electrochim. Acta* **2021**, *391*. DOI: https://doi.org/10.1016/j.electacta.2021.138947.
(57) Rodes, A.; Herrero, E.; Feliu, J. M.; Aldaz, A. Structure sensitivity of irreversibly adsorbed tin on gold single-crystal electrodes in acid media. *J. Chem. Soc. Faraday Trans.* **1996**, *92* (20), 3769-3776, 10.1039/FT9969203769. DOI: https://doi.org/10.1039/FT9969203769.

(58) Hamelin, A. Underpotential deposition of lead on single crystal faces of gold: Part I. The influence of crystallographic orientation of the substrate. *J. Electroanal. Chem. Interfacial Electrochem.* **1984**, *165* (1), 167-180. DOI: https://doi.org/10.1016/S0022-0728(84)80095-9.
(59) Hamelin, A.; Lipkowski, J. Underpotential deposition of lead on gold single crystal faces: Part II. General discussion. *J. Electroanal. Chem. Interfacial Electrochem.* **1984**, *171* (1), 317-330. DOI: https://doi.org/10.1016/0022-0728(84)80123-0.
(60) Zhang, Y.; Li, D.; Compton, R. G. Arsenic (III) detection with underpotential deposition on gold. *J. Electroanal. Chem.* **2022**, *909*. DOI: https://doi.org/10.1016/j.jelechem.2022.116154.
(61) Lebedeva, N. P.; Rodes, A.; Feliu, J. M.; Koper, M. T. M.; van Santen, R. A. Role of Crystalline Defects in Electrocatalysis: CO Adsorption and Oxidation on Stepped Platinum Electrodes As Studied by in situ Infrared Spectroscopy. *J. Phys. Chem. B* **2002**, *106* (38), 9863-9872. DOI: https://doi.org/10.1021/jp0203806.
(62) Kishioka, S.-y.; Nishino, J.; Sakaguchi, H. Fabrication of Stable, Highly Flat Gold Film Electrodes with an Effective Thickness on the Order of 10 nm. *Analytical Chemistry* **2007**, *79* (17), 6851-6856. DOI: 10.1021/ac070603u.
(63) Kim, M.; Ha, W.-J.; Anh, J.-W.; Kim, H.-S.; Park, S.-W.; Lee, D. Fabrication of nanoporous gold thin films on silicon substrate by multilayer deposition of Au and Ag. *J. Alloys Compd.* **2009**, *484*, 28-32. DOI: 10.1016/j.jallcom.2009.05.067.
(64) WHO. *Arsenic Fact Sheet*. World Health Organization, 2010. https://www.who.int/news-room/fact-sheets/detail/arsenic (accessed 2022 07/21).
(65) Weber, F.-A.; Hofacker, A. F.; Voegelin, A.; Kretzschmar, R. Temperature Dependence and Coupling of Iron and Arsenic Reduction and Release during Flooding of a Contaminated Soil. *Environ. Sci. Technol.* **2010**, *44* (1), 116-122. DOI: 10.1021/es902100h.
(66) Shi, Z.; Hu, S.; Lin, J.; Liu, T.; Li, X.; Li, F. Quantifying Microbially Mediated Kinetics of Ferrihydrite Transformation and Arsenic Reduction: Role of the Arsenate-Reducing Gene Expression Pattern. *Environ. Sci. Technol.* **2020**, *54* (11), 6621-6631. DOI: 10.1021/acs.est.9b07137.
(67) Wilkin, R. T.; Ford, R. G.; Costantino, L. M.; Ross, R. R.; Beak, D. G.; Scheckel, K. G. Thioarsenite Detection and Implications for Arsenic Transport in Groundwater. *Environ. Sci. Technol.* **2019**, *53* (20), 11684-11693. DOI: 10.1021/acs.est.9b04478.
(68) Renock, D.; Voorhis, J. Electrochemical Investigation of Arsenic Redox Processes on Pyrite. *Environ. Sci. Technol.* **2017**, *51* (7), 3733-3741. DOI: 10.1021/acs.est.6b06018.
(69) Hung, D. Q.; Nekrassova, O.; Compton, R. G. Analytical methods for inorganic arsenic in water: a review. *Talanta* **2004**, *64* (2), 269-277, Periodical. From EBSCOhost edsbl.
(70) Das Joyati, J.; Sarkar, P.; Panda, J.; Pal, P. Low-cost field test kits for arsenic detection in water. *J. Environ. Sci. Health., A* **2014**, *49* (1), 108-115. From http://worldcat.org /z-wcorg/.
(71) *Determination of arsenic in water with the scTRACE Gold*; 416; Metrohm.
(72) Bullen, J. C.; Torres-Huerta, A.; Salaun, P.; Watson, J. S.; Majumdar, S.; Vilar, R.; Weiss, D. J. Portable and rapid arsenic speciation in synthetic and natural waters by an As(V)-selective chemisorbent, validated against anodic stripping voltammetry. *Water Res* **2020**, *175*, 115650. DOI: https://doi.org/10.1016/j.watres.2020.115650.
(73) Cox, J. A.; Rutkowska, I. A.; Kulesza, P. J. Critical Review—Electrocatalytic Sensors for Arsenic Oxo Species. *J. Electrochem. Soc.* **2020**, *167* (3), 037565. DOI: https://doi.org/10.1149/1945-7111/ab697d.

(74) Welch Christine, M. C.; Compton, R. G. The use of nanoparticles in electroanalysis: a review. *Anal. Bioanal. Chem.* *384* (3), 601-619. From http://worldcat.org /z-wcorg/.
(75) Burke, L. D.; Nugent, P. F. The electrochemistry of gold: I the redox behaviour of the metal in aqueous media. *Gold Bull.* **1997**, *30* (2), 43-53.
(76) Gu, T.; Bu, L.; Huang, Z.; Liu, Y.; Tang, Z.; Liu, Y.; Huang, S.; Xie, Q.; Yao, S.; Tu, X.; et al. Dual-signal anodic stripping voltammetric determination of trace arsenic(III) at a glassy carbon electrode modified with internal-electrolysis deposited gold nanoparticles. *Electrochem. Commun.* **2013**, *33*, 43-46. DOI: https://doi.org/10.1016/j.elecom.2013.04.019.
(77) Huang, J.-F.; Chen, H.-H. Gold-nanoparticle-embedded nafion composite modified on glassy carbon electrode for highly selective detection of arsenic(III). *Talanta* **2013**, *116*, 852-859, Article. DOI: https://doi.org/10.1016/j.talanta.2013.07.063.
(78) Jena Bikash Kumar, B. K.; Raj, C. R. Gold nanoelectrode ensembles for the simultaneous electrochemical detection of ultratrace arsenic, mercury, and copper. *Anal. Chem.* **2008**, *80* (13), 4836-4844. From http://worldcat.org /z-wcorg/.
(79) Dai Xuan, X.; Wildgoose, G. G.; Salter, C.; Crossley, A.; Compton, R. G. Electroanalysis using macro-, micro-, and nanochemical architectures on electrode surfaces. Bulk surface modification of glassy carbon microspheres with gold nanoparticles and their electrical wiring using carbon nanotubes. *Anal. Chem.* **2006**, *78* (17), 6102-6108. DOI: https://doi.org/10.1021/ac060582o.
(80) Song, Y.; Swain, G. M. Total inorganic arsenic detection in real water samples using anodic stripping voltammetry and a gold-coated diamond thin-film electrode. *Anal. Chim. Acta.* **2007**, *593* (1), 7-12. DOI: 10.1016/j.aca.2007.04.033.
(81) Viltchinskaia E. A., Z. L. L., Garcia D.M., Santos P.F. Simultaneous determination of Mercury and Arsenic by Anodic Stripping Voltammetry. *Electroanalysis* **1996**, *9*, 633 - 640.
(82) Wu, J.; Yang, M.; Xiao, J.; Fu, X.; Jin, J.; Li, L.; Chang, W.; Xie, C. Gold Nanoparticle Dropped Titania Microsphere Hybrids as an Enhanced Sensitive Material for Stripping Voltammetry Determination of As (III). *J. Electrochem. Soc.* **2013**, *160* (11), B225-B230. DOI: 10.1149/2.103311jes.
(83) Kato, D.; Kamata, T.; Kato, D.; Yanagisawa, H.; Niwa, O. Au Nanoparticle-Embedded Carbon Films for Electrochemical As(3+) Detection with High Sensitivity and Stability. *Anal. Chem.* **2016**, *88* (5), 2944-2951. DOI: 10.1021/acs.analchem.6b00136.
(84) Kumar, S. A.; Wang, S.-F.; Chang, Y.-T. Poly(BCB)/Au-nanoparticles hybrid film modified electrode: Preparation, characterization and its application as a non-enzymatic sensor. *Thin Solid Films* **2010**, *518* (20), 5832-5838. DOI: https://doi.org/10.1016/j.tsf.2010.05.076.
(85) Mehran, Q. M.; Fazal, M. A.; Bushroa, A. R.; Rubaiee, S. A Critical Review on Physical Vapor Deposition Coatings Applied on Different Engine Components. *Crit. Rev. Solid State Mater. Sci.* **2017**, *43* (2), 158-175. DOI: 10.1080/10408436.2017.1320648.
(86) Shahidi, S.; Moazzenchi, B.; Ghoranneviss, M. A review-application of physical vapor deposition (PVD) and related methods in the textile industry. *Eur. Phys. J. Appl. Phys.* **2015**, *71* (3), 31302. DOI: 10.1051/epjap/2015140439.
(87) Mo, A. K.; Brown, V. L.; Rugg, B. K.; DeVore, T. C.; Meyer, H. M.; Hu, X.; Hughes, W. C.; Augustine, B. H. Understanding the Mechanism of Solvent-Mediated Adhesion of Vacuum Deposited Au and Pt Thin Films onto PMMA Substrates. *Adv. Funct. Mater* **2013**, *23* (11), 1431-1439. DOI: 10.1002/adfm.201201955.

(88) Tanami, S.; Ichida, D.; Hashimoto, S.; Seo, H.; Yamashita, D.; Itagaki, N.; Koga, K.; Shiratani, M. Low temperature rapid formation of Au-induced crystalline Ge films using sputtering deposition. *Thin Solid Films* **2017**, *641*, 59-64. DOI: 10.1016/j.tsf.2017.02.067.
(89) Kim, K.; Park, J.; Kim, H.; Jung, G. Y.; Kim, M.-G. Solid-Phase Photocatalysts: Physical Vapor Deposition of Au Nanoislands on Porous TiO2 Films for Millimolar H2O2 Production within a Few Minutes. *ACS Catal.* **2019**, *9* (10), 9206-9211. DOI: 10.1021/acscatal.9b02269.
(90) van der Zalm, J.; Chen, S.; Huang, W.; Chen, A. Review—Recent Advances in the Development of Nanoporous Au for Sensing Applications. *J. Electrochem. Soc.* **2020**, *167* (3), 037532. DOI: https://doi.org/10.1149/1945-7111/ab64c0.
(91) Jiang, J.; Wang, C. Review—Electrolytic Metal Atoms Enabled Manufacturing of Nanostructured Sensor Electrodes. *J. Electrochem. Soc.* **2020**, *167* (3), 037521. DOI: 10.1149/2.0212003jes.
(92) Thangphatthanarungruang, J.; Lomae, A.; Chailapakul, O.; Chaiyo, S.; Siangproh, W. A Low-cost Paper-based Diamond Electrode for Trace Copper Analysis at On-site Environmental Area. *Electroanalysis* **2020**, *33* (1), 226-232. DOI: https://doi.org/10.1002/elan.202060305.
(93) Pringkasemchai, A.; Hoshyargar, F.; Lertanantawong, B.; O'Mullane, A. P. Lightweight ITO Electrodes Decorated with Gold Nanostructures for Electrochemical Applications. *Electroanalysis* **2019**, *31* (11), 2095-2102. DOI: 10.1002/elan.201900152.
(94) Devi, N. R.; Sasidharan, M.; Sundramoorthy, A. K. Gold Nanoparticles-Thiol-Functionalized Reduced Graphene Oxide Coated Electrochemical Sensor System for Selective Detection of Mercury Ion. *J. Electrochem. Soc.* **2018**, *165* (8), B3046-B3053. DOI: https://doi.org/10.1149/2.0081808jes.
(95) Carmo, M.; Linardi, M.; Poco, J. G. R. Characterization of nitric acid functionalized carbon black and its evaluation as electrocatalyst support for direct methanol fuel cell applications. *Appl. Catal. A Gen.* **2009**, *355*, 132-138, Article. DOI: 10.1016/j.apcata.2008.12.010 From EBSCOhost edselp.
(96) Prati, L.; Martra, G. New gold catalysts for liquid phase oxidation. *Gold Bull.* **1999**, *32* (3), 96-101. DOI: Doi 10.1007/Bf03216617.
(97) Blake, J. M.; Vore, C. L. D.; Avasarala, S.; Ali, A.-M.; Roldan, C.; Bowers, F.; Spilde, M. N.; Artyushkova, K.; Kirk, M. F.; Peterson, E.; et al. Uranium mobility and accumulation along the Rio

Paguate, Jackpile Mine in Laguna Pueblo, NM. *Environ. Sci. Process Impacts* **2017**, *19*, 605-621.
(98) Palli, S.; R. Dey, S. Thermal stability of pulse electroplated gold films: SEM-EBSD studies. *Adv. Mater. Sci.* **2017**, *2* (1), 1-6. DOI: 10.15761/ams.1000118.
(99) Thompson, C. V. Structure Evolution During Processing of Polycrystalline Films. *Annu. Rev. Mater. Sci.* **2000**, *30* (1), 159, Article. DOI: 10.1146/annurev.matsci.30.1.159 From EBSCOhost bth.
(100) Wei, P.; Katmis, F.; Chang, C. Z.; Moodera, J. S. Induced Superconductivity and Engineered Josephson Tunneling Devices in Epitaxial (111)-Oriented Gold/Vanadium Heterostructures. *Nano Lett.* **2016**, *16* (4), 2714-2719. DOI: 10.1021/acs.nanolett.6b00361.

(101) Luo, X.; Morrin, A.; Killard, A. J.; Smyth, M. R. Application of Nanoparticles in Electrochemical Sensors and Biosensors. *Electroanalysis* **2006**, *18* (4), 319-326. DOI: 10.1002/elan.200503415.
(102) Copeland, T. K. Analytical applications of pulsed voltammetric stripping at thin film mercury electrodes. *Anal. Chem.* **1973**, *45*, 2171-2174. From http://worldcat.org /z-wcorg/.
(103) Kachoosangi, R. T.; Compton, R. G. Voltammetric determination of Chromium(VI) using a gold film modified carbon composite electrode. *Sens. Actuators B Chem.* **2013**, *178*, 555-562. DOI: 10.1016/j.snb.2012.12.122.
(104) Sikdar, S.; Kundu, M. A Review on Detection and Abatement of Heavy Metals. *ChemBioEng Rev.* **2017**, *5* (1), 18-29. DOI: https://doi.org/10.1002/cben.201700005.
(105) Ferguson, J. F.; Gavis, J. Review of the arsenic cycle in natural waters. *Water Res.* **1972**, *6*, 1259-1274, Article. DOI: https://doi.org/10.1016/0043-1354(72)90052-8.
(106) Korte, N. E. Q., Fernando. A review of arsenic (III) in groundwater. *Crit. rev. environ. control* **1991**, *21*, 1-39. DOI: https://doi.org/10.1080/10643389109388408.
(107) Stuckey, Jason W.; Schaefer, Michael V.; Kocar, Benjamin D.; Benner, Shawn G.; Fendorf, S. Arsenic release metabolically limited to permanently water-saturated soil in Mekong Delta. *Nat. Geosci.* **2016**, *9* (1), 70-76. DOI: https://doi.org/10.1038/ngeo2589.
(108) deLemos, J. L.; Bostick, B. C.; Renshaw, C. E.; StÜrup, S.; Feng, X. Landfill-Stimulated Iron Reduction and Arsenic Release at the Coakley Superfund Site (NH). *Environ. Sci. Technol.* **2006**, *40* (1), 67-73. DOI: https://doi.org/10.1021/es051054h.
(109) He, C.; Tao, M.; Zhang, C.; He, Y.; Xu, W.; Liu, Y.; Zhu, W. Microelectrode-Based Electrochemical Sensing Technology for in Vivo Detection of Dopamine: Recent Developments and Future Prospects. *Crit. Rev. Environ. Control* **2022**, *52*, 544-554, Periodical. DOI: https://doi.org/10.1080/10408347.2020.1811946.
(110) Fleischmann, M.; Pons, S. The behavior of microelectrodes. *Anal. Chem.* **1987**, *59* (24), 1391A-1399A. DOI: https://doi.org/10.1021/ac00151a001.
(111) Compton, R. G.; Wildgoose, G. G.; Rees, N. V.; Streeter, I.; Baron, R. Design, fabrication, characterisation and application of nanoelectrode arrays. *Chem. Phys. Lett.* **2008**, *459* (1), 1-17. DOI: https://doi.org/10.1016/j.cplett.2008.03.095.
(112) Borrill, A. J.; Reily, N. E.; Macpherson, J. V. Addressing the practicalities of anodic stripping voltammetry for heavy metal detection: a tutorial review. *Analyst* **2019**, *144* (23), 6834-6849. DOI: https://doi.org/10.1039/c9an01437c.
(113) Buffa, A.; Mandler, D. Arsenic(III) detection in water by flow-through carbon nanotube membrane decorated by gold nanoparticles. *Electrochim. Acta* **2019**, *318*, 496-503. DOI: https://doi.org/10.1016/j.electacta.2019.06.114.
(114) Garcia-Gonzalez, R.; Fernandez-Abedul, M. T.; Costa-Garcia, A. Nafion(R) modified-screen printed gold electrodes and their carbon nanostructuration for electrochemical sensors applications. *Talanta* **2013**, *107*, 376-381. DOI: https://doi.org/10.1016/j.talanta.2013.01.034.
(115) Hamilton, E. T. W. J.; Florence, T. M. Determination of arsenic and antimony in electrolytic copper by anodic stripping voltammetry at a gold film electrode. *Anal. Chim. Acta* **1980**, *119* (2), 225-233, Article. DOI: https://doi.org/10.1016/S0003-2670(01)93621-9.
(116) Casuse, T. Q.; Benavidez, A.; Plumley, J. B.; Tsui, L.-k.; Ali, A.-M.; Cerrato, J. M.; Garzon, F. H. DC Sputtered Ultralow Loading Gold Nanofilm Electrodes for Detection of As (III) in Water. *ECS Sens. Plus* **2022**, *1* (1), 014602. DOI: https://doi.org/10.1149/2754-2726/ac6d67.

(117) Udayan, A. P. M.; Kachwala, B.; Karthikeyan, K. G.; Gunasekaran, S. Ultrathin quasi-hexagonal gold nanostructures for sensing arsenic in tap water. *RSC Adv.* **2020**, *10* (34), 20211-20221. DOI: https://doi.org/10.1039/d0ra02750b.
(118) Jiang, X.; Ma, J.; Jiang, G.; Xu, M.; Huang, X.; Gao, G.; Dai, X. Preparation of Gold Nanoplates Using Ortho Carbonyl Compounds as Capping Agents for Electrochemical Sensing of Lead Ions. *Nanoscale Res. Lett.* **2021**, *16* (1), 57. DOI: https://doi.org/10.1186/s11671-021-03521-2.
(119) Salinas, S.; Mosquera, N.; Luis, Y.; Emerson, C.; Germán, Y.; Edgar, G. Surface Plasmon Resonance Nanosensor for the Detection of Arsenic in Water. *Sens. Transducers* **2014**, *183* (12), 97-102, article. DOI: https://doaj.org/article/4f3c21b9962f414cae3b42938e984c77.
(120) Bentley, C. L.; Kang, M.; Unwin, P. R. Nanoscale Surface Structure–Activity in Electrochemistry and Electrocatalysis. *J. Am. Chem. Soc.* **2019**, *141* (6), 2179-2193. DOI: https://doi.org/10.1021/jacs.8b09828.
(121) Clavilier, J.; Faure, R.; Guinet, G.; Durand, R. Preparation of monocrystalline Pt microelectrodes and electrochemical study of the plane surfaces cut in the direction of the {111} and {110} planes. *J. Electroanal. Chem. Interfacial Electrochem.* **1980**, *107* (1), 205-209. DOI: https://doi.org/10.1016/S0022-0728(79)80022-4.
(122) Technologies, P. *Ultra-Flat Gold Surfaces*. https://www.platypustech.com/gold-thin-films/ultra-flat-gold-films (accessed 10/25/2021).
(123) Hamelin, A. Cyclic voltammetry at gold single-crystal surfaces. Part 1. Behaviour at low-index faces. *J. Electroanaly. Chem.* **1996**, *407* (1/2), 1-11. DOI: https://doi.org/10.1016/0022-0728(95)04499-X.
(124) Dinan, T. E.; Jou, W. F.; Cheh, H. Y. Arsenic Deposition onto a Gold Substrate. *J. Electrochem. Soc.* **1989**, *136* (11), 3284-3287. DOI: https://doi.org/10.1149/1.2096439.
(125) Orozco, J.; Fernández-Sánchez, C.; Jiménez-Jorquera, C. Underpotential Deposition−Anodic Stripping Voltammetric Detection of Copper at Gold Nanoparticle-Modified Ultramicroelectrode Arrays. *Environ. Sci. Technol.* **2008**, *42* (13), 4877-4882. DOI: https://doi.org/10.1021/es8005964.
(126) Desimoni, E.; Palmisano, F.; Sabbatini, L. Simultaneous determination of tin and lead at the parts-per-billion level by coupling differential pulse anodic stripping voltammetry with a matrix exchange method. *Anal. Chem.* **1980**, *52* (12), 1889-1892. DOI: https://doi.org/10.1021/ac50062a026.
(127) Villegas, I.; Stickney, J. L. PRELIMINARY STUDIES OF GAAS DEPOSITION ON AU(100), (110), AND (111) SURFACES BY ELECTROCHEMICAL ATOMIC LAYER EPITAXY. *J. Electrochem. Soc.* **1992**, *139* (3), 686-694. DOI: https://doi.org/10.1149/1.2069285.
(128) Blum, L.; Huckaby, D. A. Underpotential deposition of Cu on Au(111): implications of the HB model. *J. Electroanal. Chem.* **1994**, *375* (1), 69-77. DOI: https://doi.org/10.1016/0022-0728(94)03336-6.
(129) Kopanica, M.; Novotný, L. Determination of traces of arsenic(III) by anodic stripping voltammetry in solutions, natural waters and biological material. *Analytica Chimica Acta* **1998**, *368* (3), 211-218. DOI: https://doi.org/10.1016/S0003-2670(98)00220-7.
(130) Wu, X.; Bowers, B.; Kim, D.; Lee, B.; Jun, Y. S. Dissolved Organic Matter Affects Arsenic Mobility and Iron(III) (hydr)oxide Formation: Implications for Managed Aquifer

Recharge. *Environ. Sci. Technol.* **2019**, *53* (24), 14357-14367. DOI: 10.1021/acs.est.9b04873.
(131) Murray, A.; Hall, A.; Weaver, J.; Kremer, F. Methods for Estimating Locations of Housing Units Served by Private Domestic Wells in the United States Applied to 2010. *JAWRA Journal of the American Water Resources Association* **2021**, *57* (5), 828-843. DOI: https://doi.org/10.1111/1752-1688.12937.
(132) Bo, Y.; Zhou, F.; Zhao, J.; Liu, J.; Liu, J.; Ciais, P.; Chang, J.; Chen, L. Additional surface-water deficit to meet global universal water accessibility by 2030. *Journal of Cleaner Production* **2021**, *320*. DOI: 10.1016/j.jclepro.2021.128829.
(133) Smedley, P. L. K., D.G. . A review of the source, behaviour and distribution

of arsenic in natural waters. *Appl. Geochem.* **2002**, *17*, 517-568. DOI: https://doi.org/10.1016/S0883-2927(02)00018-5.
(134) Forsberg, G.; Olaughlin, J. W.; Megargle, R. G.; Koirtyohann, S. R. DETERMINATION OF ARSENIC BY ANODIC-STRIPPING VOLTAMMETRY AND DIFFERENTIAL PULSE ANODIC-STRIPPING VOLTAMMETRY. *Analytical Chemistry* **1975**, *47* (9), 1586-1592. DOI: https://doi.org/10.1021/ac60359a057.
(135) Liu, Z.-G.; Huang, X.-J. Voltammetric determination of inorganic arsenic. *TrAC Trends in Analytical Chemistry* **2014**, *60*, 25-35. DOI: https://doi.org/10.1016/j.trac.2014.04.014.
(136) Hu Haibing, H. B.; Hu, H.; Xie, B.; Lu, Y.; Zhu, J. Advances in Electrochemical Detection Electrodes for As(III). *Nanomaterials* **2022**, *12* (5), 781. DOI: https://doi.org/10.3390/nano12050781.
(137) Adeloju, S. B.; Young, T. M.; Jagner, D.; Batley, G. E. Constant current cathodic stripping potentiometric determination of arsenic on a mercury film electrode in the presence of copper ions. *Analytica Chimica Acta* **1999**, *381* (2), 207-213. DOI: https://doi.org/10.1016/S0003-2670(98)00700-4.
(138) Yogarajah Nevetha, N.; Yogarajah, N.; Tsai, S. S. H. Detection of trace arsenic in drinking water: challenges and opportunities for microfluidics. *ENVIRONMENTAL SCIENCE-WATER RESEARCH TECHNOLOGY* **2015**, *1* (4), 426-447. From http://worldcat.org /z-wcorg/.
(139) Moreira, A.; Benedetti, A. V.; Cabot, P.; Sumodjo, P. Electrochemical behaviour of copper electrode in concentrated sulfuric acid solutions. *Electrochimica Acta* **1993**, *38* (7), 981-987.
(140) Kuzume, A.; Herrero, E.; Feliu, J. M.; Nichols, R. J.; Schiffrin, D. J. Copper underpotential deposition at high index single crystal surfaces of Au. *Journal of Electroanalytical Chemistry* **2004**, *570* (2), 157-161. DOI: https://doi.org/10.1016/j.jelechem.2004.02.012.
(141) Herrero, E.; Glazier, S.; Buller, L. J.; Abruña, H. D. X-ray and electrochemical studies of Cu upd on single crystal electrodes in the presence of bromide: comparison between Au(111) and Pt(111) electrodes1Dedicated to Professor W. Vielstich on the occasion of his 75th birthday.1. *Journal of Electroanalytical Chemistry* **1999**, *461* (1), 121-130. DOI: https://doi.org/10.1016/S0022-0728(98)00066-7.
(142) Vélez, P.; Cuesta, A.; Leiva, E. P. M.; Macagno, V. A. The underpotential deposition that should not be: Cu(1×1) on Au(111). *Electrochemistry Communications* **2012**, *25*, 54-57. DOI: https://doi.org/10.1016/j.elecom.2012.09.024.

(143) Frittmann, S.; Schuster, R. Role of Anions During the Cu Underpotential Deposition on Au(111): A Microcalorimetric Investigation. *The Journal of Physical Chemistry C* **2016**, *120* (38), 21522-21535. DOI: 10.1021/acs.jpcc.6b06624.
(144) Shi, Z.; Wu, S.; Lipkowski, J. Coadsorption of metal atoms and anions: Cu upd in the presence of SO42−, Cl− and Br−. *Electrochimica Acta* **1995**, *40* (1), 9-15. DOI: https://doi.org/10.1016/0013-4686(94)00244-U.
(145) Dai, X. X.; Dai, X.; Compton, R. G. Detection of As(III) via oxidation to As(V) using platinum nanoparticle modified glassy carbon electrodes: arsenic detection without interference from copper. *ANALYST* **2006**, *131* (4), 516-521. From http://worldcat.org /z-wcorg/.
(146) Mödlinger, M.; de Oro Calderon, R.; Haubner, R. Arsenic loss during metallurgical processing of arsenical bronze. *Archaeological and Anthropological Sciences* **2019**, *11* (1), 133-140. DOI: 10.1007/s12520-017-0534-1.
(147) Teppo, O.; Taskinen, P. ASSESSMENT OF THE THERMODYNAMIC PROPERTIES OF ARSENIC-COPPER ALLOYS. *Scandinavian Journal of Metallurgy* **1991**, *20* (2), 141-148.
(148) Casuse-Driovínto, T. Q.; Rizo, R.; Benavidez, A.; Brearley, A. J.; Cerrato, J. M.; Garzon, F. H.; Herrero, E.; Feliu, J. M. Increased Sensitivity and Selectivity for As(III) Detection at the Au(111) Surface: Single Crystals and Ultraflat Thin Films Comparison. *The Journal of Physical Chemistry C* **2022**, *126* (48), 20343-20353. DOI: 10.1021/acs.jpcc.2c05541.
(149) Madry, B.; Wandelt, K.; Nowicki, M. Deposition of copper multilayers on Au(111) in sulfuric acid solution: An electrochemical scanning tunneling microscopy study. *Surface Science* **2015**, *637-638*, 77-84. DOI: https://doi.org/10.1016/j.susc.2015.03.017.
(150) Shi, Z.; Lipkowski, J. Coadsorption of Cu2+ and SO42− at the Au (111) electrode. *Journal of Electroanalytical Chemistry* **1994**, *365* (1-2), 303-309.
(151) Verbruggen Florian, F.; Verbruggen, F.; Ostermeyer, P.; Bonin, L.; Prevoteau, A.; Marcoen, K.; Hauffman, T.; Hennebel, T.; Rabaey, K.; Moats, M. S. Electrochemical codeposition of arsenic from acidic copper sulfate baths: The implications for sustainable copper electrometallurgy. *Minerals Engineering* **2022**, *176*. From http://worldcat.org /z-wcorg/.
(152) Maroun, F. F.; Maroun, F.; Morin, S.; Lachenwitzer, A.; Magnussen, O. M.; Behm, R. J. Admetal-induced substrate surface restructuring during metal-on-metal electrochemical deposition studied by in situ scanning tunneling microscopy. *Surface Science* **2000**, *460* (1-3), 249-263. From http://worldcat.org /z-wcorg/.
(153) Green, M. P.; Hanson, K. J. Alloy formation in an electrodeposited monolayer. *Surface Science* **1991**, *259* (3), L743-L749. DOI: https://doi.org/10.1016/0039-6028(91)90545-4.
(154) Chen Shaohua, S. H.; Chen, S.; Ding, Y.; Zhao, D.; Lu, D.; Wang, J. Electrochemical Behaviour of Arsenic on Copper Deposition Reaction in the Low Copper Concentration Electrolyte. *ASIAN JOURNAL OF CHEMISTRY* **2013**, *25* (10), 5707-5709. From http://worldcat.org /z-wcorg/.
(155) Madry, B.; Wandelt, K.; Nowicki, M. Deposition of copper and sulfate on Au(1 1 1): New insights. *Applied Surface Science* **2016**, *388* (Part B), 678-683, Article. DOI: 10.1016/j.apsusc.2016.02.151 From EBSCOhost ScienceDirect.

Appendix A: Supplemental Materials for DC sputtered Ultralow Loading Gold Nanofilm Electrodes for Detection of As (III) in Water

Supplemental Materials

DC sputtered Ultralow Loading Gold Nanofilm Electrodes for Detection of As (III) in Water

Authors Names: Tybur Q. Casuse [*], Angelica Benavidez [2], John B. Plumley [2], Lok-kun Tsui [2], Abdul-Mehdi Ali [3], José M. Cerrato [1] and Fernando H. Garzon [2*]

* Corresponding authors' email address: garzon@unm.edu

[1] Department of Civil Engineering, MSC01 1070, 1 University of New Mexico, Albuquerque, New Mexico 87131, USA

[2] Center for Micro Engineered Materials, 1001 University Dr., Albuquerque, New Mexico 87106, USA

[3] Department of Earth & Planetary Sciences, MSC03 2040, 1 University of New Mexico, Albuquerque, New Mexico 87131, USA

Manuscript Published in ECS Sensors Plus.

Keywords: Arsenic, Aqueous Electrochemical Detection, Gold Electrode, Thin Films,

Accessible Electrochemistry

Summary of Supplemental Materials

Journal: ECS Sensors Plus

Date: April 11th, 2022

10 pages (including cover page)

4 Tables

3 Figures

Table A-S1 X-ray fluorescence film builder calculation of PVD Au nanofilm thickness due to intensity of characteristic x-rays in comparison to a bulk phase Au sample.

Area	Intensity	XRF Orbis film builder film thickness (nm)
A	10.94	7.0875
B	9.787	6.3391
C	10.875	7.044
Average		6.82 ± 0.42

Table A-S2 Summary of Particle size determined using Jade software from XRD pattern data.

Sample Synthesis Attempt	Particle size in XRD (nm)
1	~8
2	~4
3	~4
4	~7
5	~3

Table A-S3 Area and charge density for As (III) standard additions method calibration curve in ultrapure conditions and 0.5 M H_2SO_4 supporting electrolyte. The region of interest was analyzed with a straight line from 0.14 to 0.3 for each of the curves. The electrochemical surface area was determined to be 21.96 cm^2 using Au reduction peak analysis from cyclic voltammetry and a specific capacitance of 400 µC cm^{-2} for gold.

	Area (µA V)	Charge (µC)	Charge Density (µC cm^{-2})
50 µg/L	1.477	147.686	6.723
	1.446	144.592	6.582
	1.381	138.141	6.288
25 µg/L	0.715	71.534	3.256
	0.755	75.497	3.437
	0.763	76.260	3.471
15 µg/L	0.468	46.774	2.129
	0.405	40.489	1.843
	0.405	40.473	1.842
10 µg/L	0.313	31.256	1.423
	0.308	30.790	1.402
	0.308	30.842	1.404
5 µg/L	0.156	15.569	0.709
	0.148	14.774	0.673
	0.124	12.410	0.565
Blank 1	0.005	0.046	0.002
Blank 2	-0.019	-0.186	-0.012
Blank 3	-0.013	-0.128	-0.011

Table A-S4 Area and charge density for As (III) standard additions method calibration curve in Rio Paguate Moquino river water sample and 0.5 M H_2SO_4 supporting electrolyte. The region of interest was analyzed with a straight line from 0.1 to 0.4 for each of the curves. The electrochemical surface area was determined to be 21.23 cm^2 after Au reduction peak analysis from cyclic voltammetry and a specific capacitance of 400 µC cm^{-2} for gold.

	Area (µA V)	Charge (µC)	Charge Density (µC cm^{-2})
175 µg/L	3.454	345.380	16.268
	3.609	360.893	16.999
	3.759	375.850	17.704
125 µg/L	2.470	246.989	11.634
	2.727	272.654	12.843
	2.633	263.270	12.401
100 µg/L	2.047	204.694	9.642
	2.260	226.032	10.647
	2.366	236.643	11.147
75 µg/L	1.631	163.108	7.683
	1.786	178.619	8.414
	1.731	173.145	8.156
50 µg/L	1.501	150.090	7.070
	1.452	145.247	6.842
	1.507	150.730	7.100
25 µg/L	1.044	104.409	4.918
	0.986	98.633	4.646
	1.046	104.583	4.926
15 µg/L	0.838	83.841	3.949
	0.770	77.046	3.629
	0.954	95.444	4.496
10 µg/L	0.802	80.226	3.779
	0.865	86.459	4.072
	0.750	75.044	3.535
5 µg/L	0.302	30.203	1.423
	0.172	17.150	0.808
	0.341	34.138	1.608
Blank 1	-0.374	-37.398	-1.762
Blank 2	-0.446	-44.636	-2.102
Blank 3	-0.435	-43.494	-2.049

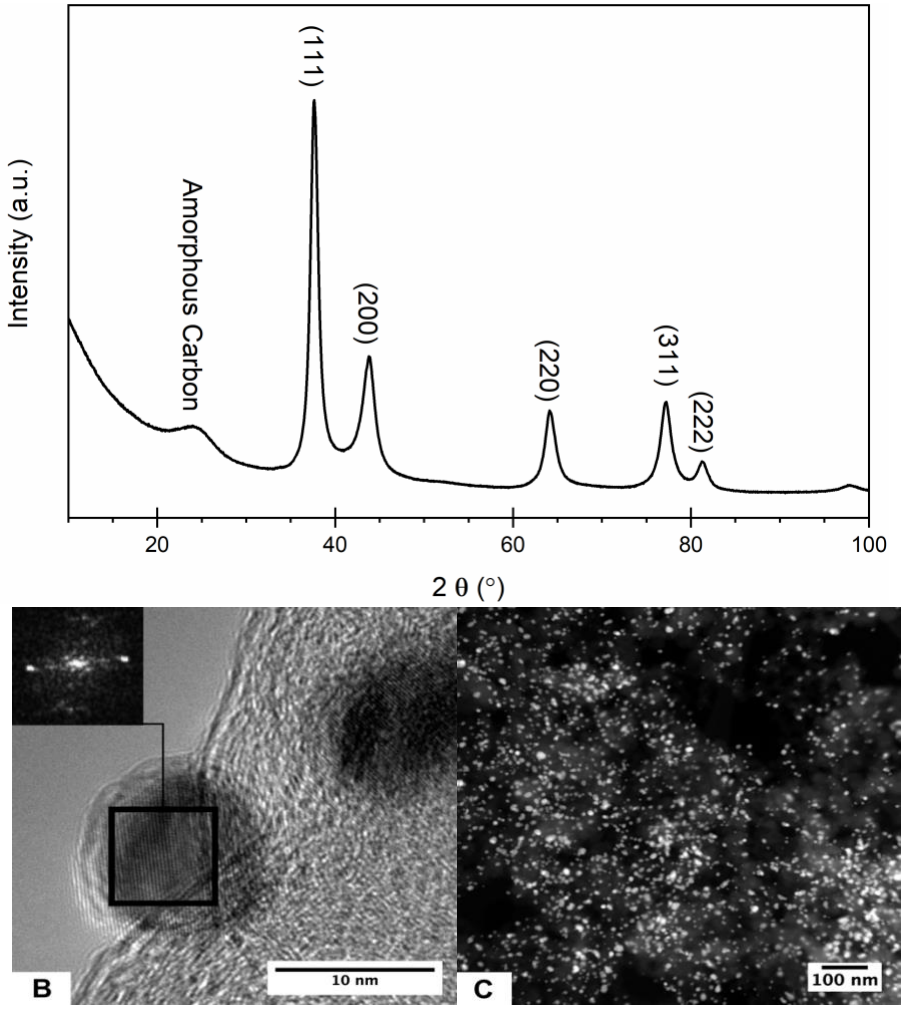

Figure A-S1. Gold nanoparticles deposited onto Vulcan XC 72R: (A) X-ray Diffraction pattern International Centre for Diffraction Data (ICDD) card (PDF# 00-066-0091); (B) High Resolution TEM inset Fast Fourier Transform of boxed region; dark area is Au nanoparticles and lighter patterned region is XC 72R carbon; (C) Dark Field TEM; light regions are Au particles and dark region is space or XC 72R.

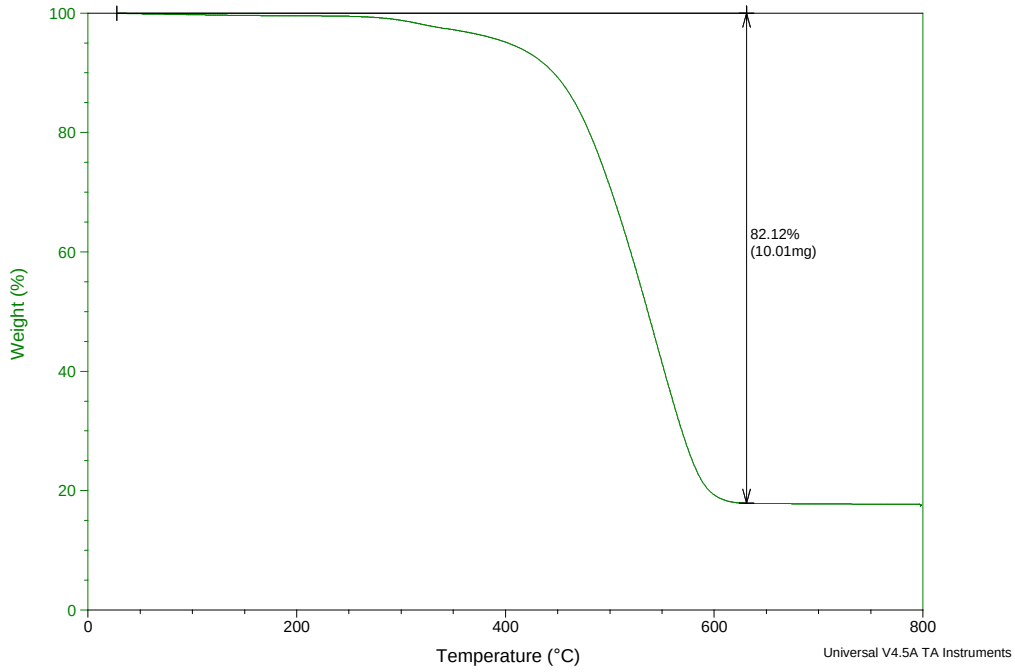

Figure A-S2. Thermogravimetric analysis of first Au nanoparticle synthesis.

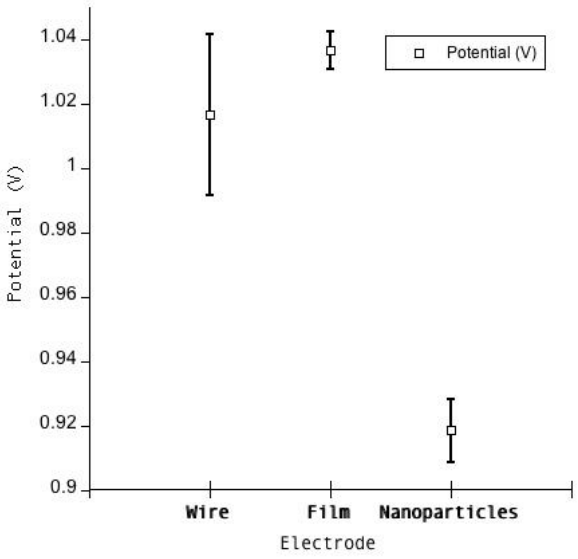

Figure A-S3. Potential of reduction peak for each of the electrodes in Figure 2 with a 50 mV s^{-1} scan rate. Anova single parameter test in Microsoft Excel showed no significant difference between PVD Au nanofilm and Au Wire. There is significant difference between Au wire and Au nanoparticles reduction peak potentials.

Appendix B: Supporting Information for Increased Sensitivity and Selectivity for As (III) Detection at Au(111) Surface: Single Crystals and Ultraflat Thin Films Comparison

Tybur Q. Casuse,[1,3*] Rubén Rizo,[2] Angelica Benavidez,[3] Adrian Brearley,[3,4] Jose M. Cerrato,[1,3] Fernando H. Garzon,[3*] Enrique Herrero,[2] Juan M. Feliu [2]

[z] Corresponding email addresses: garzon@unm.edu; tcasuse@unm.edu

Telephone: (001) 505-934-6971

Fax: (001) 505-277-1988

[1] Department of Civil, Construction & Environmental Engineering, 1 University of New Mexico, MSC01 1070, Albuquerque, NM, USA 87131

[2] Instituto de Electroquímica, Universidad de Alicante, Apdo. 99, E'0308, Alicante, Spain.

[3] Center for Micro-Engineered Materials, University of New Mexico, 1001 University Blvd SE, Albuquerque, NM, USA 87106

[4] Department of Earth & Planetary Sciences, MSC03 2040, 1 University of New Mexico, Albuquerque, New Mexico 87131, USA

Summary of Supplemental Information

Journal: Journal of Physical Chemistry C

Date: July 31st, 2022

11 pages (including cover page)

2 Tables

6 Figures

Table B-S1. AFM analysis of Au(UTF) data for calculating root mean square roughness.

Statistical Quantities

Image: Scan_012_Topography_F

Selected area: 256 × 256 at (0, 0) px

0.000000 × 0.000000 at (0.000000, 0.000000) m

Mask in use: No

Average value: -5.85331 µm

RMS roughness (Sq): 2.54736 nm

RMS (grain-wise): 2.54736 nm

Mean roughness (Sa): 1.19266 nm

Skew (Ssk): 4.76679

Excess kurtosis: 50.5297

Minimum: -5.87094 µm

Maximum: -5.81644 µm

Median: -5.85348 µm

Maximum peak height (Sp): 0.03687 µm

Maximum pit depth (Sv): 0.01763 µm

Maximum height (Sz): 0.05450 µm

Projected area: 4.00000 µm²

Surface area: 4.05758 µm²

Surface slope (Sdq): 0.183978

Volume: -23.4132 µm³

Variation: 588307 nm²

Inclination θ: 0.00 deg

Inclination φ: 131.82 deg

Scan line discrepancy: 147.187×10^{-6}

Table B-S2. Table of charge density of Arsenic reduction and oxidation and oxidation peak potential for cyclic voltammetry in 10^{-1} and 10^{-3} M As with 0.5 M H_2SO_4 supporting electrolyte.

	Reduction Charge Density	Oxidation Charge Density	Oxidation Peak Potential
	μC cm^{-2}	μC cm^{-2}	V vs. SHE
10^{-1} M As (III)	-2160	2450	0.554
10^{-3} M As (III)	-1480	1570	0.402

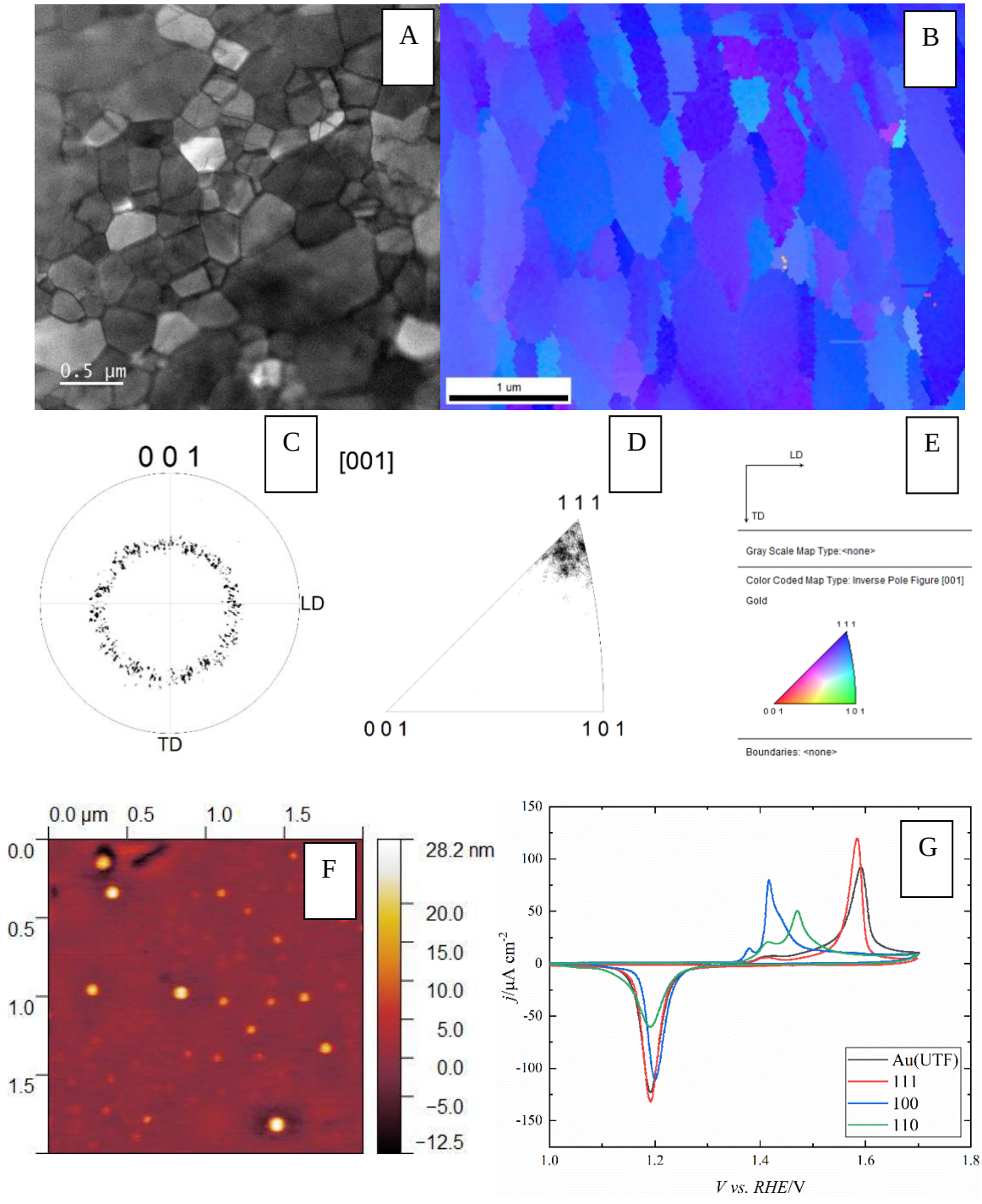

Figure B-S1. Characterization of Au(UTF): A) Dark Field transmission electron microscopy, B) Electron Backscatter Diffraction Image, C) pole figure for the [100] pole direction, D) Inverse pole figure by EBSD analysis, E) legend associated with figures B, C and D, F) Atomic force microscopy image, G) Electrochemical Au oxidation and reduction peaks for Au(UTF), Au(111), Au(110) and Au(100) surfaces in 0.5 M H2SO4.

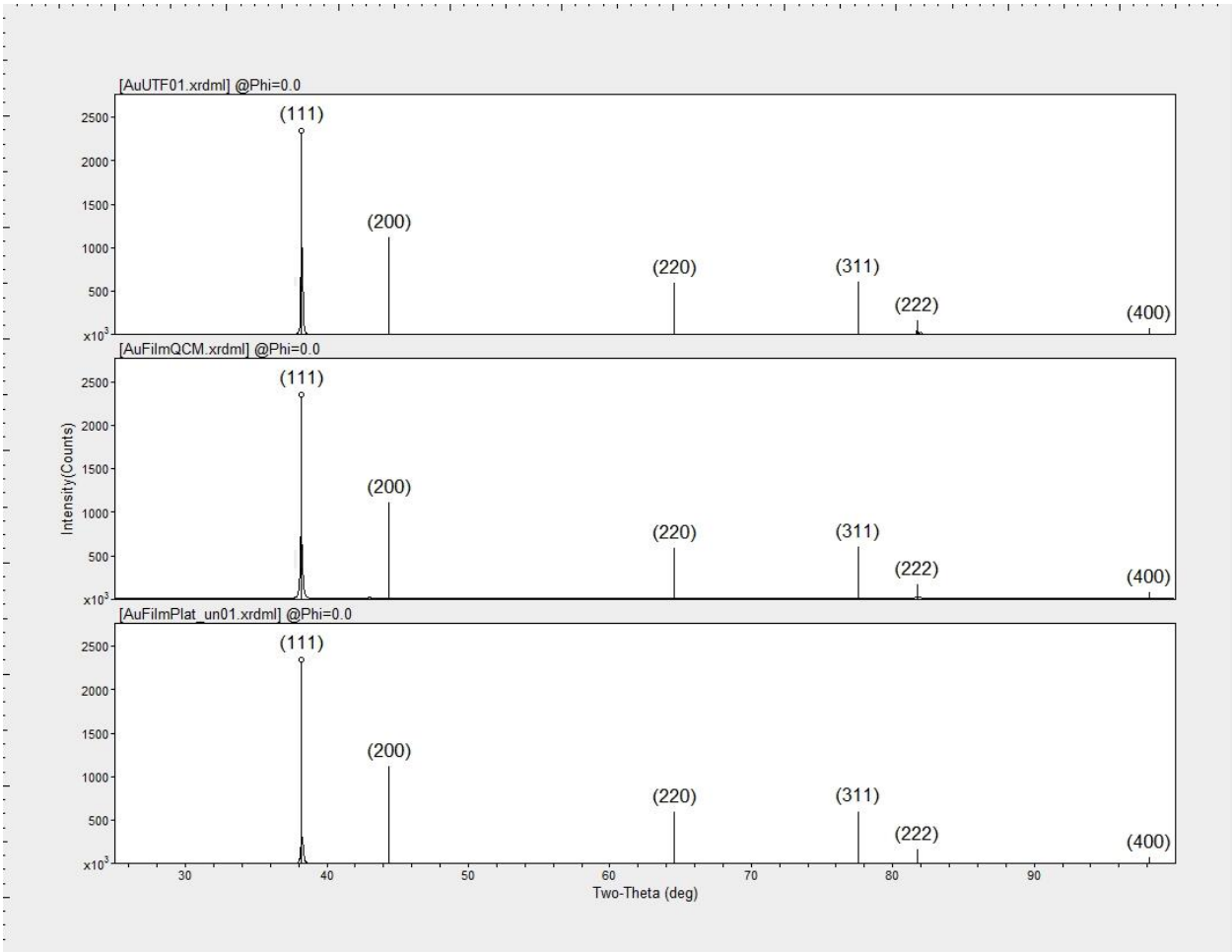

Figure B-S2. X-ray diffraction analysis of: Top: Au(UTF) thin film. Middle, EQCM electrode and Bottom, not intentionally oriented Au thin film electrode, (111) normal texture noted in all three samples.

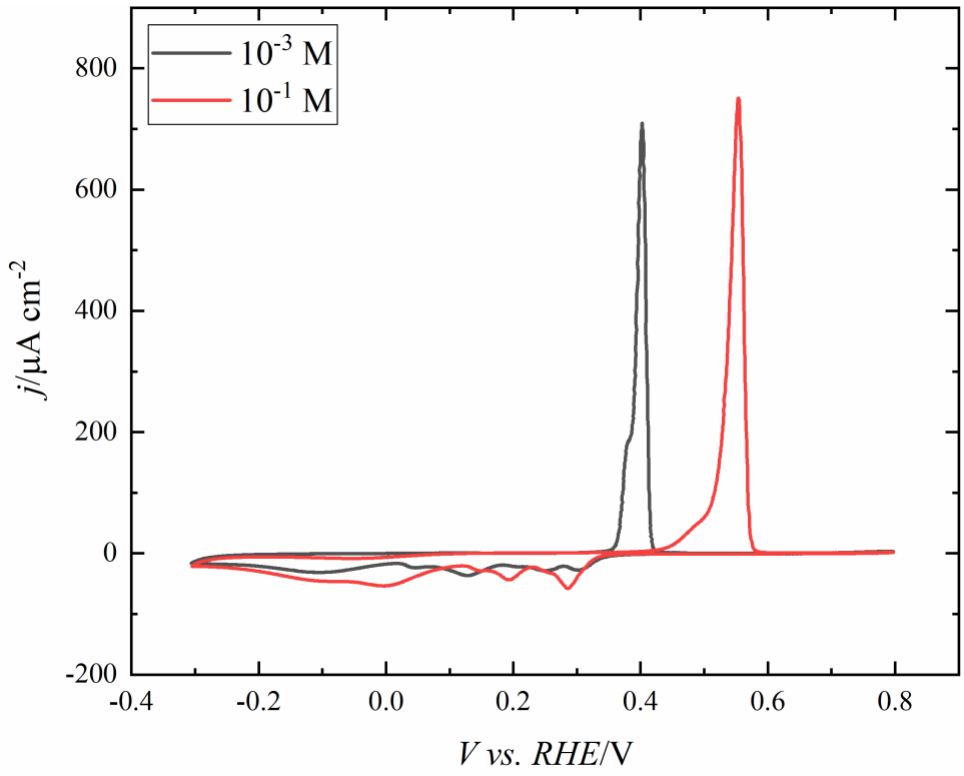

Figure B-S3. Cyclic voltammetry of 10-3 and 10-1 M As (III) in 0.5 M H2SO4 solution at 10 mV s-1.

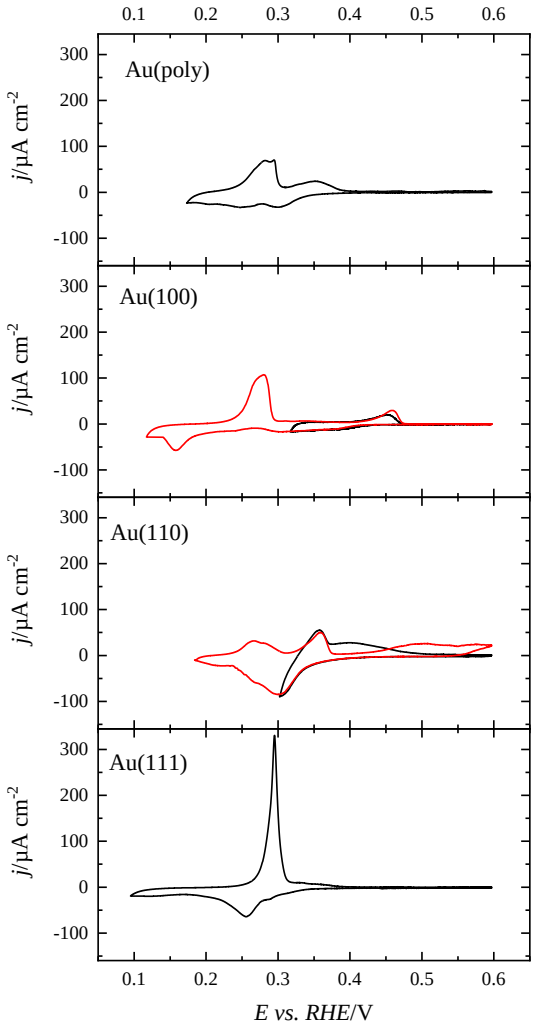

Figure B-S4. Cyclic voltammetry in 10-3 M As (III) with 0.5 M H2SO4 supporting electrolyte with more positive lower limit potentials on a smaller potential scale to inform Figures 1 and 2 in the main manuscript.

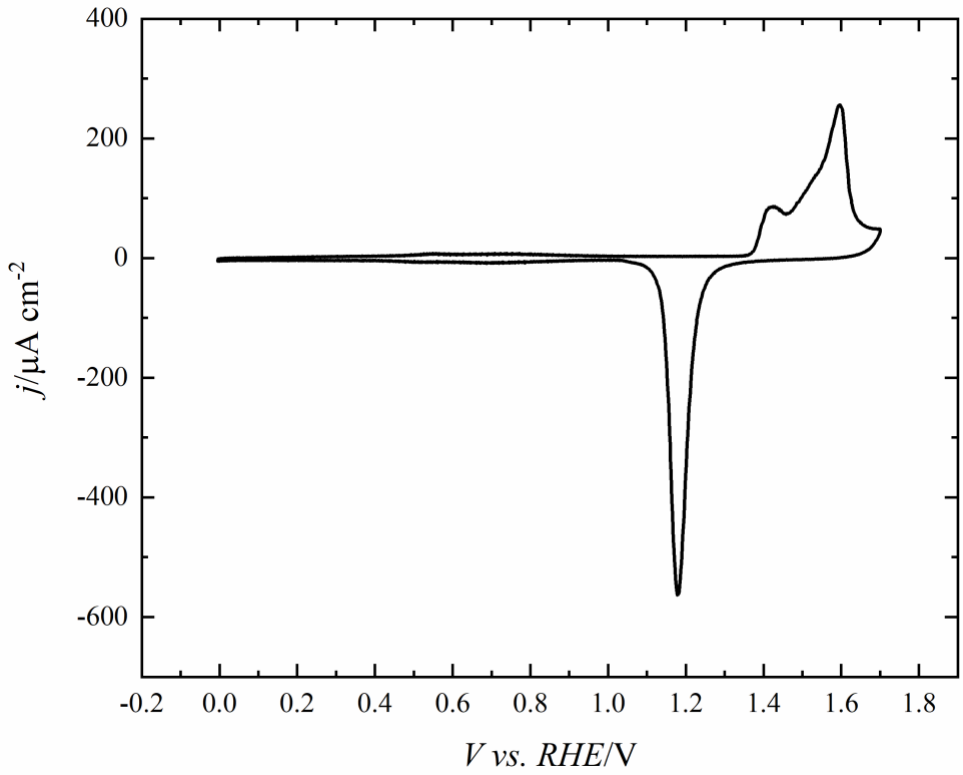

Figure B-S5. Cyclic voltammetry of EQCM in 0.5 M H2SO4 at 50 mV s-1.

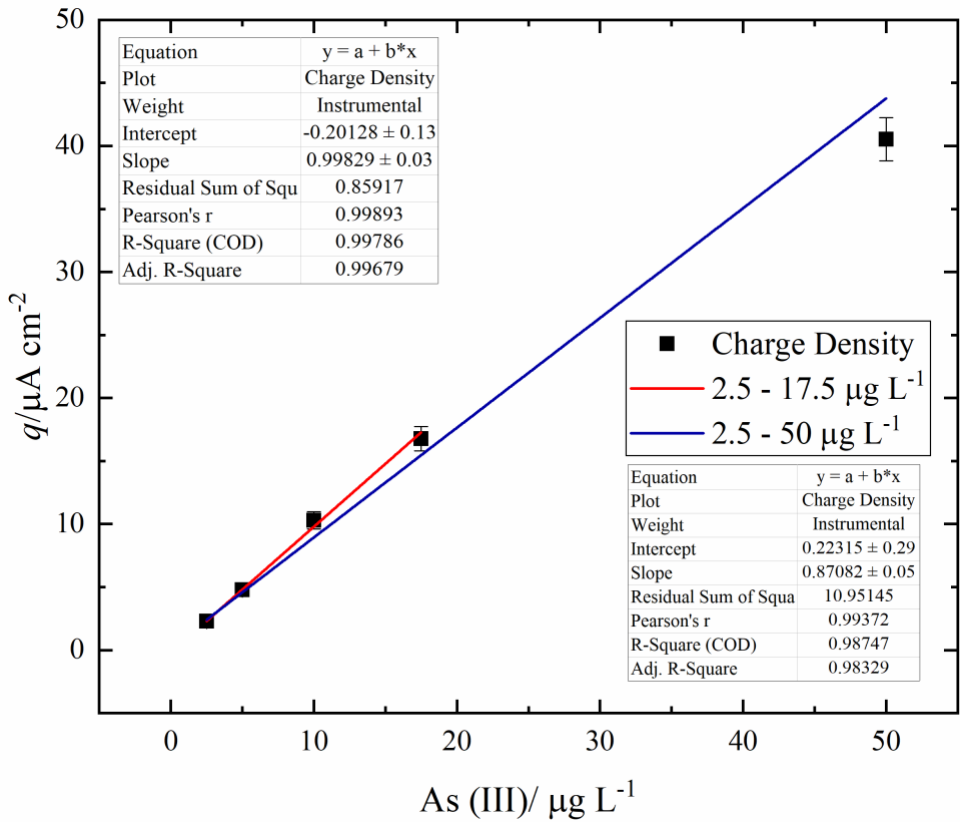

Figure B-S6. Linear regressions between charge density for 2.5 to 17.5 and 2.5 to 50 µg L^{-1}. The upper left data is related to 2.5 to 17.5 µg L^{-1} and the lower right data is related to 2.5 to 50 µg L^{-1}.

Appendix C: Supplemental Information for Electrochemical Redox of Arsenic (III) and Cu (II) Mixtures with Ultraflat Au(111) Thin Films in Water

Tybur Q. Casuse-Driovínto,[1,2] Angelica Benavidez,[2] Noah Jemison,[2] José M. Cerrato,[1,2] Juan Feliu,[3] Fernando H. Garzon,[2z]

[z] Corresponding email addresses: garzon@unm.edu

Telephone: (001) 505-934-6971

Fax: (001) 505-277-1988

[1] Department of Civil, Construction & Environmental Engineering, 1 University of New Mexico, MSC01 1070, Albuquerque, NM, USA 87131

[2] Center for Micro-Engineered Materials, University of New Mexico, 1001 University Blvd SE, Albuquerque, NM, USA 87106

[3] Instituto de Electroquímica, Universidad de Alicante, Apdo. 99, E'0308, Alicante, Spain.
[*]Corresponding Author

Summary of Supplemental Information

Journal: TBD

Date: June 25th, 2023

4 pages (including cover page)

2 Figures

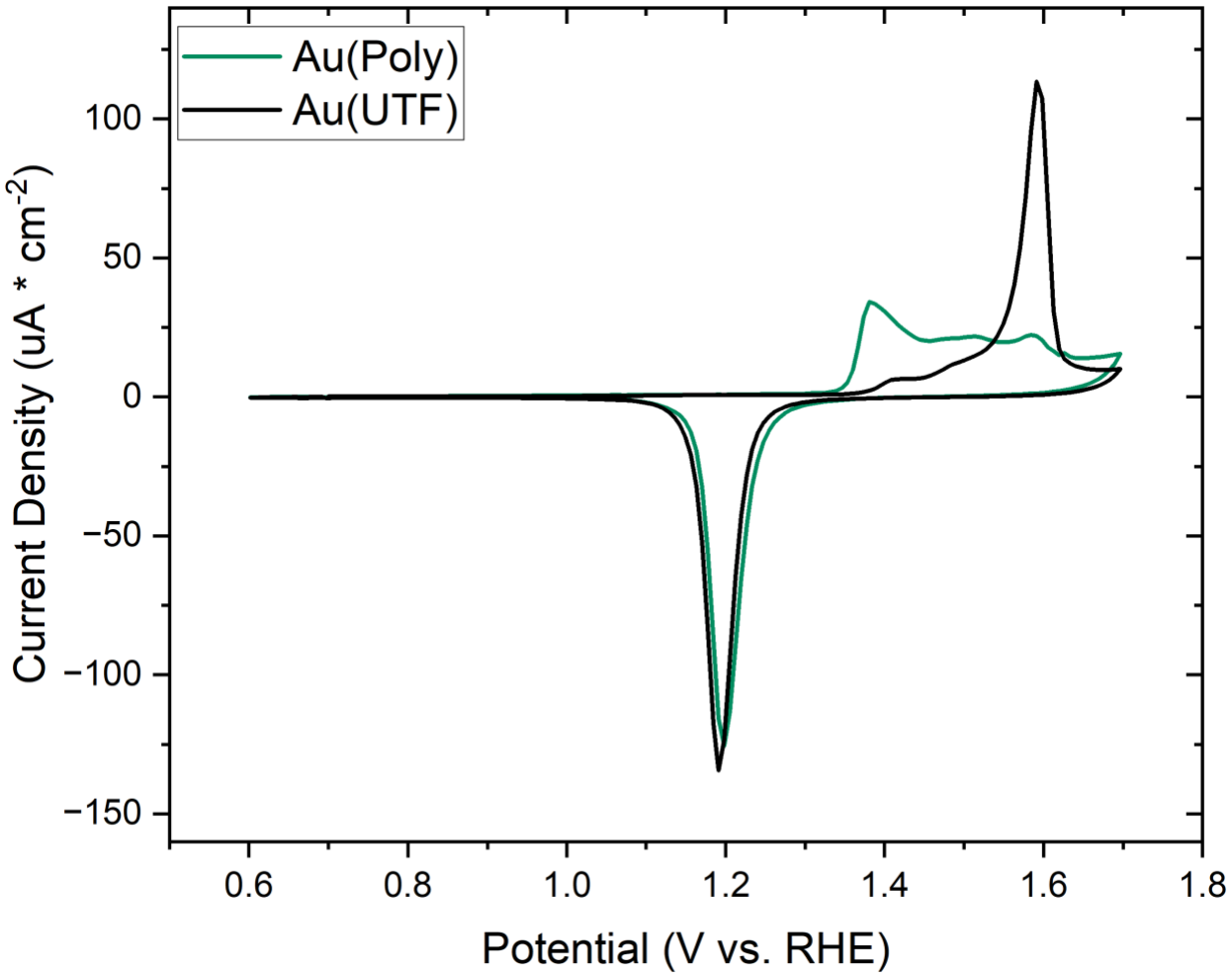

Figure C-S1. Comparison of Gold Oxidation and Reduction at the Au(UTF) and Au(Wire) electrode surfaces.

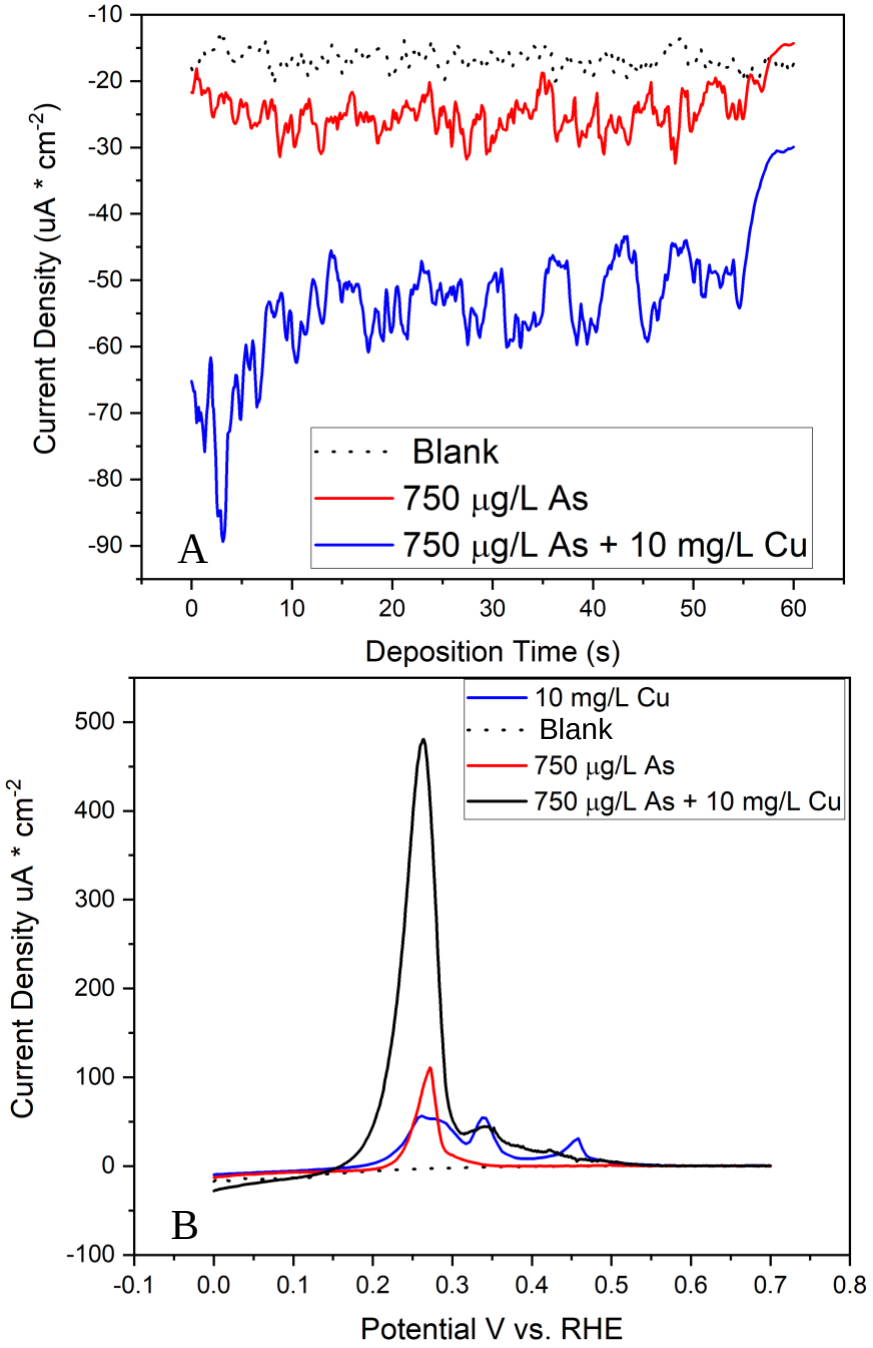

Figure C-S2. A) Chronoamperometry during 60 s of deposition at 0 V vs. RHE and B) Linear stripping voltammetry after chronoamperometry with a scan rate of 10 mV s^{-1}, for 750 µg L^{-1} As (III) and a 750 µg L^{-1} As (III) + 10 mg L^{-1} Cu (II) mixture with 0.5 M H_2SO_4 supporting electrolyte.